NTNU

Norwegian University of
Science and Technology

# Low Temperature Plate Freezing of Fish on boats using R744 as Refrigerant and Cold Thermal Energy Storage

**Espen Halvorsen Verpe**

Master of Science in Mechanical Engineering
Submission date: June 2018
Supervisor: Armin Hafner, EPT
Co-supervisor: Ignat Tolstorebrov, EPT

Norwegian University of Science and Technology
Department of Energy and Process Engineering

NTNU

Norwegian University
of Science and Technology

Department of Energy
and Process Engineering

EPT-M-2018-105

# MASTER THESIS

for

student Espen Halvorsen Verpe

Spring 2018

**Low Temperature Plate Freezing of Fish on Boats Using R744 as Refrigerant and Cold Thermal Energy Storage**

*Lavtemperatur platefrysing av fisk på båt ved bruk av R744 som kuldemedium og kald termisk energilagring*

## Background and objective

Synthetic refrigerants, for example HCFC-22 (R22), were earlier used in onboard freezing systems because of their high COP, non-toxicity and manageable system pressures and temperatures. Because of their ozone depleting potential and effect on global warming when released to the atmosphere, restrictions and bans on several synthetic refrigerants have been introduced. This has forced the marked to invest in refrigeration systems with more climate friendly natural refrigerants, such as R744 ($CO_2$, carbon dioxide) and R717 ($NH_3$, ammonia). R717 is common in land based refrigeration systems and in refrigerated sea water systems (RSW) onboard of fishing boats. Ammonia systems do have high COPs and manageable system pressures. However, when applied in freezing systems, it is recommended to avoid temperatures in the evaporator below -35 °C. Below this value, the saturation pressure in the system will be sub atmospheric and there is a risk of air (and water vapor) leaking into the system. Instead, when applying R744, evaporating temperatures down to -50 °C are possible. Lower freezing temperatures (-50 °C compared with -35 °C) will freeze the same amount of fish faster, which is beneficial for the total production onboard.

This Master Thesis will continue on the preliminary studies of the summer job work and a project work, and further improve some of the models developed, including CFD freezing model, and system COP model. Comparison between results obtained with the models and industry plate freezer are performed during and after field test campaigns.

## The following tasks are to be considered:

1. Literature survey on low temperature plate freezers
2. Describe and further improve the numerical model, including air voids in and on the product surface, and optimization/influence of block thickness.
3. Describe and improve the refrigeration system model, by including compressor capacity control devices. Consider implementation of cold storage devices and analyses the energy saving potential.
4. Prepare HSE documents required to perform tests in the field / laboratory. Develop a plan for required measurement equipment to be able to evaluate the performance of the $CO_2$ / R744 refrigeration systems. Establish a plan for dedicated experimental campaigns to be coordinated with the manufacture / system operator and the availability of the laboratory equipment.

7. Master Thesis report including results, summary, discussion and conclusions.
8. Make a scientific paper with main results from the thesis.
9. Make proposals for further work

-- ” --

Within 14 days of receiving the written text on the master thesis, the candidate shall submit a research plan for his project to the department.

When the thesis is evaluated, emphasis is put on processing of the results, and that they are presented in tabular and/or graphic form in a clear manner, and that they are analyzed carefully.

The thesis should be formulated as a research report with summary both in English and Norwegian, conclusion, literature references, table of contents etc. During the preparation of the text, the candidate should make an effort to produce a well-structured and easily readable report. In order to ease the evaluation of the thesis, it is important that the cross-references are correct. In the making of the report, strong emphasis should be placed on both a thorough discussion of the results and an orderly presentation.

The candidate is requested to initiate and keep close contact with his/her academic supervisor(s) throughout the working period. The candidate must follow the rules and regulations of NTNU as well as passive directions given by the Department of Energy and Process Engineering.

Risk assessment of the candidate's work shall be carried out according to the department's procedures. The risk assessment must be documented and included as part of the final report. Events related to the candidate's work adversely affecting the health, safety or security, must be documented and included as part of the final report. If the documentation on risk assessment represents a large number of pages, the full version is to be submitted electronically to the supervisor and an excerpt is included in the report.

Pursuant to “Regulations concerning the supplementary provisions to the technology study program/Master of Science” at NTNU §20, the Department reserves the permission to utilize all the results and data for teaching and research purposes as well as in future publications.

The final report is to be submitted digitally in DAIM. An executive summary of the thesis including title, student’s name, supervisor's name, year, department name, and NTNU's logo and name, shall be submitted to the department as a separate pdf file. Based on an agreement with the supervisor, the final report and other material and documents may be given to the supervisor in digital format.

☒ Work to be done in lab (Water power lab, Fluids engineering lab, Thermal engineering lab)
☒ Field work

Department of Energy and Process Engineering, 15. January 2018

_____
Prof. Dr.-Ing. Armin Hafner
Academic Supervisor

Research Advisor: Dr. Ignat Tolstorebrov (ignat.tolstorebrov@ntnu.no)

# Preface

This is a master thesis for the Department of Energy and Process Engineering at NTNU Trondheim. The master thesis is valued at 30 credit points at NTNU. It was carried out the spring semester of 2018, in collaboration with SINTEF Energy. It is also a part of the international research project HighEff which goal is to ensure a more energy efficient industry. It was based on the project thesis of the same author, in addition to some research for the internship program at SINTEF Energy 2017.

Espen Halvorsen Verpe

Trondheim, 11 June 2018

# Acknowledgment

I would like to thank the following persons for the help I received during the past semester: Dr. Armin Hafner and Dr. Michael Bantle for formulating and administrating the project work. Also, they have been helping out with some technical details. Dr. Ignat Tolstorebrov for great technical help and assistance regarding technical help and in experimental work.

Thanks to SINTEF Energy for the opportunity to start with preliminary work during summer 2017, and for the collaboration in the following project work. Michael Bantle was, also here, my supervisor and of great technical and administrative support.

This thesis has been partly funded by HighEFF - Centre for an Energy Efficient and Competitive Industry for the Future, an 8-year Research Centre under the FME-scheme (Centre for Environment-friendly Energy Research, 257632/E20). The author gratefully acknowledge the financial support from the Research Council of Norway and partners of HighEFF.

Given the opportunity here, the author would like to give special gratitude to Yves Ladam from Kuldeteknisk AS for helping out with the planning and execution of the experiment carried out on MS Arnøytind in Tromsø, where important validation was performed in plate freezer.

E.H.V.

# Abstract

The introduction of R744 based freezing systems enables lower evaporating temperatures and faster freezing times, however, also a lower system efficiency (COP). This thesis will investigate how low temperature $CO_2$ compares to traditional refrigerants in plate freezers, regarding energy efficiency and product capacity, where the latter is of special importance for fishing vessels.

A numerical freezing model was made to simulate freezing of fish blocks in a plate freezer, and was validated by freezing of a phase changing test material in an industrial plate freezer. COP was estimated for the freezing system, and selected natural refrigerants was modeled. The freezing model relied on a two-dimensional, heat capacity-temperature, implicit finite difference method with time dependent temperature boundary conditions. The evaporating temperature is not static, as one might expect, but dynamic due to varying heat load from the product side. The reason being the compressor cannot deliver the required freezing capacity for peak loads. The elevation of the evaporating temperature results in prolonged freezing times and reduced product capacity, compared to ideal freezing with constant plate temperature. The conditions in the low pressure receiver was modeled to estimate the temperature increase, which was also validated. A thermal storage with $CO_2$ as phase change material was investigated, with objective to eliminate the elevated temperature in the beginning of the freezing process by storing energy when compressor capacity is larger than the heat load, and release that energy when the compressor struggles to maintain the low evaporating pressure. Ice formation/melting in the storage tank was modeled to determine the dimensioning properties.

The numerical freezing model demonstrated good agreement with experiments, with a deviation in freezing time of only 3 %. Numerical calculations revealed that low temperature freezing, down to -50 °C, require 71 % and 57 % more energy per kilo fish than for -30 °C and -40 °C, respectively, assuming R744 COP and 100 mm thick blocks. The higher energy consumption is mainly due to decreased COP for lower evaporation temperatures, which was estimated to be 1.75, 2.25 and 2.98 for the abovementioned temperatures, using R744. In addition, product capacity (kg frozen fish per hour) is increased by correspondingly 66 % and 34 % by lowering the evaporating temperature to -50 °C. When implementing a energy storage system, shorter freezing times were obtained, because the pressure in the low pressure receiver is not elevated as much in the beginning of the freezing process. Results suggest a product capacity increase of 2.92 % for a low temperature R744 freezer with thermal energy storage solution. The tank volume was determined to be between 614 and 422 liters, and required between 1377 and 702 tubes, of 1 meter length and 10 mm radius.

# Sammendrag

Introdusering av $CO_2$ baserte frysesystemer tilrettelegger for lavere fordampningstemperaturer og raskere innfrysningstider, men også lavere systemeffektivitet (COP). Denne masteroppgaven undersøker hvordan $CO_2$ egner som kjølemiddel, i forhold til mer tradisjonelle kjølemidler. Sentrale sammenligningsindikatorer er energibruk [kWh per kilo fisk] og produktkapasistet [kilo frossen fisk per time], hvor den sistnevnte er av spesiell betydning.

COP ble estimert for et totrinns fryseanlegg, for forskjellige kjølemidler og fordampningstemperaturer. I tilleg ble det laget en numerisk frysemodell for å simulere innfrysning av fiskeblokker i en platefryser. Modellen ble validert ved å fryse et testmateriale, med lignende egenskaper som fisk, i en industriell platefryser. Frysemodellen er basert på en todimensjonal, varmekapasitet/temperatur, implisitt «finite difference» metode, med tidsavhengige grensebetingelser. Platetemperaturen i fryseren er ikke konstant, men dynamisk ettersom varmelasten varierer, og er i begynnelsen større enn varmen som kompressorene klarer å fjerne. Dette fører til en oppsamling av kjøleemediegass i lavtrykkstanken, og midlertidig økning av trykket. En trykkøkning medfører også temperaturøkning av kjølemediet inn til platene i fryseren, som igjen påvirker frysetiden. Det ble derfor laget en numerisk modell til å forutsi denne temperaturøkningen, som også ble validert, med data fra et landbasert anlegg med lignende frysere. Denne varierende platetemperaturen ble implementert i frysemodellen som de tidsavhengige grensebetingelsene. Til slutt ble en det sett på hvordan en energilagringsenhet kan redusere denne platetemperaturøkningen med å lagre «kald» overskuddsenergi i et faseendringsmateriale (PCM), og bruke denne energien til å tilføre mer kjøling i begynnelsen av innfrysningen.

Den numeriske frysemodellen samsvarte bra med de eksperimentelle verdiene. Bare 3 % forskjellig innfrysningstid ble målt. Resultater fra modellen avslørte at lavtemperatursfrysing på -50 °C krevde 57 % og 71 % mer energi, enn henholdsvis -40 °C og -30 °C når 100 mm fiskeblokker ble modellert. Den økte energibruken har bakgrunn i en lavere COP for reduserte fordampningstemperaturer, henholdsvis 1.75, 2.25 og 2.98 for de overnevnte temperaturene med bruk av $CO_2$. I tillegg ble produktkapasistet økt med 65 % og 34 % ved å senke fordampningstemperaturen til -50 °C og -40 °C. Videre ble det også konkludert med at et energilagringssystem kan øke produktkapasiteten inntil 2.92 %, som er en effekt av begrenset trykkøkning i lavtrykkstanken. Størrelsen på energilagringstanken ble estimert til mellom 614 og 422 liter, og krevde mellom 1377 og 720 rør av 1 meter lengde og 10 mm radius.

# Contents

# Chapter 1 Introduction

## 1.1 Background

Freezing and cooling is one of the most applicable preservation methods for food products there is. Frozen food has an image of preserving freshness, at least more than canned or dried food. Fish, especially fish caught from fishing vessels, may be frozen one, two or in some cases three times before it is consumed. The first time is on the fishing vessel while the capacity of the boat is being filled up. The frozen fish block is ideally held frozen until it reaches the slaughter facility, which might be in another country and must be transported in containers, boats, trains or trucks. The frozen fish is thawed, filleted, packaged, re-frozen and transported to a storage of the supermarket. This project thesis will focus on what is usually the first freezing of the fish, caught at sea.

For many years synthetical refrigerants like R22 have been the dominant refrigerant on-board fishing vessels due to high efficiency, manageable operation pressure, non toxicity and non flammability. However, recent change in industries all over the world have shifted focus to more environmental friendly alternatives, with help from political induced taxes and phase-out of synthetically refrigerants. Global Warming Potential and Ozone Depletion Potential, referred to as GWP and ODP, are central values to estimate the harm when the refrigerant is leaked into the atmosphere. For example, R22 has a GWP of 1810, which means it contributes to global warming nearly 2000 times as much as for the same amount of $CO_2$, often referred to as R744.

This has led to recent development in systems using naturally occurring refrigerants, like $CO_2$, ammonia and other hydro carbons which have no or low GWP and ODP values. Nowadays, $CO_2$ and ammonia are the predominant refrigerants in the industry, but ammonia have a crucial weakness when it comes to evaporating temperature. Below -33.3 °C, the evaporating pressure is sub-atmospheric, risking leakage of water and air *into* the system. This is not the case for $CO_2$ which can, in theory, reach temperatures to -56.5 °C. In practice it is limited to around -50 °C to reduce the risk of dry ice formation.

Plate freezers are often used as the preferred freezing method on boats because of space and capacity requirements. Plate freezers are small, and have relatively short freezing time due to direct contact between product and plates, in which refrigerant is evaporating. Fish is distributed in stations, formed by the evaporating plates. Multiple fish is packed in one station, forming frozen fish blocks with varying thickness, depending on plate freezer design.

Fast freezing time, leading to increased capacity, is crucial to fishing vessels. Higher capacity

means that fishing boats can empty the RSW tank faster, where unfrozen fish is stored. Reduced time in the RSW tank improve the quality of fish. Furthermore, boats can harvest more fish while the fish is present. This reduces time at sea, and therefore fuel consumption and cost. At last, higher capacity means fewer boats can harvest the same amount of fish, further reducing fuel consumption and cost for the owner. Therefore, prediction of freezing time is an important parameter when designing new freezing systems or freezing facilities.

As of today, there was not found available software specifically designed to predict freezing time in plate freezer. The institute of Energy and Process Engineering (EPT) at NTNU want to implement a low stage $CO_2$ cycle on the existing transcritical $CO_2$ booster system. The new low stage cycle can be connected to for example a plate freezer for further testing. Furthermore, a numerical model opens up for more precise information about heat load. This is not gained by a simple analytical freezing time calculation.

## 1.2 Related work

Proper freezing time calculation was first introduced by *Plank* (1941) [41]. Almost every analytical freezing time prediction is based on this simple equation. This is a model which only predict the time for phase change to occur at single temperature. He later, in 1963, developed a correctional model to account for sensible heat from initial to frozen temperature[42]. Food properties are hard to determine and vary greatly because of different composition. An extensive collection of thermal properties for different food was created by *Miles et al. (1983)* [37]. They also developed a computer aided model to predict the properties. The American Society of Heating, Refrigerating and Air-Conditioning Engineers (ASHRAE) has in recent years developed, gathered and updated standards on how to measure thermal properties. *ASHRAE* (2010) [39] contains theory and tables on thermal properties for all kinds of food. It is not possible to have a continuous update of thermal properties with respect to temperature in an analytical freezing time equation, but there have been attempts to further modify Plank equation and to use thermal properties at different proposed temperature levels. Such modified equations are described by *Nagaoka et. al (1955)*[38] and *Cleland and Earle (1976-1979)*[12][13][11].

These analytical equations have proven to be somewhat inaccurate compared to numerical simulations, especially for complex geometry of the food product. *Lees (1966)*[32] suggested a numerical equation using the apparent heat capacity, which includes both sensible and latent energy required to reduce the temperature in food product when freezing occurs over a temperature range below initial freezing point. The method described, involved a fixed temperature boundary condition and is a one dimensional problem. *Bonacina and Comini (1971)* [8] used the same formulation, while modifying for the peak jump in apparent heat capacity, to simu-

late freezing in tylose, a phase changing material. *Cleland (1977)*[10] extended this method to convective boundary conditions. Also, he updated the numerical scheme to avoid numerical error involving oscillations. The extension to two dimensional computation was made by *Rebellato et al. (1978)*[43]. Their method included fixed boundary temperature, fixed heat flux and convective boundary conditions.

Numerical methods based on enthalpy, rather than temperature and heat capacity, has also been used. The discontinuity in enthalpy is not as sharp as for apparent heat capacity [27]. Examples on this method are described by, among others, *Rose (1960)*[45], *Crowley (1978)*[14] and *Marmapperuma & Singh, (1988)* [44].

There are few published experimental studies on low temperature R744 plate freezing of fish. Manufacturers claim they have reduced freezing time by 25-50% in R744 systems compared to systems using a higher evaporating temperature refrigerants, such as ammonia [19]. *Fernandez-Seara et al. (2012)*[23] used a horizontal plate freezer as evaporator in the low stage of a $NH_3/CO_2$ cascade system. They measured temperature in water contained in tin cans while determining optimum condenser temperature for $CO_2$. Evaporating temperature on the low stage refrigerant was measured to be between -40°C and -50°C. Water is not the ideal freezing product when used to compare freezing times in food. Water will circulate due to density differences and the ice front development might deviate from what is assumed. The combination of horizontal orientation and circulating water in gravitational field might cause ice to form stratificationally, resulting in the thermal center being different from the geometrical center. Therefore, the result highly dependent on probing, which might explains the observed difference in freezing time up to 16 minutes for the same experiment in two different boxes.

The Norwegian Ministry of Fisheries published in 1949 a detailed experimental setup of a R717 plate freezer test rig, with indirect brine cooling, to be used for fish freezing [1]. Cod filet was frozen for different plate temperatures, with and without packaging, different thickness, multiple probe depth and detailed size and weight data was given. Unfortunately, R744 was not used as a refrigerant and the brine temperature circulating the plates was at the lowest -32°C. Also, indirect cycle with brine solution will cause a temperature gradient within the plates. Even though the experiments seem thorough, this was done almost 70 years ago when measuring and refrigeration equipment can be regarded as underdeveloped.

In regard to cold thermal energy storage (CTES), there has been published a lot of papers and case studies. In general, these papers mainly describes system for use in combination to air conditioning in buildings, in addition to high temperature storage related to solar power. *Dincer & Rosen, (2001)*[17] did meta study on installed thermal energy storages (TES) for heating and cooling in large buildings around the world. They found large economical saving potential when energy used for heating and cooling could be generated and stored at night, when electricity prices are lower. Furthermore, a facility in the Netherlands using natural gas for peak load

heating, was found to reduce the natural gas consumption by 44 %, using a TES system with payback time of 6.5 years. *Agyenim et al. (2009)*[4] made a detailed review of PCM materials, heat transfer rates and problem formulation of CTES over the last three decades, with 135 cited sources. They found that most papers studied phase change at temperatures ranging between 0 °C and 60 °C. Anyhow, the theory for heat transfer and storage tank design is still valid for low temperature storage. Numerical (1D, 2D and 3D), experimental and analytical studies are included. They argue for a cylindrical shell and tube heat exchanger/storage tank with PCM at the shell side. Most PCM have unacceptably low thermal conductivity, which requires fins or other heat transfer enhancements to be able to store the energy when needed. It is reported that the effective thermal conductivity could be improved up to 10 times that of the PCM itself. However, advanced numerical schemes or experiments is required to calculate most heat transfer techniques. Values of melting rates, heat transfer and temperature gradients are tabulated, using dimensionless numbers like Reynolds number, Fourier number and Stefan number. The paper is very thorough, and much of the theory can be applied, but the operating temperatures is far off what is needed. When storing temperatures of -50°C, special PCM must be used. Also, on the tube side, solid CO2 is produced because of the required temperature difference. Sublimation occurs inside the tubes, making models for liquid/gas evaporation ineffective.

*Hafner et al. (2011)*[6] described an ammonia based tunnel freezer for fish, with a installed cascade CTES system, using $CO_2$ as both refrigerant and PCM. An energy analysis was done based on required and available freezing energy in the system, and they concluded with a potential 30% electricity saving. However, the pressure and temperature levels in tank (both shell and tube side) is not mentioned, and energy input from the added compressor seems to be missing. Also, it is not clear how the total energy savings are calculated. Dry ice growth in storage tank is not described nor is the storage tank dimensioned for the system. They concluded a more detailed review of CTES system should be done.

It is well known that when freezing food, a system cannot deliver the cooling required to maintain the low pressure in the evaporator. There was not found studies that relates heat load and compressor capacity to evaporating pressure, which in turn affects the freezing time. Unpublished work from *Lund, (2006)* described experiments on R744 based plate freezers, while logging compressor capacity, plate temperature and freezing time (of water). He also illustrated the circulation rate's influence on the UA value, confirming the most used circulation rate of between 3-6 is best in regard to heat transfer. The paper highlights the problem of initial instabilities in plate freezer flowrate due to high temperature difference between refrigerant and product.

## 1.3 Objectives

### What remains to be done?

Every numerical freezing problem is unique, and therefore a numerical solution must be made specifically for the problem at hand. Boundary conditions, equation to be solved and thermal property solutions are some of the assumptions to be made before solving the problem. It was therefore necessary to develop own numerical models. Experimental freezing times for fish using low temperature plate freezers are also not widely published. The few studies that appear lack vital information to be used as comparison. Validating the model is therefore essential to this thesis.

One of the main objectives of this thesis is to predict freezing times of fish blocks in a plate freezer using $CO_2$, enabling faster freezing than can be expected for ammonia based systems. In fact, plate freezer manufacturers, such as Dybvad Stål Industri in Denmark, claim that freezing time can be reduced by 25-50 %. At the same time, lowering the evaporation temperature increases the pressure ratio of the compressors, resulting in lower system COP. Moreover, different thermodynamic properties of the different refrigerants will influence the efficiency when comparing $CO_2$ to other refrigerants.

For economical reasons, installed compressor capacity in freezing facilities are normally dimensioned for the average heat load from product, meaning that during peak heat load, compressors cannot deliver required freezing capacity. This leads to elevated pressure and evaporating temperature in low receiver, resulting in prolonged freezing time. To reduce this effect, installation of energy storage system will be investigated. The objective of the energy storage is to store energy when available, and release that energy, supplementing the compressor with freezing capacity.

The following measures is to be done:

1. Develop numerical freezing model to predict freezing time for fish blocks in plate freezer
2. Develop numerical model to predict dynamic pressure in low receiver, caused be insufficient compressor capacity
3. Validate the numerical models with experimental data from industrial plate freezers
4. Theoretically compare COP for different system solutions using natural refrigerants
5. Estimate the effect on key performance indicators of low temperature plate freezer, compared to traditional refrigerants

6. Propose a CTES system to be used with plate freezers and evaluate its benefits on key performance indicators of the freezing systems
7. Describe control system for use in R744 systems

## 1.4 Approach

The numerical freezing model is to be developed in MATLAB, as the author's preferred programming language.

The low pressure receiver temperature must be modeled, as early calculations reveals dynamic conditions which influences the freezing temperature.

The freezing model will be verified by experiments performed on industrial R744 plate freezer. A water based gel will be used as test material, due to cost and simple probing setup. The gel block is expected to have similar thermodynamic properties as water, including phase change, without the water circulating in the freezing stations, and a lot of nucleation sites. Measurements on thermal conductivity, by TPS HotDisk method, will be performed to ensure correct model input. Validation of the pressure receiver model will be done by comparing with data from land based freezing facility.

Experimentally comparing COP for different system, using different refrigerant is not an easy task. The systems would need to have more measuring equipment than what is normal for industrial systems. Also, freezing systems often include separate freezing rooms which further complicates the comparison. Therefore, a theoretical Excel model will be used to compare different systems with the same load, using selected natural refrigerants.

The CTES system will be described, using information on similar systems. Calculations will be done numerically.

Description of control systems will be done by a literature survey on similar systems, and information from industry partners.

# Chapter 2 Theory

## 2.1 Food freezing

Freezing is a widely used conservation method. In fact, International Institute of Refrigeration, IIR, estimates the total amount of refrigeration equipment, air-conditioning units and heat pump units to be over 3 billion worldwide in 2015. Nearly 12 million employees work in the refrigeration industry, and refrigeration alone contribute for about 17% of the worlds electricity need [30].

Freezing slows the process of food deterioration and have an image of preserving freshness, at least more than canned or dried food. Normally one can define a product to be deep frozen when core temperature is less or equal to -18°C.

### 2.1.1 Freezing point depression

Pure water has a well known freezing point of 0°C at 1 atm. Therefore, water cannot exist in equilibrium for negative Celsius temperatures. Let us take a look at the *freezing curve*, (figure 2.1), which is illustrating the temperature of water during freezing.

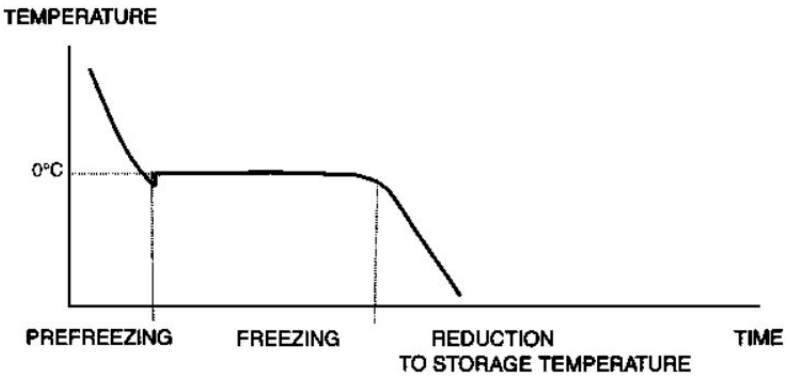


Figure 2.1: Freezing of pure water, from [34]

During prefreezing the *sensible heat* is removed, which means that the core temperature is decreased. It is not uncommon that sub-cooling occurs, which means that the temperature is below the initial freezing point. This is possible because the ice crystals have not been formed yet. When ice crystalls are formed, the temperature rapidly rise to the equilibrium temperature. Now, the *latent heat* must be removed. The latent heat is the energy required to change phase from liquid to solid, which is measured to be 333.6 $\frac{kJ}{kg}$ for water. After all the water has changed phase, the temperature drops again.

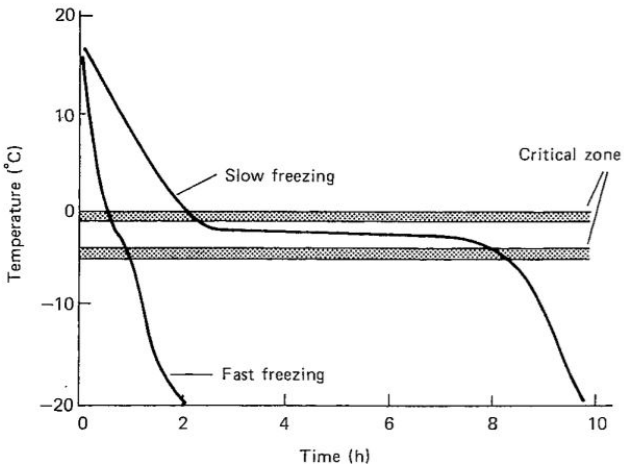


Figure 2.2: Freezing of food, from [33]

For food products, the freezing curve is quite different due to the high concentration of impurities (fat, protein, carbohydrate and ash), see Table 2.1. First of all, the initial freezing point is always lower than for water. Also, when ice formation starts, the remaining liquid water has a higher concentration of impurities, which depresses the freezing point even further. This is continued while the water undergoes freezing and therefore freezing occurs over a wide temperature range, creating a slightly declined freezing plateau. Notice from Figure 2.3 that over 65 % of the ice is formed before core temperature has reached -5°C, which is in the area called the *critical zone*.

### 2.1.2 Change in thermal properties of food product

Unprocessed food generally have a high water content, typically around 60-90% [39]. The rest is distributed to lipides (fat), proteins, carbohydrates and ash. Ash can be seen as what is left after burning the food, typically salts and other minerals. Table 2.1, below, shows composition of selected fish species.

Table 2.1: Composition of selected fish, extracted from [39]

| | Moisture content | Protein | Fat | Carbohydrates | | Ash |
|---|---|---|---|---|---|---|
| | % | % | % | Total % | Fiber % | % |
| Food item | $x_{wo}$ | $x_p$ | $x_f$ | $x_c$ | $x_{fb}$ | $x_a$ |
| Herring | 59.70 | 24.58 | 12.37 | 0.00 | 0.00 | 1.84 |
| Salmon | 76.35 | 19.94 | 3.45 | 0.00 | 0.00 | 1.22 |
| Cod | 81.22 | 17.81 | 0.67 | 0.00 | 0.00 | 1.16 |
| Mackerel, Atlantic | 63.55 | 18.16 | 13.89 | 0.00 | 0.00 | 1.35 |

The different components have different thermal properties, and they are slightly dependent on temperature. Although for practical purposes the thermal properties can be considered to be constant for values above the initial freezing point. When the food product reaches temperatures below initial freezing temperature, ice formation occurs, and the thermal properties

change dramatically. This can be explained by ice being a structured crystalline, and for example have a higher thermal conductivity [16]. In food, or generally substances with high concentration of impurities, ice formation is gradually formed over a wide temperature range, not for a single temperature, as described in Chapter 2.1.1. For cod, thermal properties are illustrated in the figure below.

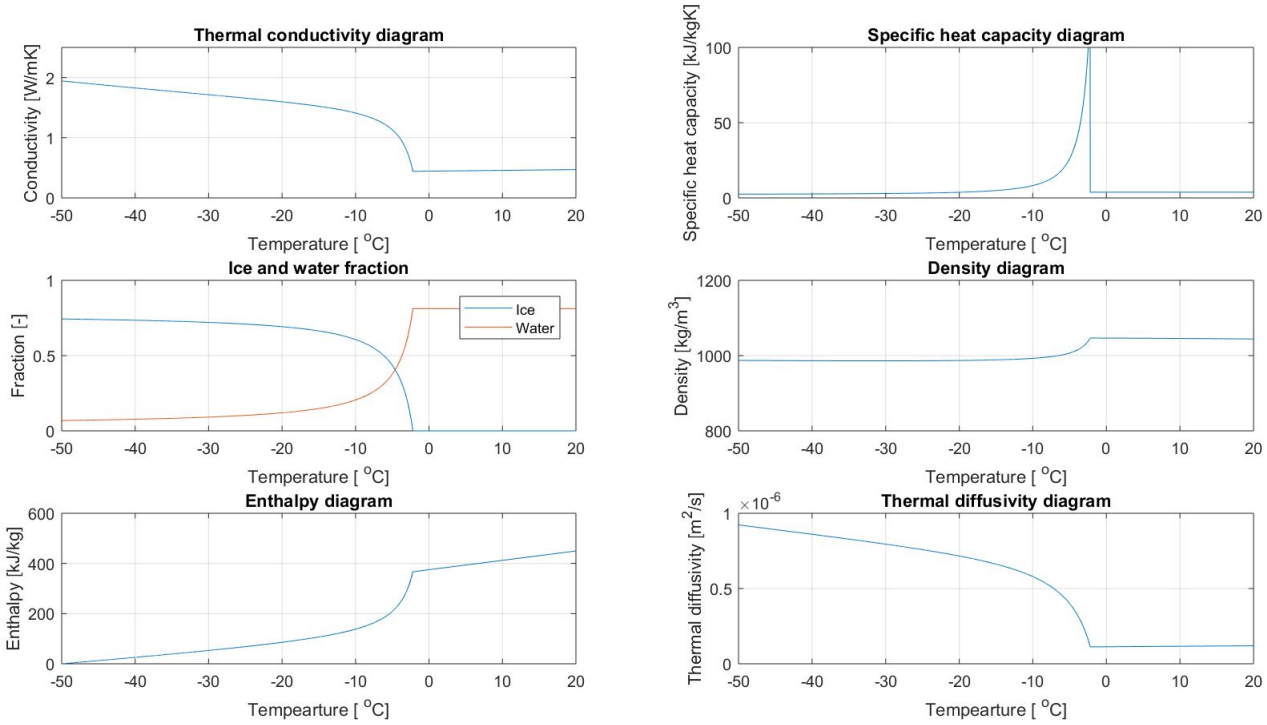


Figure 2.3: Calculated thermal properties for cod, using equations from [39]

Let us investigate further, how certain thermodynamical properties are affected by temperature and composition:

### Ice and bound water fraction

While not being a thermal property, ice fraction still has a great influence on thermal properties, and is therefore described in this section.

As described in chapter 2.1.1, after the first ice crystalls has been formed, the remaining liquid water has a higher concentration of impurities, decreasing the freezing point. Ice is therefore formed over a wide temperature range. However, there will always be some liquid water present due to the increased impurity concentration. This is called the *bound water fraction*, or the

unfrozen water fraction, $x_b$. A simple way to approximate the bound water fraction is

$$x_b = 0.4 x_p \tag{2.1}$$

Where $x_p$ is the mass fraction of protein in the food. To calculate the ice fraction, the following method from ASHRAE [39] is used.

$$x_{\text{ice}} = \frac{x_s \cdot R \cdot T_0^2 \cdot (t_f - t)}{M_s \cdot L_0 \cdot t_f} \tag{2.2}$$

where:
$x_s$ = mass fraction of solids in food
$M_s$ = relative molecular mass of soluble solids, kg/kmol
$R$ = universal gas constant = 8.314 kJ/(kg mol·K)
$T_0$ = freezing point of water = 273.2 K
$L_0$ = latent heat of fusion of water at 273.2 K = 333.6 kJ/kg
$t_f$ = initial freezing point of food, °C
$t$ = food temperature, °C
and

$$M_s = \frac{x_s \cdot R \cdot T_0^2}{-(x_{\text{wo}} - x_b) L_0 \cdot t_f} \tag{2.3}$$

where:
$x_{\text{wo}}$ = initial water fraction before freezing

Inserting equation 2.3 into equation 2.2 yields

$$x_{\text{ice}} = (x_{\text{wo}} - x_b) \cdot (1 - \frac{t_f}{t}) \tag{2.4}$$

Notice in figure 2.3 that ice fraction never reaches the value of initial water fraction due to the bound water.

### Density

Density [kg/m$^3$] can be calculated as the inverse of the weighted sum of the individual densities for the components present, described in [27].

$$\frac{1}{\rho} = \sum_i \frac{x_i}{\rho_i} \tag{2.5}$$

The main contribution to the density change around the freezing point, visualized in figure 2.3 is of course the change in water density. Ice have approximately 9% higher volume (at 0°C), and ice fraction is gradually increasing as the freezing temperature is depressed. A common mistake is to think that also food will expand by 9%, but this is not true for two reasons

- **The mass fraction** of water in food is not 1
- **The structure** of the food usually allows for the expanding ice to form in voids between cells and tissue. For example the relative volume increase in strawberries ($x_{wo}$ = 91.57) is only around 3%, while coarsely grounded, having lost its original structure, strawberries increases by 8.2%

### Thermal Conductivity

Thermal conductivity [W/mK], is a measure of how the material is conducting heat. It is in theory dependent on composition, phase, temperature and structure arrangement. For example, thermal conductivity *across* fibres is lower than *along* fibres. Since this will be hard to calculate in real freezing application, the structure arrangement is disregarded in this thesis. The food composition, the phase and the temperature will be the dependent variable. The calculation is done in a similar fashion as for density, using reciprocal sum of the individual volume fractioned conductivities:

$$k = \frac{1}{\sum_i \frac{x_i^v}{k_i}} \tag{2.6}$$

Where $x^v_i$ indicates the volume fraction of component i

$$x_i^v = \frac{x_i/\rho_i}{\sum \frac{x}{k}} \tag{2.7}$$

As mentioned before, the crystalline structure of ice results in higher thermal conductivity for frozen food. After the initial freezing point, the conductivity sharply increases as ice develops.

For porous media, which will later be used to model fish block with air voids, thermal conductivity will be lower than in a continuous phase. Eucken's adaption of Maxwell's equation (Eucken 1940) can be used to find an altered conductivity of fish/air mixture.

$$k = k_c \frac{1 - [1 - a(k_d/k_a)]b}{1 + (a-1)b} \tag{2.8}$$

where:
$k$ = thermal conductivity of porous material

$k_c$ = thermal conductivity of continuous material
$k_a$ = thermal conductivity of air
$a = 3k_c/(2k_c + k_a)$
$b$ = volumetric void fraction $(V_a/(V_a + V_c))$

### Specific heat capacity

Specific heat capacity is the energy required to change the temperature by one degree, resulting in the unit [J/kgK]. The heat capacity is rather constant for unfrozen food around normal storage temperatures. Below initial freezing point however, the energy required to change the temperature is much higher because of the latent heat of fusion. Also, the heat capacity is strongly dependent by temperature below freezing because the amount of water to be frozen changes considerably as the freezing point is depressed. When the latent heat of fusion is considered in specific heat capacity, it is normally refereed to as *apparent heat capacity*.

To calculate the apparent heat capacity, the method by Schwartsberg (1976) [47] was used

$$c_a = c_u + (x_b - x_{wo})\Delta c + \frac{M_w}{M_s} \cdot x_s \left( \frac{R \cdot T_0^2}{M_w \cdot t^2} - 0.8\Delta c \right) \tag{2.9}$$

where:
$c_a$ = apparent specific heat capacity, kJ/(kg·K)
$c_u$ =specific heat capacity of food above initial freezing point
$\Delta c$ = difference between specific heat capacity of water and ice, at 0°C
$M_w$ = molecular mass of water
$c_u$ is calculated using weighted sum for the individual components present.

### Enthalpy

In food engineering, the change in enthalpy for the product during freezing can be seen as energy that must be removed by freezer. This is clear from the unit [J/kg]. Specific heat capacity, $c_p$ for constant pressure, is defined

$$c_p = \left( \frac{\partial H}{\partial T} \right)_p \tag{2.10}$$

By integrating from a reference temperature, $T_r$, to an arbitrary temperature t, defining enthalpy to be zero at the lowest temperature, one can define an expression for enthalpy

$$H = c_a \partial T = \int_{T_r}^{t} c_a dT = (t - T_r) \cdot \left[ c_u + (x_b - x_{\text{wo}})\Delta c + \frac{M_w}{M_s} x_s \left( \frac{RT_0^2}{M_w (T_0 - T_r)(T_0 - t)} - 0.8\Delta c \right) \right] \tag{2.11}$$

where, once again:
$t$ = Temperature of food, K
$T_0$ = Freezing temperature of water = 273.2 K
$T_\text{r}$ = Reference temperature for zero enthalpy, K
$M_\text{s}$ = Relative molecular mass of soluble solids, kg/kmol
$M_\text{w}$ = Molecular weight of water, kg/kmol

Other methods of determining apparent heat capacities exists, some of them described in [47]

**Thermal diffusivity**

The most widely used parameter in numerical heat transfer models is the thermal diffusivity, $\alpha$ [$\text{m}^2/\text{s}$].

$$\alpha = \left( \frac{k}{\rho c_p} \right) \tag{2.12}$$

Thermal diffusivity is a measure of change in temperature with respect to time per change in temperature with respect to space, in other words, how fast an impulse (sharp increase in temperature) is propagated through the material. It is often used in the thermal energy diffusion equation:

$$\frac{\partial T}{\partial t} = \alpha \nabla^2 T \tag{2.13}$$

In equation 2.12, the apparent heat capacity $c_\text{a}$ should be used when the product undergoes phase change. This results in a low thermal diffusivity at initial freezing point, and the immediate temperatures below, due to the sharp increase in apparent heat capacity. As a result, the food temperature barely respond to a temperature gradient, around the initial freezing point, crating the freezing plateau.

### 2.1.3 Ice formation

It has already been explained how impurities are the reason why ice formation occurs over a temperature range, and not for a single temperature like in water. But how are ice crystals formed?

Before ice crystals starts to form, water starts to *nucleate*. Nucleation precedes ice crystal formation because it can be seen as the first step to solidification . There are two forms of nucleation [22] :

- **heterogeneous nucleation** happens on a surface of suspended particles, impurities, cell walls, or other surfaces. This is the fastest and most common type.
- **homogeneous nucleation** happens without presence of the surfaces mentioned above.

High rates of heat transfer has a tendency to create many small nuclei, while slow heat transfer tends to create fewer, but larger nuclei. This can be explained by the energy required to form new nuclei is larger than for water molecules to attach to existing nuclei. However, large differences in ice crystals are found in different food with same heat transfer [22], making prediction complex.

Most ice crystals are formed in the *critical zone*, see figure 2.2. Therefore the time required to pass the critical zone determines the size and number of ice crystals in the food product. The rate of mass transfer, water migrating towards ice crystals and solutes moving away, does not control the rate of crystal growth except for the end of the freezing process [22].

### 2.1.4 Fast vs slow freezing

Faster freezing may result in notable better food quality. This can be explained by how the formation of ice crystalls works. From figure 2.4 a), one can observe that for slow freezing, the ice crystal formation starts on the cell surface, and is growing in intercellular spaces. The ice crystal develops and destroys the surrounding cells. For fast freezing however, illustrated in 2.4 b), smaller and greater number of ice crystals form more uniformly, both inside and outside of the cells. These ice crystalls will not have the same damaging effect.

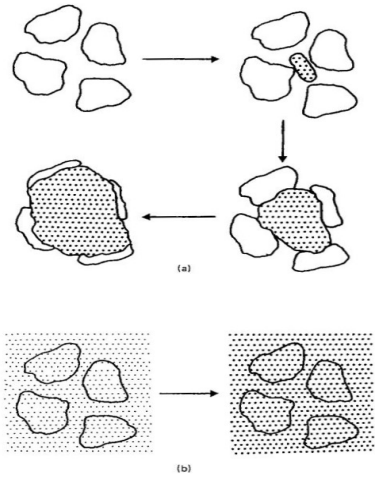


Figure 2.4: Freezing of plant tissues for slow freezing (a), and fast freezing (b) [36]

### 2.1.5 Food freezing impact

As seen in figure 2.4, plant tissue can be very sensitive to freezing time. Animal tissue has less rigid cell structure, therefore fibre structures tend to separate instead of braking, resulting in less damage. There are negligible change in taste, nutrition and colour during the freezing itself, however, these effects may come from later storage and thawing [22]. A main contributor to loss in food quality is the *drip loss*. During slow freezing, ice crystals tend to form outside cells, resulting in a water gradient. Water migrate out from the cells to the ice crystal surface, dehydrating the cells. During thawing, the water does not migrate back to the damaged cells, but drips out of the product and into the packaging [22]. This is easily seen from any thawed product taken out from a normal freezer. If the drip loss is not consumed, water soluble vitamins may be lost. Drip loss is less significant if the freezing time in the critical zone is reduced.

### 2.1.6 Product heat load

Heat load can be defined as energy absorbed to the food product during freezing, not to be confused with freezing- or compressor capacity. Compressor capacity is how much energy is removed from the evaporator by the compressor, while heat load is how much energy is absorbed by the product. Larger heat load than compressor capacity results in a increased evaporating pressure and vice versa. The heat load vary during the freezing process, peaking at the very beginning. The high peak at the onset of freezing can be explained by the large temperature difference in food/heat transfer surface and the rapid ice formation at the start. Heat load is an important parameter as it sets design conditions for the main components, like compressor and pressure receiver. Typical heat load for food product is illustrated in figure 2.5.

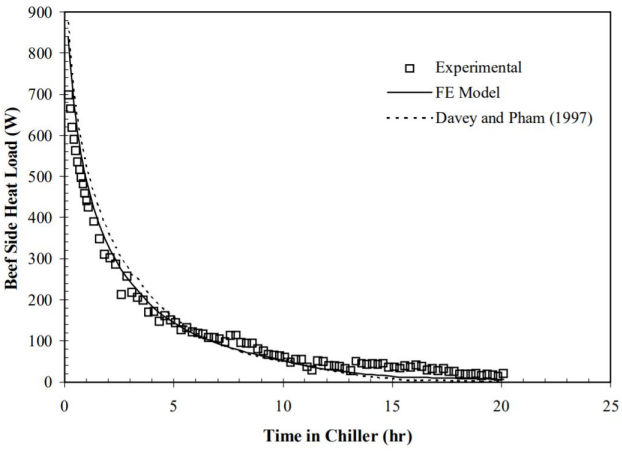


Figure 2.5: Typical heat load curve for food freezing in freezing tunnel, from [40]

Compressors are not designed to cover the peak load, which would lead to over dimensioning of the compressor and part-load performance during most of the process. In stead, one acknowledge the under performance of the compressor at the start of the freezing process, leading to increased pressure in pressure receiver, or early dry evaporation in evaporator if direct expansion is used. Both lead to increased temperature in evaporator and longer freezing times.

## 2.2 Freezing time calculation

Freezing time calculations are critical when designing new freezing systems. The most used definition of freezing time is the time required to change the temperature from an initial value to a desired freezing temperature in the slowest cooling location, usually in the geometrical center or where the product is thickest [27]. An alternative definition would be to change the temperature from a initial value to a temperature where the mass average enthalpy equals the desired enthalpy for an evenly distributed temperature. This definition of freezing time is somewhat shorter and might increase product capacity and lower energy use.

### 2.2.1 Analytical methods

The easiest, most frequently used methods for determining freezing times are the analytical methods. One of the most popular equations to use is the plank equation, which includes latent heat and some of the sensible heat to be removed. The initial condition is that the product starts *on* the freezing point [25].

Consider an infinite slab, initially at its freezing point. The slab is being frozen from both sides, creating two ice fronts moving to the center, see figure 2.6

The overall heat transfer coefficient can be defined as:

$$\frac{1}{U} = \frac{1}{h_a} + \sum_i \frac{\delta_i}{k_i} + \frac{x}{k_f} \tag{2.14}$$

where:
$U$ = The overall heat transfer coefficient [W/m$^2$K]
$h_a$ = convective heat transfer coefficient at border [W/m$^2$K]
$\delta_i$ =thickness of packaging material [m]
$k_i$ = thermal conductivity of packaging material [W/mK]
$x$ = thickness of ice front [m]
$k_f$ = thermal conductivity for ice[W/mK]

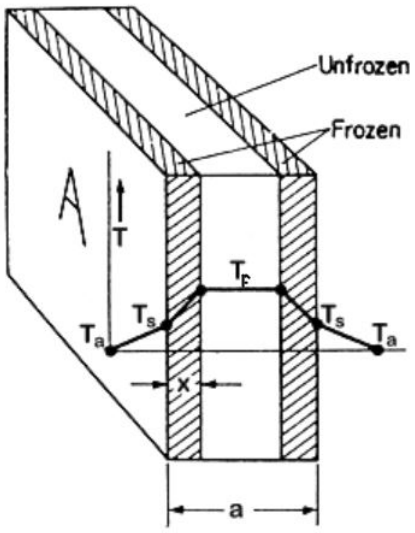


Figure 2.6: Infinite slab to be frozen, after a certain amount of time in freezer [20]

To increase the frozen layer thickness, the heat to be removed is described by:

$$dQ = L \cdot \rho \cdot A \cdot dx \tag{2.15}$$

where:
dQ = Heat to be removed [J]
L = Latent heat of fusion for chosen product [kJ/kg] ($L=L_{water}{}^{*}x_{wo}$)
$\rho$ =density of frozen product [kg/m$^3$]
A = Contact area of slab [m$^2$]
dx= infinitesimal increase of ice front [m]

Heat transported through the product can be defined as

$$dQ = U \cdot A \cdot \Delta T \cdot d\tau \tag{2.16}$$

where:
$\Delta T = (T_f - T_a)$
d$\tau$ = infinitesimal time

Inserting equation 2.15 into equation 2.16, solving for time reveals:

$$d\tau = \frac{L\rho dx}{U\Delta T} \tag{2.17}$$

Inserting equation for U, disregarding any packaging and integrating from surface to center b=a/2, yields en expression for the analytical freezing time.

$$\int_0^{\tau_f} d\tau = \int_0^b \frac{L\rho}{\Delta T}\left(\frac{1}{h_a} + \frac{x}{k_f}\right) \cdot dx \tag{2.18}$$

$$\tau_f = \frac{L\rho}{\Delta T}\left(\frac{1}{h_a} + \frac{b}{2k_f}\right) \cdot b \tag{2.19}$$

A more general formula, which is valid for multiple shapes can be defined:

$$\tau_f = \frac{L\rho}{\Delta T}\left(\frac{Pa}{h_a} + \frac{Ra^2}{k_f}\right) \tag{2.20}$$

Here, P and R are shape factors, found in Table 2.2

One must remember that Plank´s equation defines freezing time as time for ice front to reach the center. With other words, there is no temperature drop in the center of the product, only phase change. Also, one must assume constant thermal properties.

| Shape | **P** | **R** |
|---|---|---|
| Infinite Slab | 0.500 | 0.125 |
| Infinite Cylinder | 0.240 | 0.053 |
| Sphere | 0.167 | 0.042 |

Table 2.2: Shape factors in Plank´s equation

There are modified Plank´s equations, by among others Nagoaka et. al. (1955) [38] and Cleland and Earle (1977)[11]. These take into consideration sensible heat above and below freezing along with more complex geometry.

### 2.2.2 Numerical methods

Numerical methods are far superior compared to analytical methods regarding accuracy, due to the possibility of implementing temperature dependent thermal properties, complex shapes and dynamic boundary conditions (for example change in plate temperature in a plate freezer, or changing air velocity or temperature in blast freezer). They are, however, far more time consuming, both in computation and implementation [27]. A detailed description of the numerical freezing model used in this thesis can be found in chapter 3.1.

## 2.3 Heat pump technology

Heat pump technology can be used both for heating and cooling, sometimes at the same time. The four critical components are compressor, condenser, expansion device and evaporator. The four components, in that order and together with a circulating media, constitutes a simple 1-stage heat pump.

Evaporation takes place in the evaporator, which requires thermal energy. This energy is extracted from whatever is in physical contact with the evaporator, which may be air, water, other refrigerant or more relevant to this thesis: food product. After the refrigerant has evaporated, it is drawn into the compressor, which maintains the low evaporation pressure, and compress the refrigerant to

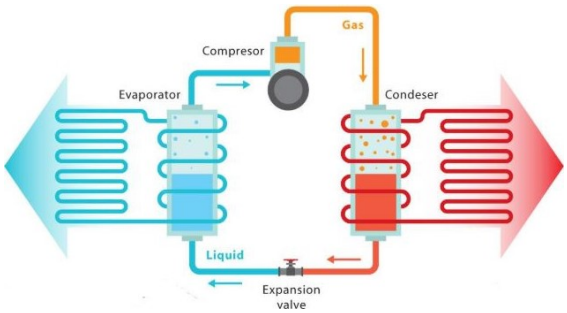


Figure 2.7: Simple heat pump, from Vecteezy.com

match the pressure in the condenser.The refrigerant is condensed, which releases energy. Heat is delivered to whatever is in physical contact with the condenser, which is usually air or water. To be able to evaporate the refrigerant in the lower temperature evaporator, the pressure has to be decreased. The simplest way is to use an expansion device.

More complex heat pump systems include multistage compression with intermediate cooling, internal heat exchangers, ejectors and intermediate pressure receivers for better efficiency and more advanced requirements.

### 2.3.1 R744 as refrigerant

Before 1930 $CO_2$ and ammonia were the most widespread refrigerant. Natural refrigerants virtually seized to exists after the invention of the far superior synthetical refrigerants like Chlorofluorocarbon refrigerants. CFC refrigerants was used up to 1980's, until scientist discovered the damage related to the ozone (ODP). This led to the replacement of CFC to HFC, like R134-a and R22. These synthetic refrigerants have no or low ODP values. Still, they have a Global Warming Potential (GWP) of several thousand. Due to regulations [15], the phase out of HFC has already started and the demand for natural refrigerants has made the use of $CO_2$ and $NH_3$ widespread again.

#### Thermodynamic properties

R744 has many good qualities as a refrigerant. Firstly, it is non flammable and non toxic, which is important in for example offshore applications. High operating pressures has for a long time made R744 challenging to implement due to requirements of special made components, demanding higher safety classifications. However, the high operating pressure gives R744 an advantage in low temperature applications. Many refrigerants, including the popular R717 (Ammonia), R134-a and R22, is limited to evaporating temperatures around -35°C due to sub atmospheric evaporating pressures. This has made R744 popular for bottom cycle cascade systems, as it can be evaporated down to around -50°C.

The high system pressure has other unique qualities. For example, R744 has high specific volumetric capacity, resulting in smaller compressors and thinner piping. High operating pressure also gives rise to steeper saturation pressure curve. This results in lower saturation temperature difference from pressure loss ($\Delta T_{sat}/\Delta P$). This gives a significant advantage related to system efficiency [26].

In the liquid phase, R744 has relative low viscosity, resulting in less pumping power for systems with large piping (supermarkets). Together with low surface tension, R744 has excellent heat

transfer properties, especially in the nucleate boiling regime.

Theoretically, R744 is not the most efficient refrigerant, due to the low critical temperature (31.1 °C) and the high expansion loss that follows, for condensing around the critical temperature.

However, if losses related to condenser/evaporator temperature difference, compressor efficiency and system pressure loss are included, R744 is comparable and for some applications even more efficient than other refrigerants [24].

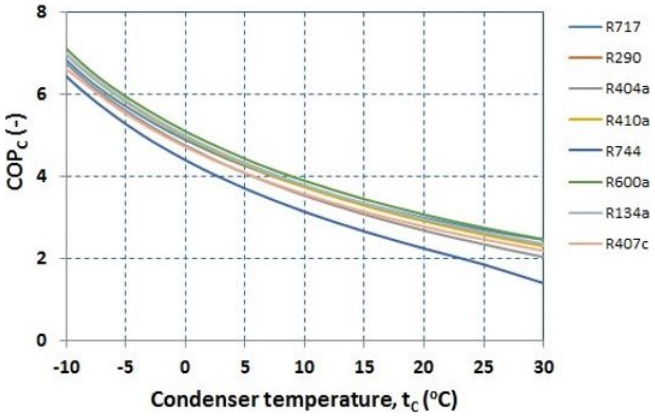


Figure 2.8: Theoretical COP for different refrigerants ($T_0$=-40 °C) [26]

### 2.3.2 Plate freezers

Plate freezers are only one of many industrial freezers. More detailed description of other freezers can be found in for example [51]. There are two versions of plate freezers, which refers to the orientation of the plates, **horizontal** and **vertical**. Common for both is that the refrigerant is evaporated in channels inside the plates.

In horizontal plate freezers, food is placed in between plates. Hydraulic press makes sure of good contact between product and plates. Flat and evenly shaped products, like hamburgers, fish filet or packaged food, are best suited.

Vertical plate freezers are often used for more irregular shaped products, like whole fish. The products are poured into sections, created by the vertical plates, resulting in frozen blocks with multiple products in one block. Block size are usually in the size order of 550x550x100mm.

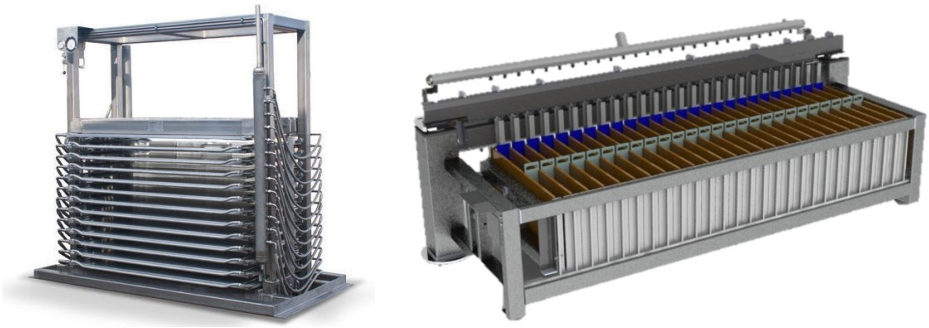

Figure 2.9: Horizontal and vertical plate freezer, from [7]

Plate freezers are popular where space is limited, like offshore. They have relatively high product capacity, where 1250 kg fish may be frozen in less than 3 hours for a single freezer. High heat transfer coefficients ensure fast freezing rates, compared to other methods (see Table 2.3). After freezing, a quick defrost, for example using hot gas, is performed before the frozen blocks are lifted up from the freezer using a hydraulic system at the bottom.

Table 2.3: Typical heat transfer coefficients for various freezers

| Method of freezing | Typical heat transfer coefficients [W/m$^2$K] |
|---|---|
| Still air | 6-9 |
| Blast freezer (5 m/s) | 25-30 |
| Blast freezer (3 m/s) | 18 |
| Spiral Belt | 25 |
| Fluidized bed | 90-140 |
| Plate freezer, good contact | 200-500 |
| Plate freezer, poor contact | 50-100 |
| Immersion (freon) | 500 |
| Cryogenic Freezers ($N_2$) | 1500 |

### 2.3.3 Evaporators and pressure drop

In freezing applications, the purpose of an evaporator is to remove heat from the food product to the refrigerant. Most of the heat removed comes from phase change, evaporation, of the refrigerant. The rest comes from temperature change of refrigerant gas, if there is superheating inside the evaporator. Evaporators can either be based on convection/conduction or nucleate boiling. As mentioned before, CO2 has relatively low surface tension, so it will easily start to nucleate, making nucleation the predominant heat transfer mechanism. Ammonia, on the other hand, will largely be governed by convection [26]. Different flow boiling regimes is a complex, not fully understood subject, mainly governed by empirical equations [50].

Evaporators can be divided into two types:

- **DX**, direct expansion evaporators
- **Flooded**, or wet evaporators

In direct expansion evaporators, an expansion device is mounted at the inlet of the evaporator. The refrigerant is usually expanded down in the two phase area, with a vapour fraction of around 0.1-0.3, depending on the system. DX-evaporators usually operates with superheating of the refrigerant, meaning that vapor fraction is increased to 1, and from that point and downstream the vapor is superheated to ensure that only vapor enters the compressor.

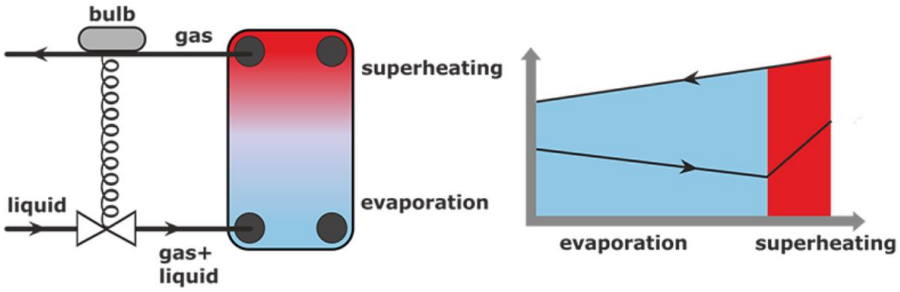


Figure 2.10: Direct expansion evaporator [50]

In flooded evaporators, the evaporator is operating in conjugation with a low pressure receiver, functioning as a separator, see figure 2.11. Saturated liquid leaves the separator, and subcooled liquid enters the evaporator, due to pressure increase from height difference. Refrigerant with vapor fraction between 0.2 and 0.8 exits the evaporator, and is transported back to the pressure receiver. The flooded evaporator ensures good heat transfer as nucleate boiling is the main flow boiling regime, resulting in large heat transfer rates.

It is common to use the term *circulation rate*, defined as the inverse of the vapour fraction at the freezer exit. A circulation number of 3 means that, theoretically, the refrigerant must circulate the evaporator three times on order to evaporate completely.

Forced flow evaporators use pumps or ejectors to bring flow trough the evaporator. However, thermophison evaporators is circulated without the use of electrical powered pumps, or ejectors. The refrigerant is instead density driven. The lower density of the evaporated gas, allows more liquid to enter the evaporator. No regulation is required from the expansion device, as the flow is self-regulating [50].

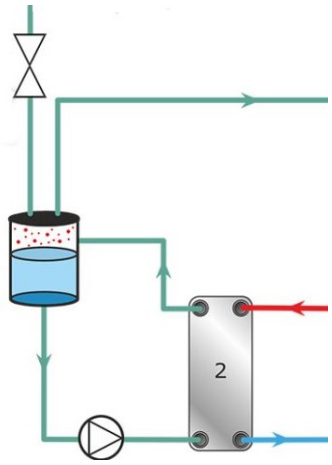


Figure 2.11: Flooded evaporator [50]

**Pressure loss in evaporator**

Pressure loss along the evaporating tubes results in a lowered evaporating temperature. Pressure loss can be divided into four main contributors

- Acceleration loss, $\Delta P_a$
- Friction, $\Delta P_f$
- Height difference, $\Delta P_z$

A method for calculating evaporator pressure loss is described in [46]. They use a mixture density for two phase flow calculated by:

$$\rho_m = (1-\epsilon)\rho_L + \epsilon\rho_G \tag{2.21}$$

where

$$\epsilon = \left[1 + \left(\frac{1-x}{x}\right)\left(\frac{\rho_G}{\rho_L}\right)\left(\frac{\mu_L}{\mu_G}\right)\right]^{-1} \tag{2.22}$$

Here, x is the vapour fraction. The pressure loss contributions is calculated by following equations:

$$\Delta P_a = G^2\left(\frac{1}{\rho_{m,out}} - \frac{1}{\rho_{m,in}}\right) \tag{2.23}$$

$$\Delta P_f = \frac{2fG^2L}{D_h\rho_m}\left[1 + \frac{x\rho_L}{2\rho_G}\right] \tag{2.24}$$

$$\Delta P_g = (\rho_m g z)_i - (\rho_m g z)_o \tag{2.25}$$

$$\Delta P_{tot} = \Delta P_a + \Delta P_f + \Delta P_g \tag{2.26}$$

Here, G is the mass flux $[\frac{kg}{sm^2}]$, f is the darcy friction factor, L is the tube length, $D_h$ is the hydraulig diameter and z is the height.

## 2.4 Thermal energy storage

Thermal energy storage is used when there is a mismatch between supply and demand of energy, or to be able to cover peak loads without over-dimensioning the system. It is often being used in conjunction with solar power, where energy is stored by warming up water or other substances. It is also frequently used in the HVAC industry, where large buildings consume a lot of energy for heating and cooling. When electricity prices vary considerably during the day, it could be beneficial to store the energy in applicable medias at night, when electricity prices are low, and use that energy when it is needed during the day. Some buildings manage to store all the necessary cooling during the night, in order for no "expensive" electricity to be used for cooling during the day [17].

Design of thermal energy storage tanks can be done in many ways, which will not be discussed in this thesis. However, it is customary to use a phase change material, PCM, as the energy absorbent when space is limited because the latent energy will results in a high energy density for the tank [4]. Because of generally low conductivity of most PCMs, heat transfer enhancements methods should be implemented [52]. This can be done by implementing shell and tube heat

exchangers as the storage tank. Esen et al. (1997) [21], did a theoretical analysis on different models altering various parameters, including mass flow, tank volume, pipe radii, PCMs, and temperature levels, and suggested to have the PCM at the shell side and refrigerant at the tube side for optimal heat transfer rate.

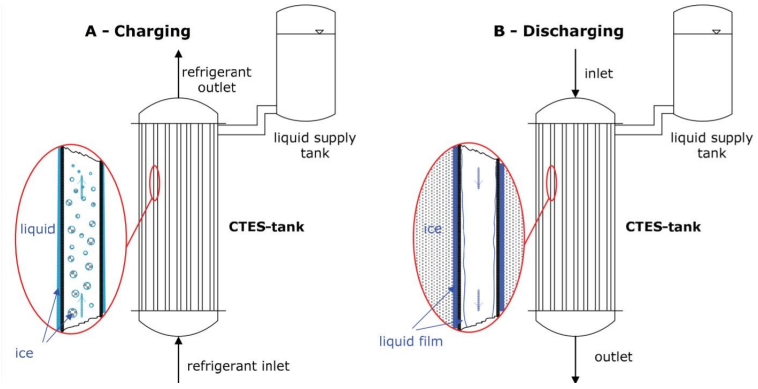


Figure 2.12: Illustration of storage tank during charge and discharge [6]

A CTES solution has two modes: *charge* and *discharge*, see figure 2.12. During charging of the tank, PCM is solidifying and storing energy. Colder refrigerant is evaporated inside the tubes in the tank, and s solid layer will start to form at the outside of the tubes. During discharge, the PCM releases the stored energy by melting against the hotter refrigerant in the tubes.

### Solid PCM formation

As mentioned in chapter 1.2, shell and tube heat exchangers with PCM is the most frequently used set-up for a TES system. In charge mode, solid PCM will start to form at the outside of the evaporating tubes, and grow until the cycle is finished, see figure 2.13.

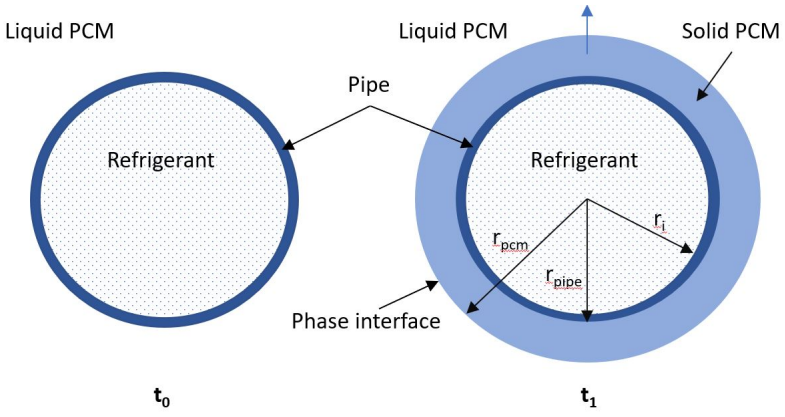


Figure 2.13: Illustration how solid PCM grows as refrigerant evaporates in tubes, at time instances $t_0$ and $t_1$

It can be desirable to estimate the growth rate of solid PCM on tubes. One must then conduct a energy balance from pipe center to interface between solid/liquid PCM.

$$Q = (U \cdot A)\Delta T = \frac{\Delta H \Delta m}{\Delta t} \tag{2.27}$$

where:
$Q$ is heat, W
$UA$ product is the overall heat transfer coefficient, W/K
$\Delta T$ is the temperature difference from tube center to phase interface, K
$\Delta H$ is heat of fusion for PCM, J/kg
$\Delta m$ is the added mass of solid PCM for each time step, kg
$\Delta t$ is the time step, s

Rearranging equation 2.27, yields the increased mass of solid PCM for a given time step.

$$\Delta m = \frac{\Delta t (U \cdot A)\Delta T}{\Delta H} \tag{2.28}$$

### 2.4.1 R744 as PCM

When storing energy for temperatures down to -50°C, there is a limited selection of PCMs. A natural choice would be to use $CO_2$, which have high heat of fusion (340 kJ/kg) and relative high thermal conductivity (0.35 W/mK) compared to other PCMs [48]. $CO_2$ will sublimate or evaporate on pressure and temperature levels illustrated in figure 2.14.

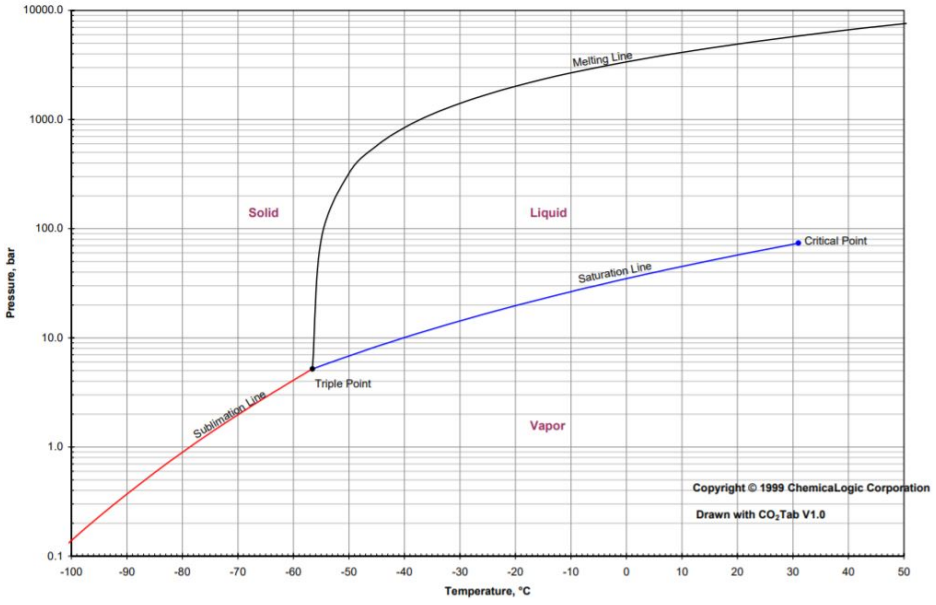


Figure 2.14: Temperature-Pressure diagram for $CO_2$, from [9]

# Chapter 3 Method

## 3.1 Numerical freezing model description

A numerical freezing model was developed to predict freezing time for fish in plate freezers. The chosen method in this thesis was to solve the two-dimensional heat diffusion equation using finite difference:

$$\rho(T)c_a(T)\frac{\partial T}{\partial t} = \nabla(k(T)\nabla T) \tag{3.1}$$

and can be rewritten to

$$\frac{\partial T}{\partial t} = \frac{1}{\rho(T)c_a(T)}\left(\frac{\partial k(T)\frac{\partial T}{\partial x}}{\partial x} + \frac{\partial k(T)\frac{\partial T}{\partial y}}{\partial y}\right) \tag{3.2}$$

Applying the implicit FTCS scheme [2] and evaluating thermal properties at the central node (i,j), the discretization formulates accordingly:

$$\frac{T_{i,j}^{n+1} - T_{i,j}^{n}}{\Delta t} = \alpha_{i,j}(T)\left(\frac{T_{i-1,j}^{n+1} - 2T_{i,j}^{n+1} + T_{i+1,j}^{n+1}}{\Delta x^2} + \frac{T_{i,j-1}^{n+1} - 2T_{i,j}^{n+1} + T_{i,j+1}^{n+1}}{\Delta y^2}\right) \tag{3.3}$$

where $\alpha$ is the thermal diffusivity $\alpha(T) = k(T)/\rho(T)c_a(T)$, $\Delta t$ is the chosen time step and $\Delta x$ and $\Delta y$ are the chosen distance between nodal points

Note that implicit scheme means that the unknowns are one time step ahead of the known solution. This is done due to the fact that implicit schemes are *unconditionally stable* for any combination of chosen time step and grid size [2]. Further rearranging the equation yields:

$$\left(a_W T_{i-1,j}^{n+1} + a_E T_{i+1,j}^{n+1} + a_N T_{i,j+1}^{n+1} + a_S T_{i,j-1}^{n+1} + a_P T_{i,j}^{n+1}\right) = T_{i,j}^{n} \tag{3.4}$$

Where $a_N = a_S = -\frac{\alpha(T)\Delta t}{\Delta y^2}$, $a_E = a_W = -\frac{\alpha(T)\Delta t}{\Delta x^2}$, $a_P = 1 + \sum_{i=N,S,E,W} |a_i|$

At the boundaries, where the fish blocks are in contact with the plates, fixed temperature was first imposed.

$$T(i,0,t) = T(i,H,t) = T_{wall} \tag{3.5}$$

Later, realizing that plate temperature varied during freezing, time dependent boundaries were implemented. The plate temperature was assumed to be equal to the dynamic low pressure receiver temperature, explained in chapter 3.2.

At the two perpendicular walls, one can assume insulated boundary conditions

$$\frac{\partial T}{\partial x}|_{x=0,x=L} = 0 \tag{3.6}$$

The unknown temperatures can be found by solving the linear system, derived from Equation 3.4

$$A \cdot T^{n+1} = B^n \tag{3.7}$$

Where A is a *pentadiagonal* matrix, composed by diagonals of the *a* coefficients. T includes the unknown temperatures at time step n+1 and B is the known solution at the previous time step with boundary conditions included. Equation 3.7 is solved by preferred solving method, for example LU-decomposition or Gauss-Seidel iteration.

It is essential that the time discretization is small enough for a numerical cell to "feel" the jump in apparent heat capacity, see chapter 2.1.2. However, Too small time discretization might result in unnecessary time consumption. Decreasing the step size (distance between nodes) by a factor of 2, increases computation time by a factor of 4, simultaneously decreases numerical error by a factor of 4. This is easily shown by Taylor expanding equation Equation 3.1.

### 3.1.1 Air voids

Air voids in between fish and on the plate surface should ideally be modeled by boundaries inside numerical domain. However, in this thesis, density and conductivity was modified assuming porous media. This method is Eucken's adaption of Maxwell's conductivity equation (Eucken 1940) and was described by equation 2.8. Now, the porous material (equally distributed, small air pockets), could be modeled by single thermodynamic properties, for respective temperatures.

The bulk porosity, or air void fraction, was calculated by

$$\epsilon_B = 1 - \frac{\rho_B}{\rho_T} = \frac{V_a}{V_a + V_c} \tag{3.8}$$

where:
$\epsilon_B$ = bulk porosity of material
$\rho_B$ = bulk density of material, measured weight divided by measured volume of material
$\rho_T$ = Theoretical calculated density
$V_a$ = Volume of air
$V_c$ = Volume of continuous phase, fish

Fish blocks was observed to have a bulk porosity between 0.05 and 0.15.

## 3.2 Pressure receiver model description

It has been made clear that the evaporation temperature will vary, due to insufficient compressor capacity and varying heat load. Therefore, a model to estimate the dynamic low receiver temperature was made. Heat load to hold plate temperature on constant levels was first calculated by imposing constant plate temperature in model. Enthalpy in the fish was monitored and heat load was calculated. Pressure in the low pressure receiver was modeled by performing a gas mas balance, see figure 3.1.

$$\dot{m}_{1,g} = \dot{m}_{2,g} + \dot{m}_{4,g} \tag{3.9}$$

when $\dot{m}_1$ is assumed to be equal to $\dot{m}_2$, equation 3.9 yields:

$$\dot{m}_{1,g} = x\dot{m}_{1,g} + \dot{m}_{4,g} \tag{3.10}$$

mass flow can be expressed by

$$\dot{m} = \frac{\dot{V}}{v} \tag{3.11}$$

Inserting equation 3.10 into equation 3.11 yields,

$$\frac{(1-x)\dot{V}_{1,g}}{v^{n+1}} = \dot{m}_{4,g} \tag{3.12}$$

finally,

$$v^{n+1} = \frac{(1-x)\dot{V}_{1,g}}{\dot{m}^{n}_{4,g}} \tag{3.13}$$

Equation 3.13 relates the specific volume , $v$, to known properties in the tank. $\dot{V}_{1,g}$ is the volume flow through compressor, which was assumed to be constant due to fixed compressor stroke volume and assumed constant compressor delivery factor. $\dot{m}_{4,g}$ was calculated from the known heat load from fish and available evaporation energy, dependent on pressure from last iteration.

Excel and RnLib was used to calculate the specific volume by marching in time with initial values corresponding to -50°C. From the newly calculated specific volume, pressure and temperatures out from the evaporator during freezing could easily be calculated with RnLib. It was also calculated that the refrigerant at time step n+1 was mixed with the liquid with temperature and pressure corresponding to time step n, which is closer to a real system, rather than an instantaneous increase in temperature for the whole liquid receiver.

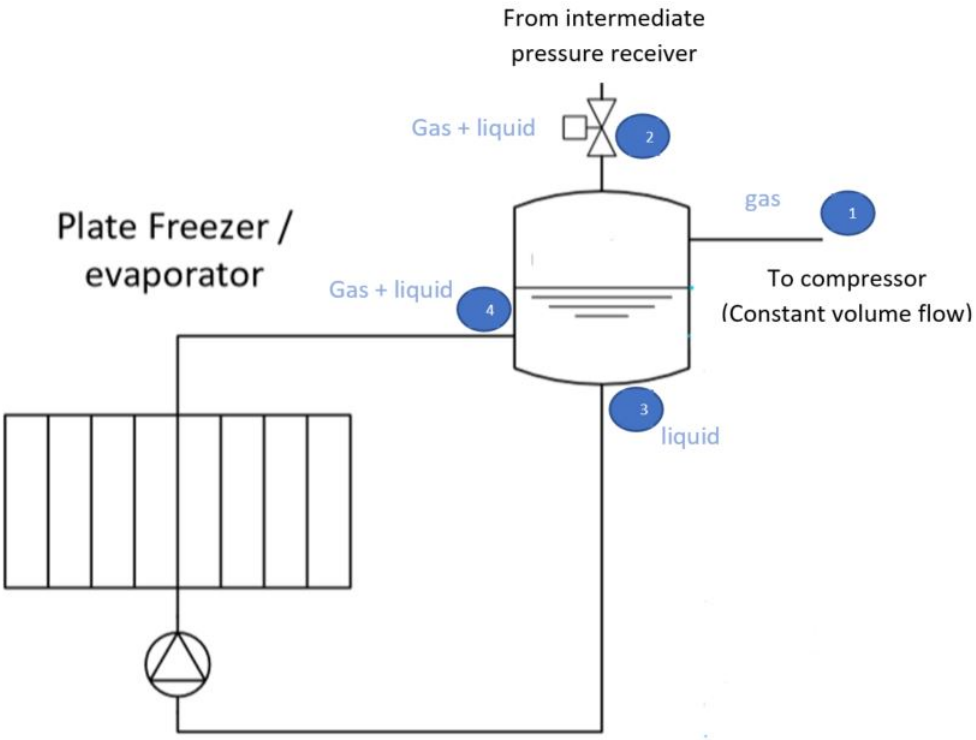


Figure 3.1: Illustration on low pressure receiver

The calculated liquid temperature was then used as boundary condition in the numerical freezing model, desribed in chapter 3.1.

## 3.3 Validation of pressure receiver- and freezing model

The pressure receiver model was validated by comparing with data from land based freezing facility, using similar plate freezers. The data was supplied by Kuldeteknisk AS.

The numerical freezing model was validated by performing experiments on a industrial plate freezer, on board MS Arnøytind. Description of the experiment is described below.

### 3.3.1 Freezing system description

The freezing system, delivered by Kuldeteknisk AS, is illustrated in figure 3.2. It was a two-stage seawater condensed system with flooded evaporator.

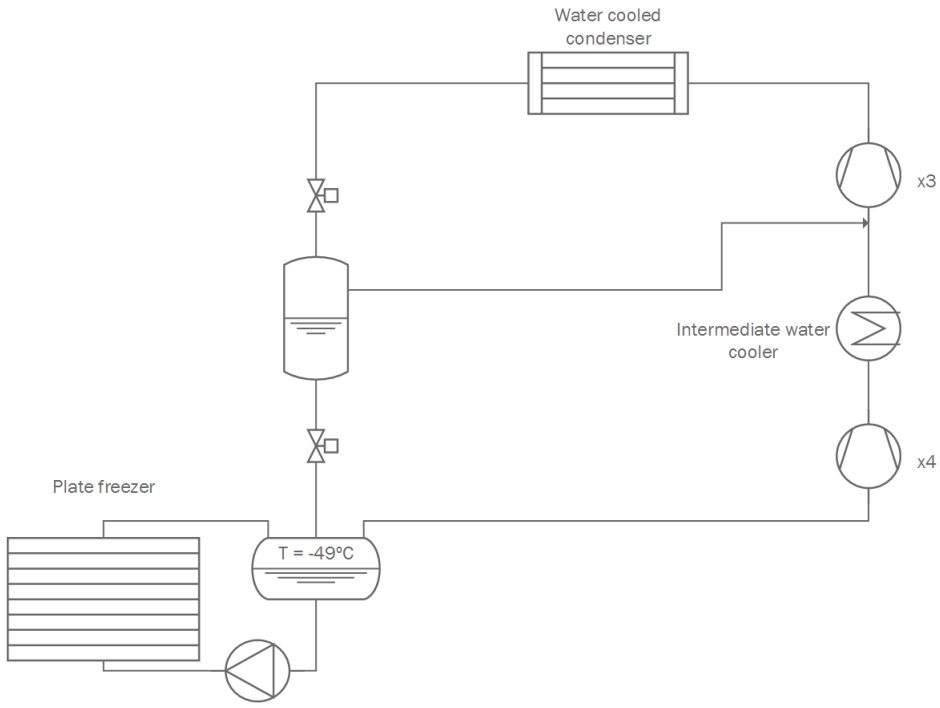


Figure 3.2: Principle solution of heat pump system on board MS Arnøytind

The evaporating temperature was held close to -50°C during the whole experiment, due to under loading of the freezer. This gave excellent conditions for constant plate temperature validations.

The plate freezers on board MS Arnøytind is three DSI V3 vertical plate freezers [18]. Each freezer have contain 48 fish blocks with a block size of 530x520x100mm, corresponding to approximately 1200 kg fish.

Figure 3.3: DSI V3 plate freezer used on board MS Arnøytind [18]

### 3.3.2 Test material

Fish is not the ideal test material considering the fish block consist of several fish, randomly structured in sections of the freezer. Therefore, the center of the fish block might be between fish (in air or frozen water) or somewhere inside a fish. Thus, measuring in the geometrical center is not an easy task and might disrupt measurements.

Water is sometimes used in freezing experiments. It is easily available, however, the water will start to circulate in the freezing section because of density change, called natural convection. Furthermore, ice formation might start under heavy sub cooling due to lack of nucleation sites. Measurement equipment in the center of the block might be a good nucleation site, which is unnatural in real applications.

For these reasons, a PCM was chosen as the test material. A cheap and readily available PCM is a water/agar-agar mix. Agar-gel will have similar freezing point and thermodynamical properties as water, is non toxic and is not prone to natural convection. Also, probing is easy due to the homogeneous, penetrable material.

Since block thickness was measured to be 103mm, the test material was made to the same thickness. Agar-agar was mixed with water (10g/L water) and brought to boiling until the liquid was clear again. Salt was added to correct for the lower initial freezing point of fish (15 g/L water). The boiling solution was quickly poured into molds with a flat bottom. It was made clear, by failed attempts, that the gel could not be made in one piece of 103mm, as the solution would not harden. Therefore, 3 separate blocks was made. It might be possible, however, to make two equally sized blocks and have the measuring equipment placed in between. Three block was made because of uncertainty of this solution and a lack of time for failure. The solution was left over night as it takes a couple of hours before it is properly hardened.

Figure 3.4: Making of agar-gel blocks in molds

**Experimental determination of thermal conductivity in agar-gel**

Agar-gel consists of nearly 99 % water, thus thermodynamical properties like heat capacity, density and thermal conductivity are expected to be similar to water. However, the structured arrangement of the gel could affect the thermal conductivity as structured materials generally have higher conductivity. Specific heat and density is not dependent on structural arrangement, and was therefore assumed to be equal to water. To be able to model agar-gel, the thermal conductivity was determined by HotDisk TPS.

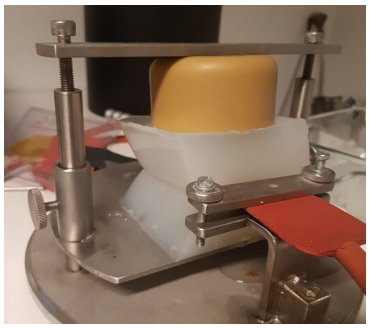

Figure 3.5: Experimental setup used for determining thermal conductivity in agar-gel

Hot disk TPS method is a well known, highly accurate method for determining thermal conductivity in fluids, solids and powder. It is approved under ISO Standard 22007-2 [31]. A HotDisk 2500 S®was used with a 6.4 mm diameter kapton sensor [28]. Logging time was set to be 160 seconds and different samples was tested in 20 °C and 0 °C. Results are illustrated in 3.6

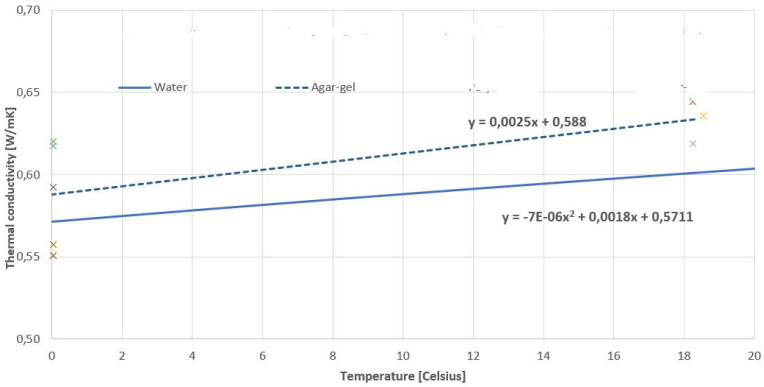


Figure 3.6: Result for experimentally determined thermal conductivity for agar-gel

As expected, thermal conductivity was measured to be slightly higher than for water, approximately 5%. Solid line is theoretical thermal conductivity for pure water, while dotted line is experimentally measured thermal conductivity for agar gel. Regression analysis was used for experiments in room temperature and 0°C.

### 3.3.3 Measuring equipment

Two kinds of temperature measuring devices were used during the plate freezer experiment.

- TC Couple
- Button censors

The TC monitor was of type Accsense Versalog™[3]. It can monitor up to 7 temperatures and has a supplementary thermistor for room temperature measurement.

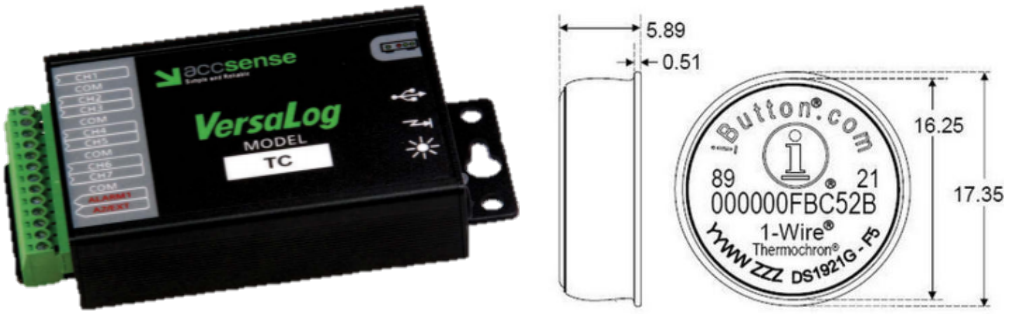


Figure 3.7: Accsence Versalog™[3] and I-Button ™[35] used in plate freezer experiment

The button censors were from Maxim Integrated™[35]. They are small, self-sufficient temperature loggers with internal memory.

### 3.3.4 Experimental plate freezer set-up

In the plate freezer , the three test material blocks was placed in a single section between two plates, forming one 103 mm block. Water was filled in three other sections, so that these could also be measured, in order to have more comparison data. Water had to be contained in bags considering the bottom of the freezer was not leak proof. Salt was added to the water (3.5g/L) to get a lower freezing point, similar to fish.

Two TC probes was inserted approximately 170 mm in the half thickness plane of the gel block, with guidance from a 1 mm thick steel rod. The TC tip (measuring point) was placed 30 mm from the steel rod tip to avoid any measuring error created by the high conductivity of the steel rod, as seen in figure 3.8.

For the water sections, custom made measuring equipment was made. A thin walled steel pipe lead the TC to the half thickness plane of the water. Also, button censors was placed on the plates, submerged in the water.

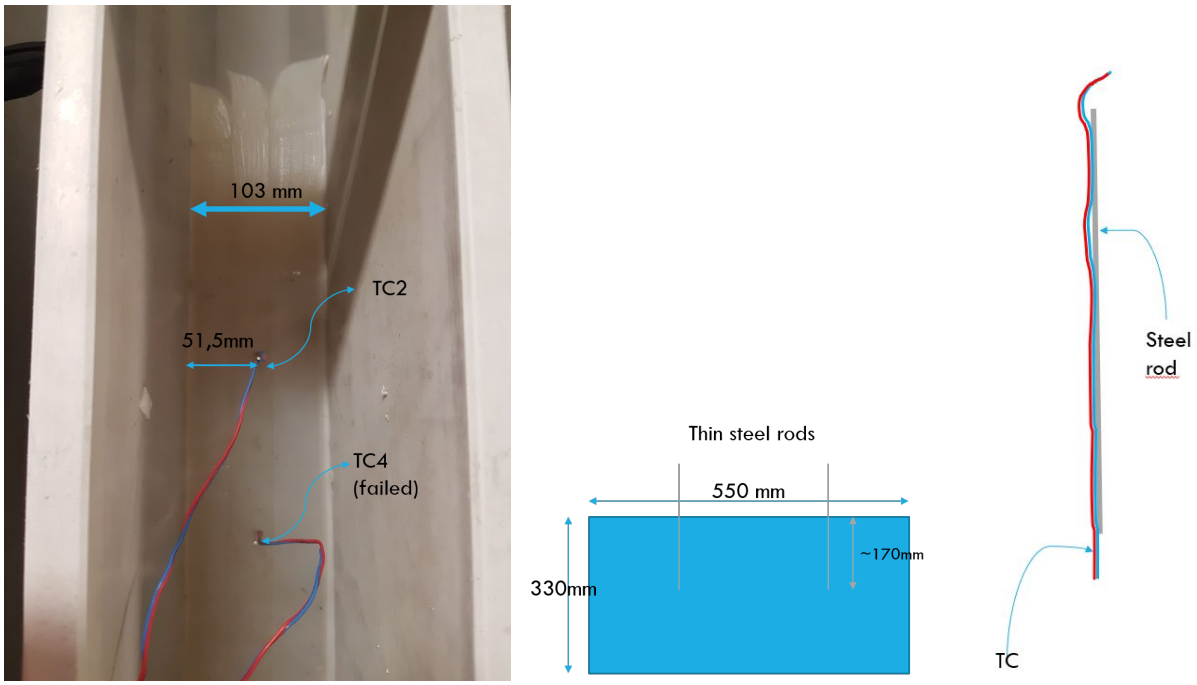


Figure 3.8: Experimental setup and measuring equipment used for agar-gel blocks

Figure 3.9: Experimental setup and measuring equipment used for water

## 3.4 Theoretical COP calculation

To be able to compare theoretical COP for various refrigerants and evaporating temperature, a two-stage system with open intermediate pressure receiver, flooded evaporator, and water cooled condenser was studied. In addition, a cascade system was investigated, both illustrated in figure 3.10.

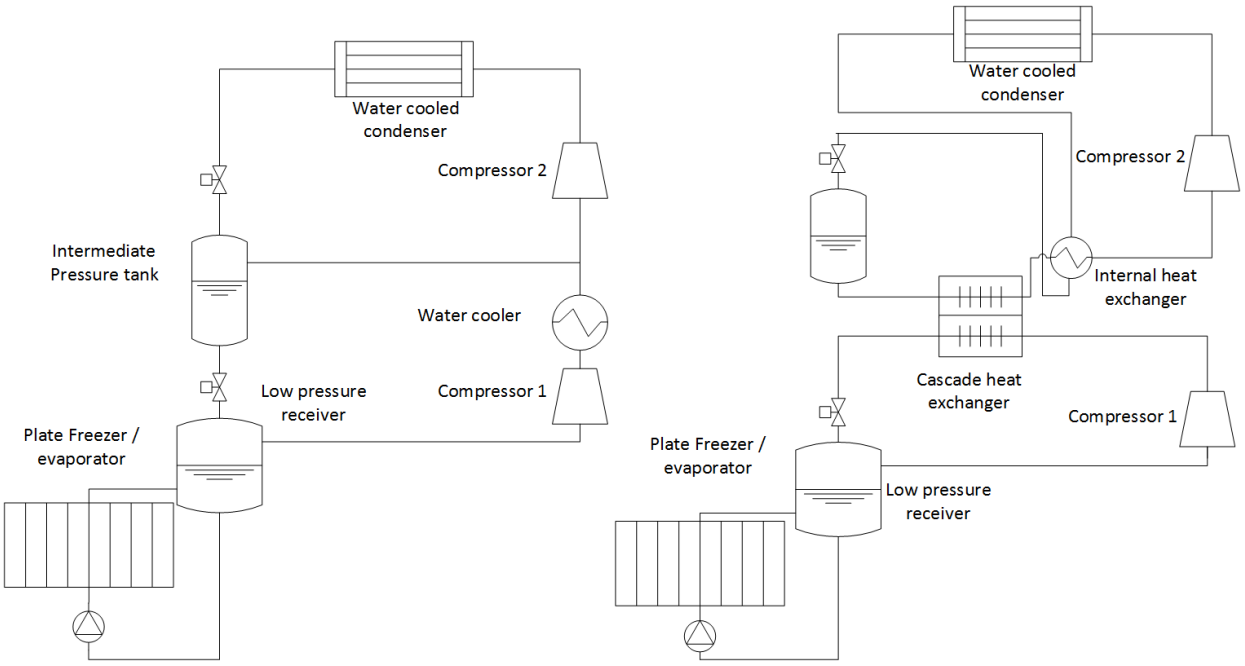


Figure 3.10: Chosen system solutions for comparison between refrigerants. Left: booster system with open intercooler, right: Cascade system

It was assumed sea water cooled condensers, with water temperature of 8°C and 3K temperature difference in condenser. The internal heat exchangers was set to an overheat of 10K, while the temperature difference in the cascade heat exchanger was set to 5K. The isentropic efficiency was chosen to be 0.71 for all compressors, while the intermediate pressure level was calculated so that both compressors had equal pressure ratio:

$$p_i = \sqrt{p_l \cdot p_h} \tag{3.14}$$

The COP was calculated using a Excel spreadsheet made by the author, by utilizing the free Excel extension Rn-Lib [49]. Rn-Lib can be used to calculate necessary properties for a comprehensive selection of refrigerants.

Pressure drop in evaporator was included by methods reviewed in chapter 2.3.3, leading to more realistic values for COP.

## 3.5 CTES solution

As already mentioned, one of this thesis main objectives are to optimize a fish freezing system, regarding freezing time and product capacity. Installed compressor capacity is not dimensioned to cover peak heat loads, leading to increased pressure and temperature in the evaporator, which

in turn prolongs freezing time. A CTES solution will aim to reduce this elevation in pressure by storing energy when available, and releasing it when needed, during peak loads.

### 3.5.1 Strategy and energy calculations

To introduce energy storage solution, it was necessary to combine it with a flooded evaporator. Simplified system solution from Kuldeteknisk AS, was used as reference, see figure 3.11.

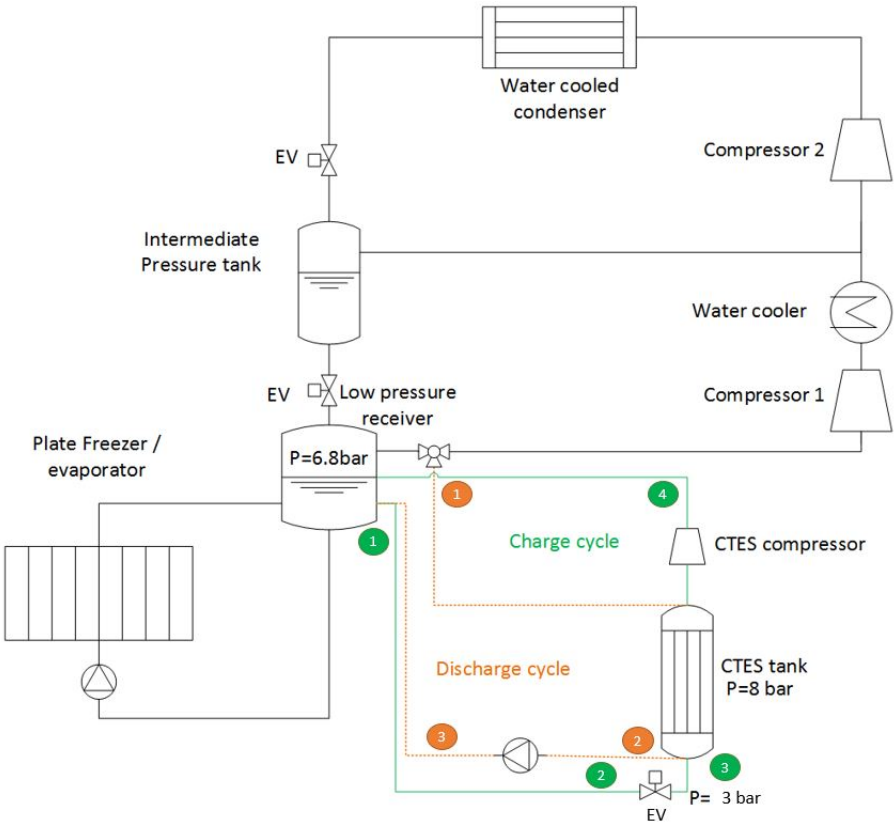


Figure 3.11: Suggested process diagram for a CTES add-on system

The intention of implementing a CTES system was to reduce the negative effect which follows by having a mismatch between supply and demand in freezing energy. The proposed solution was to run the main compressor(s) at design point, equal to the average heat load, throughout the freezing process. When the heat load is lower than the compressor capacity, the CTES system can start to run and store the available energy by expanding liquid from the low receiver to a low pressure and freeze the PCM in the CTES tank, called **charging** the tank. To be able to store energy at -50°, including a temperature difference in the CTES tank, pressures below the triple point of the $CO_2$ refrigerant had to be assumed, meaning dry ice is generated after the expansion device before the CTES tank. Energy is available for storage when the pressure in the

receiver is lower than designed, and would signal the expansion valve to open. When freezing the PCM, dry ice is sublimated and refrigerant gas exits the CTES tank. The refrigerant gas is finally compressed back to the receiver. During **discharge**, energy is released from the CTES tank by melting the PCM. Now, the compressor is struggling to maintain the low pressure in the receiver, due to excessive refrigerant vapour generation from the freezer. The receiver pressure starts to rise and signals the tree way valve to open, guiding some of the refrigerant gas through the CTES tank. The colder PCM is condensing the refrigerant, essentially helping the compressor to remove refrigerant gas in the low receiver. The liquid refrigerant from the CTES tank is pumped back to receiver.

Figure 3.12 illustrates the charge and discharge cycle in the P-H diagram. Note that logarithmic vertical axis are used above the triple point and linear axis below. Pressure and temperature levels are tabulated in table 3.1

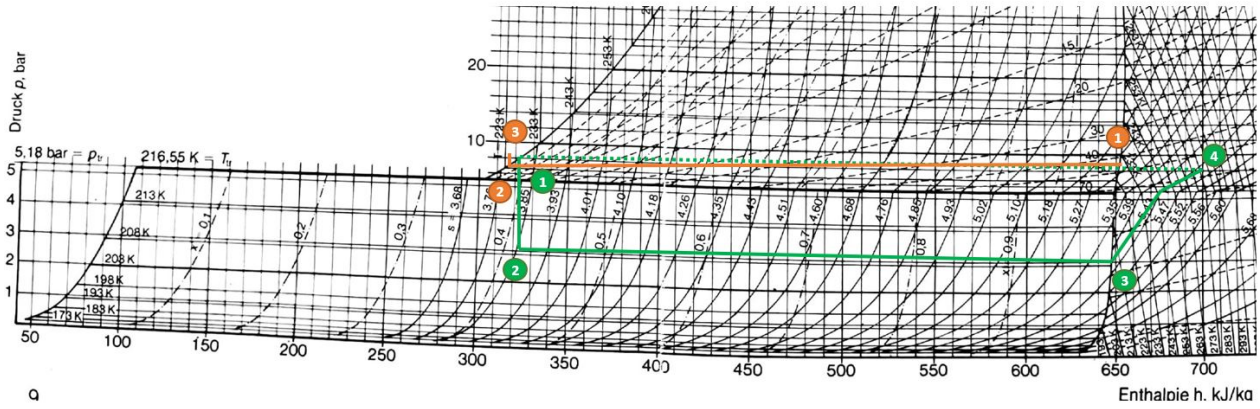


Figure 3.12: CTES cycle in P-H diagram

Illustration below takes a closer look on the CTES tank in figure 3.11. Notice the liquid supply tank, necessary to supply the tank with liquid during charging, as dry ice has approximately 20 % lower specific volume.

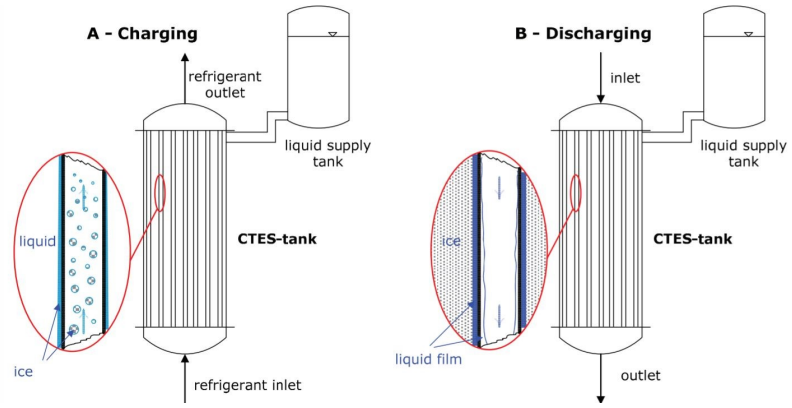


Figure 3.13: Close-up of CTES tank in figure 3.11 during charge and discharge [6]

As can bee seen from figure 3.11, an extra compressor is needed, possibly influencing the total energy input. In addition, it was important to calculate how much energy could be stored. The calculations was done as follows:

Heat load from fish was already known from simulations made to calculate the freezing time. Dimensioned compressor size was assumed to be average of the heat load. A script in MATLAB was made to calculate when heat load was smaller than compressor capacity and amount of storable energy after that point. That exact amount of energy was then added to compressor capacity in the first 15 minutes in the freezing process, simulating the discharging of the CTES tank.

Power consumption from CTES compressor could also be calculated by knowing the running time, storage time, and storable energy. Data from below the triple point of R744 is scarce, but PH- and TS-diagrams are presented in Appendix B.

### 3.5.2 Ice melting and dimensioning of CTES tank

To determine the dimensioning factors of the CTES tank, melting and solidification of PCM had to be studied. It was assumed a shell and tube heat exchanger, with PCM at the shell side. An important assumption is whether to have a two- or three dimensional model. Agyenim et al. (2010) [5] found that axial heat transfer was 2.5-3.5 % of the radial heat transfer, making the problem essentially a 2-D problem. Heat transfer was assumed from the inside of the condensing tubes, to the interface of solid/liquid PCM. Proper values for heat transfer from condensing $CO_2$ is not readily available. Therefore, a preliminary analysis was done by varying the heat transfer in the tubes from relative low values (1700 $W/m^2K$), to high values (4000 $W/m^2K$), suggested by [53]. It turns out condensing transfer has relative impact on the total melting thickness of the PCM, differencing only 5 %. This validated the assumption that heat transfer resistance is dominated by the PCM, except for the beginning.

Aluminium pipe diameter was set to be 10 mm, and pipe thickness was assumed to be 3 mm. Temperature difference between refrigerant and PCM was set to constant 8K. Assumed temperatures and pressures in the tank are tabulated in table 3.1.

Table 3.1: Designed temperatures and pressures in CTES tank

| | Tube side | | Shell side |
|---|---|---|---|
| | Refrigerant, charge | Refrigerant, discharge | PCM |
| Temperature | -65 °C | -49 °C | -57 °C |
| Pressure | 3 bar | 7 bar | 8 bar |

Figure 3.14 illustrates melting of PCM around tubes, inside which refrigerant is condensing. The tube is only one of many tubes in the shell and tube heat exchanger, illustrated in figure 2.12.

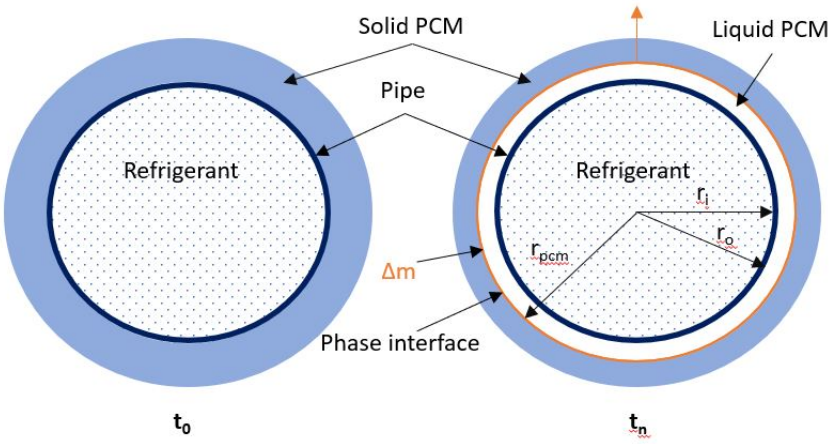


Figure 3.14: Illustration how solid PCM melts on tubes when refrigerant condenses inside

Time instance $t_0$ corresponds to the onset of discharge, while time instance $t_n$ corresponds to an arbitrary time after $t_0$.

Overall heat transfer coefficient product, UA, could be calculated by applying conductive and convective heat transfer in polar coordinates [29].

$$UA = \frac{2\pi L}{\frac{1}{r_i h_{conv}} + \frac{ln(r_o/r_i)}{k_{pipe}} + \frac{ln(r_{pcm}/r_o)}{k_{pcm}}} \tag{3.15}$$

Equation 3.15 is valid for liquid PCM at rest. However, density difference in the liquid PCM gives rise to circulation in the fluid, called natural convection, resulting in higher heat transfer in liquid layer. Nusselt number, which relates heat transfer in convective fluids to pure conduction in fluids at rest, is defined by:

$$Nu_d = \frac{hd}{k} \tag{3.16}$$

Inserting Nusselt number into equation 3.15 yields:

$$UA = \frac{2\pi L}{\frac{1}{r_i h_{conv}} + \frac{ln(r_o/r_i)}{k_{pipe}} + \frac{ln(r_{pcm}/r_o)}{k_{pcm} Nu_d}} \tag{3.17}$$

Inserting equation 3.17 into equation 2.28, and expressing $\Delta m$ by an increase in radius

$$\Delta m = 2\pi r_{pcm} \Delta r \rho_{pcm} L \tag{3.18}$$

yields,

$$\Delta r = \frac{1}{\frac{1}{r_i h_{sub}} + \frac{ln(r_o/r_i)}{k_{pipe}} + \frac{ln(r_{pcm}/r_o)}{k_{pcm} Nu_d}} \cdot \frac{\Delta T \Delta t}{\Delta H \rho_{pcm^n} r_{pcm}^n} \tag{3.19}$$

Finally,

$$r_{pcm}^{n+1} = r_{pcm}^n + \Delta r \tag{3.20}$$

where
radii can be seen from figure 3.14
$n$ is time iteration
$\Delta r$ is the increase in liquid PCM radius from time iteration $n$ to $n+1$
$k$ is thermal conductivity, 0.17 W/mK and 237 W/mK for $CO_2$ and aluminium pipes, respectively

Now, the final thickness of the dry ice could be calculated, by knowing the storing time. Furthermore, the total mass of solid PCM could be calculated, by knowing the amount of required stored energy.

# Chapter 4 Results

## 4.1 Numerical freezing and pressure receiver model

### 4.1.1 Freezing time with constant temperature boundary condition

Simulating core temperature in fish block (cod) during freezing, from +8 °C to -20 °C center temperature, and constant plate temperature, the freezing curve is illustrated below:

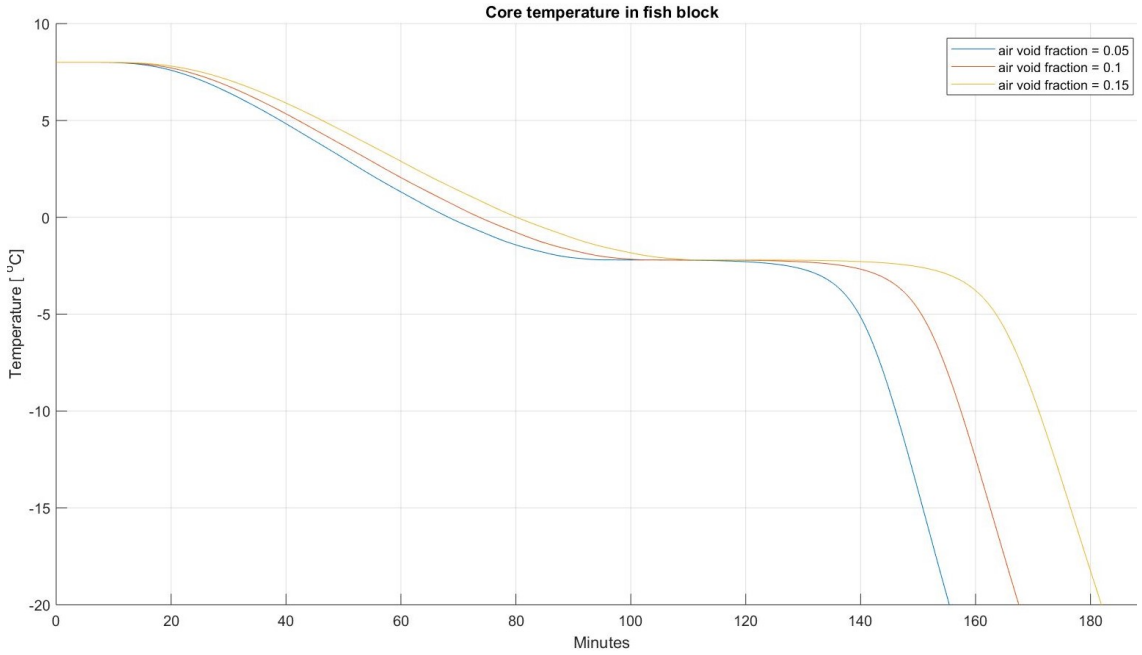


Figure 4.1: Numerical freezing time for 100mm cod with constant -50 °C plate temperature and various air void fractions

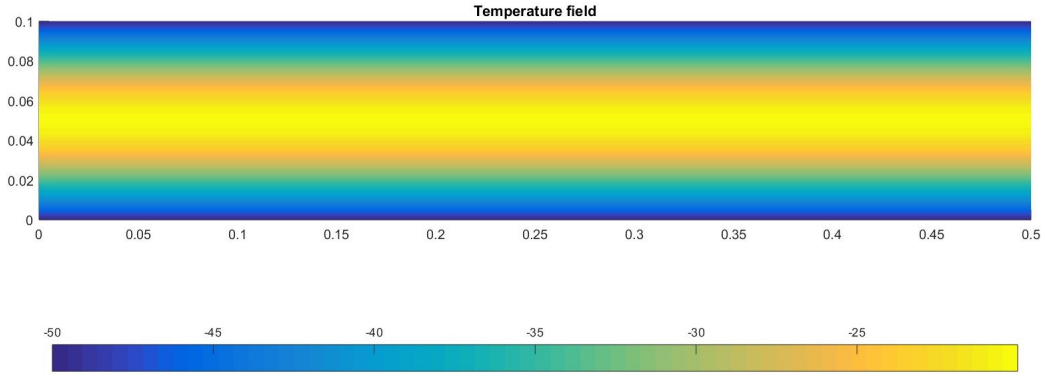


Figure 4.2: Temperature field in fish block after freezing

Figure 4.1 looks like a typical freezing curve. Temperature drop is slow in beginning due to relative low thermal diffusivity. Temperature impulse at boundary is not felt at center before some time has passed. Initial freezing point is below 0 °C, like expected, and the temperature is almost constant until most of the water has been frozen. Temperature drop at end is rapid due to the higher conductivity of ice compared to water.

Air voids between fish and on the block surface is modeled by implementing corrected thermophysical properties for porous media. In other words, small air pockets distributed in the fish block rather than larger air voids which are inconsistent in size and shape and requires special numerical boundary conditions. Air void fraction is defined as volume of air divided by total volume of fish block.

Figure 4.1 illustrates the importance of having low air volume fraction in the fish block. An increase from 5 % to 15 % in air volume fraction results in increase in freezing time of 17 %. Factors that influence air volume fraction may be fish size and shape, block thickness and flexibility of fish (rigor mortis).

### 4.1.2 Product heat load

Calculating enthalpy in fish as it freezes, it is possible to determine the or heat load.

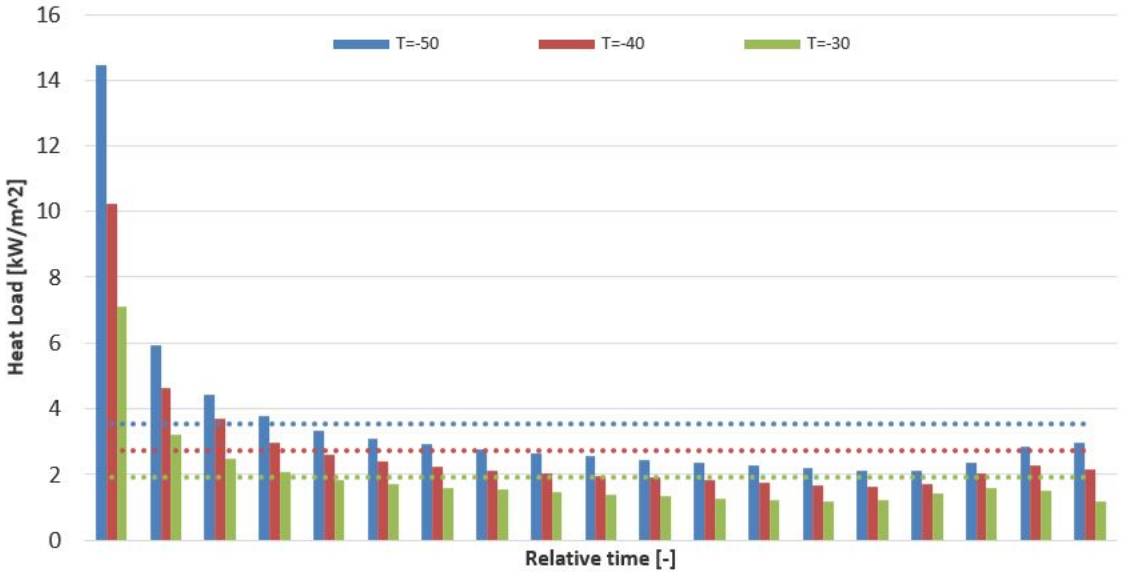


Figure 4.3: Heat load per surface area of cod blocks during freezing of 100mm blocks. Dotted lines are averages

The results reveal that heat load is large at the beginning, as temperature difference between plate and products is at it's highest. After some time, heat load is almost constant. This can

be explained by the "freezing plateau" where temperature in product is almost constant. Unit $kW/m^2$ means heat load in kW per surface area of one side of the fish block.

For all three cases, heat load is increased at the end of the freezing period. This happened around the time the core temperature starts to decrease again, see Figure 4.1. The increase might arise from increased conductivity as ice fraction is near the maximum value, which increases the overall heat transfer coefficient and in turn allowing more heat to be "extracted" from the fish.

For the different evaporating temperatures, the required energy to freeze cod is calculated by:

$$Q/m = c_u(T_i - T_f) + c_{f,avg}(T_f - T_{end,avg}) + Lx_w \tag{4.1}$$

where:
$c_u$ = Heat capacity of unfrozen fish
$c_{f,avg}$ = Average heat capacity of frozen fish
$T_i$ = Initial Temperature
$T_f$ = Freezing temperature
$T_{end,avg}$ = Average frozen temperature
$Lx_w$ = Latent energy of freezable water

Results from Equation 4.1 for relevant evaporation temperatures is tabulated in Table 4.1

Table 4.1: Specific freezing energy in cod

| | T = -50°C | T = -40°C | T = -30°C | |
|---|---|---|---|---|
| Latent Heat | 240 | 238 | 235 | kJ/kg |
| Pre-Cooling | 57.2 | 57.2 | 57.2 | kJ/kg |
| Sensible Freezing | 68.8 | 59.3 | 49.9 | kJ/kg |
| **Total freezing energy** | **366** | **354** | **342** | **kJ/kg** |

Energy required to freeze the fish increases with decreased plate temperature due to higher ice fraction in frozen product and steeper temperature gradient. Now, Figure 4.3 reveals higher heat load for lower temperatures, which is consistent with the fact that more energy is to be frozen, in a shorter time. An example of average heat loads and freezing times fore different evaporating temperatures are tabulated in table 4.2:

Table 4.2: Average heat load and freezing times for a 1250 kg freezer with 100 mm blocks

| | Evaporating temperature | | |
|---|---|---|---|
| | -50 °C | -40 °C | -30 °C |
| Average heat load [kW] | 43.6 | 33.8 | 24.0 |
| Freezing time [min] | 168 | 213 | 294 |

Notice the dimensioning installed compressor capacity is lower for higher evaporating temperatures. However, this also results in longer freezing times.

### 4.1.3 Receiver pressure modeling

To simulate the pressure increase in the receiver, due to insufficient compressor capacity, a pressure receiver model was made. In addition, experimental data from land based fish freezing facility with similar freezers was gathered to compare with real data. Theoretical and experimental temperature in pressure receiver is illustrated in figure 4.4.

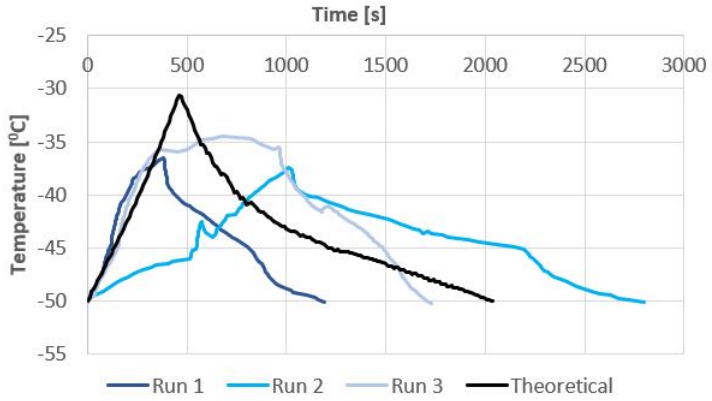


Figure 4.4: Experimental and theoretical temperature in receiver during the start of the freezing process

Note that the land based facility had two 25 station plate freezers with 120mm blocks and 7 available compressors. Only data on temperature and pressure was given, not compressor capacity.

It is clear from the experimental data, that the receiver temperature is not equal for seemingly identical freezing processes. This may be because of the unstable conditions in the receiver and complex compressor capacity regulations. These factors contribute to making the problem complex to model precisely. Nevertheless, as can be seen from Figure 4.4, the model predicts the temperature raise relatively good. An overshoot by approximately 5K can be explained by the difference in freezer facility, unknown receiver size in and by not assuming constant liquid level in the model. During freezing the liquid layer will be lowered, allowing more space to be

occupied by gas, which in turn decreases the pressure in the receiver. This is the most probable cause for the maximum pressure to be more rounded off, displayed by run 2 and 3.

Another possible reason for the deviation might be assumed constant circulation number, in the freezer. This is not possible, as the evaporator pump will remain on its characteristic. The pump characteristic is a relation between discharge and pump head. Pressure in evaporator is varying, and so will the discharged mass flow be, resulting in varying circulation number during freezing. Notice that these calculations is only valid for one single freezer. Multiple freezers in parallel will give different results.

### 4.1.4 Freezing time with time dependent boundary condition

Now that the dynamic evaporating temperature was calculated, new boundary conditions in the numerical freezing model was implemented. Figure 4.5 below shows the temperature after a short time after freezer start, where evaporating temperature is set to -50 °C. Notice the elevated temperature at the boundary, where the fish block is in contact with the freezer plates.

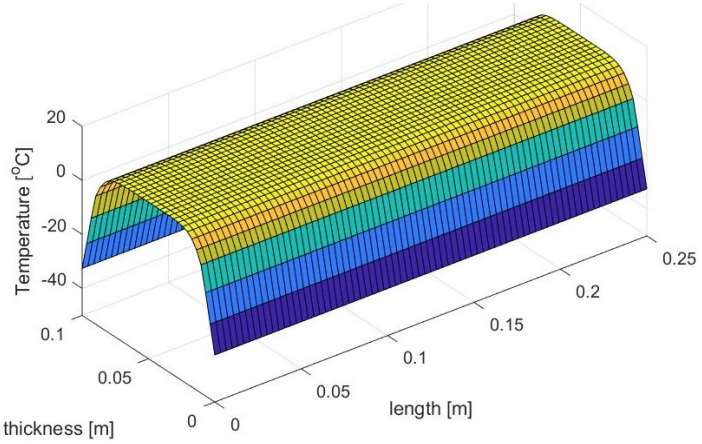


Figure 4.5: Temperature field in fish block a short time after freezer start

Corrected freezing times and average heat load is tabulated below.

Table 4.3: Correcetd average heat load and freezing times for 100 mm blocks and 1250 kg fish

| | Evaporating temperature | | |
|---|---|---|---|
| | -50 °C | -40 °C | -30 °C |
| Average heat load [kW] | 42.3 | 32.7 | 23.5 |
| Freezing time [min] | 174 | 219 | 301 |

As expected, freezing times are somewhat longer, because of the elevated temperature at boundary in the beginning. Real freezing with varying plate temperature results in approximately 5-7 minutes longer freezing times, compared to ideal freezing with constant plate temperatures.

### 4.1.5 Geometry and plate temperature influence on freezing time

As one can imagine, plate temperature and block thickness plays a major role in determining freezing time. Plank's equation ,Equation 2.20, states that freezing time is inversely proportional to reduction in plate temperature, and effectively proportional to the thickness squared for high heat transfer rates. Results from a series of simulations are displayed in table 4.4, varying fish block thickness and designed evaporating temperature between -30°C and -50°C, to simulate a variety of refrigerant. Note that air void fraction was set between 0.1 and 0.2, to model the lower bulk density obtained when trying to pack the same size fish in thinner blocks.

Table 4.4: Relative freezing times for different evaporating temperature and thickness

| | | Evaporating temperature | | |
|---|---|---|---|---|
| | | -50 °C | -40 °C | -30 °C |
| Thickness [mm] | 50 | 19 % | 23 % | 31 % |
| | 75 | 36 % | 44 % | 61 % |
| | 100 | 58 % | 73 % | 100 % |

Relative values are used in table 4.4, with evaporating temperature of -30 °C and 100 mm blocks as the reference. Note that if freezing time was directly proportional to thickness squared, relative freezing time when using 7 5mm blocks instead of 100 mm should be 56.3%. However, as table 4.4 demonstrates, we do not see this large decrease. This is mainly due to the air void fraction, which makes relative freezing times deviate from this relation.

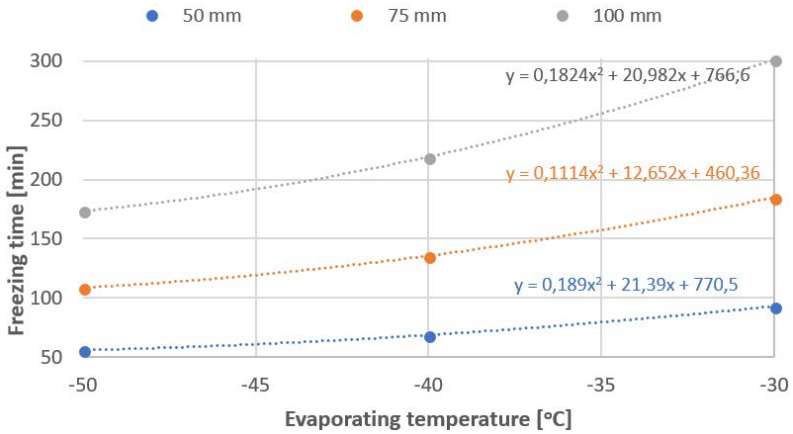


Figure 4.6: A function for freezing time based on numerical simulations

**Different fish species**

Different fish species has various thermal properties and water content. However, difference in freezing time is more likely to be a function of contact area with plates and size of air voids within the fish block, rather than varying properties. Fish with high water content obviously has more water to be frozen, which is time and energy consuming. However, water and ice have higher thermal conductivity than fat and protein, which will be the replaced components for fish with lower water content, see Table 2.1. Therefore, more data on bulk densities of different fish species must be gathered before comparison between fish species can be done.

## 4.2 Validation of numerical freezing model

The numerical freezing model was validted by conducting experiments in an industrial plate freezer. Evaporating temperature was heald close to -49 °C during the whole experiment. Distance between plates was measured to be 103 mm. Results are illustrated in below.

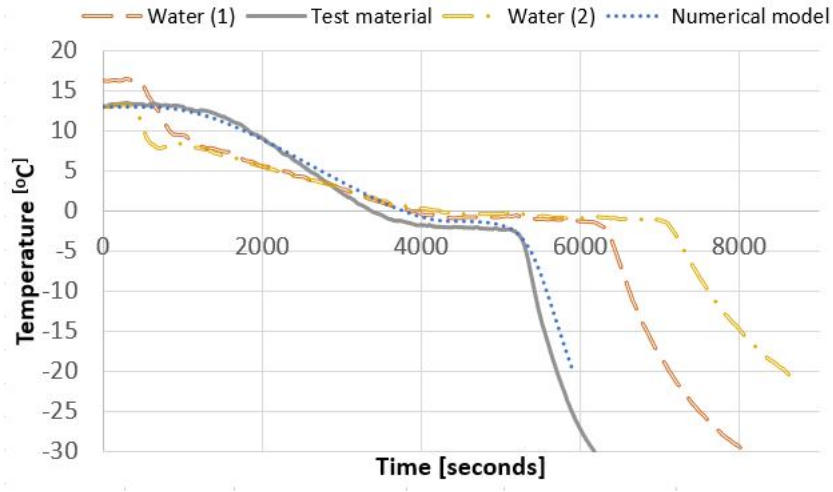


Figure 4.7: Results from plate freezer experiment and numerical model

Table 4.5: Time to reach center temperature of -20°C

| | Freezing time | |
|---|---|---|
| Numerical gel model | 98.5 | min |
| Experimental gel | 95.7 | min |
| Water (1) | 117 | min |
| Water (2) | 142 | min |

The time for agar-gel to be frozen (from +13°C to -20°C in center) was measured to be 95.7 minutes, while the numerical model predicts freezing time to be 98.5 minutes, resulting in 2.6% over-estimation. The numerical model follows the measurements closely at the beginning, but the freezing rate is slightly faster just before, and after, the critical zone.

The water blocks vary in freezing time, even though initial conditions are similar and they where measured during the same experiment. This verify the skepticism of using water as test material. Water has few nucleation sites and is prone to more homogeneous nucleation, which is much more complex to predict, compared to heterogeneous nucleation. Similar results are found in Seara et al. (2012) [23], where freezing time was in water measured to be between 5500 and 6400 seconds for the same experiment, using 9.5 cm water blocks and slightly higher evaporating temperatures.

The temperature measurements could be affected by the measuring probe itself. The TC was inserted in the gel using a thin (2 mm) steel rod, see figure 3.9. The rod's contact with warmer surrounding air might have influenced the measured temperature, even though the TC tip was placed 3cm away from the steel rod end.

Another way to validate the model is to study the ice fraction development. As the block froze during the experiment, the ice front was clearly visible and could easily be measured, see figure 4.8. After 10 minutes, the ice volume fraction was measured to be 26.6% while the model predicted just above 26%.

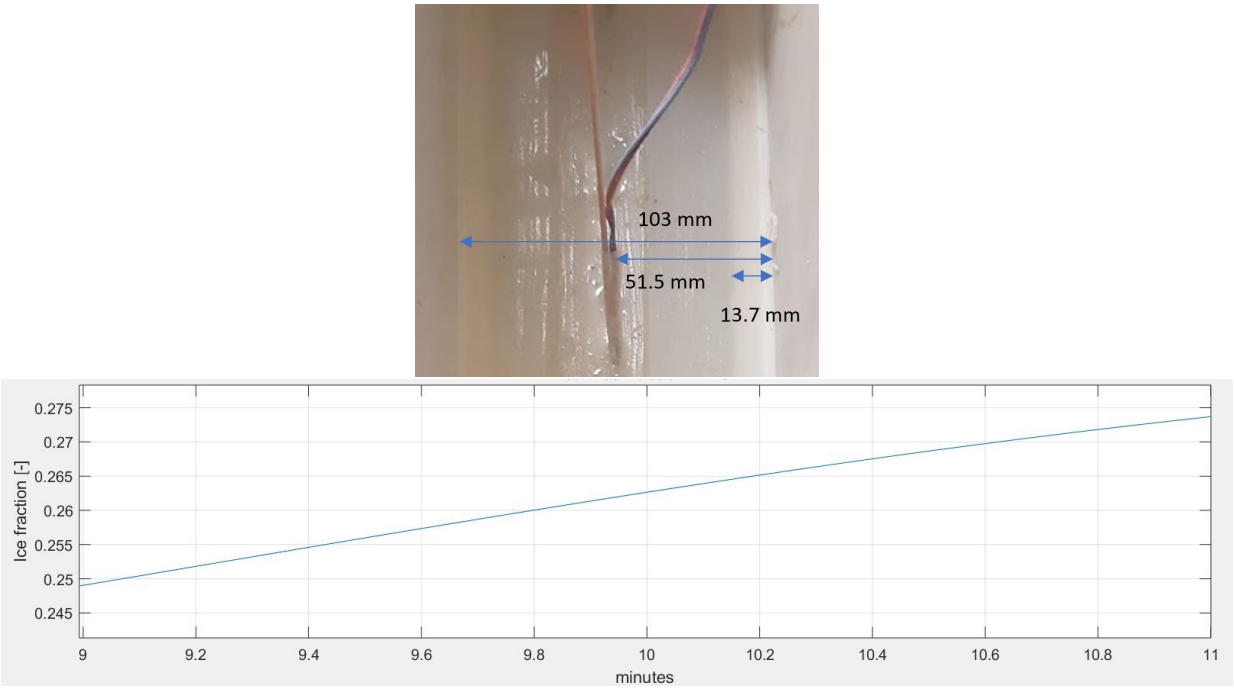


Figure 4.8: Ice fraction in gel after 10 minutes and the corresponding predicted numerical value

The small difference in freezing time, relative closely matching freezing curve and good prediction of ice volume fraction at single time instance concludes that the numerical model functions well for good contact products. For now, one might assume that the freezing model also predicts freezing time for fish, provided correct model input. More validation, especially on fish, having more irregular shapes and lower heat transfer contact area. This has been corrected for in the model by implementing thermal conductivity for porous media.

## 4.3 COP, energy use and product capacity calculations

### 4.3.1 Evaluation of system COP using natural refrigerants

COP for the systems, described in chapter 3.4 is estimated for selected natural refrigerants in figure 4.9

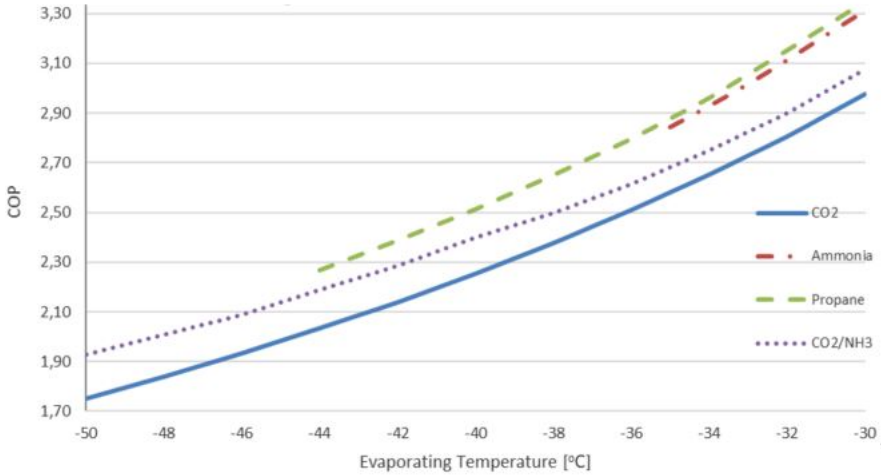


Figure 4.9: COP for cascade and two stage system for selected natural refrigerants. $T_c$=13°C

Results reveal that R744 has the lowest COP while R290 and R717 has the highest. Cascade system was somewhere in between as it uses two refrigerants, but has an additional temperature difference in the cascade heat exchanger. COP for all refrigerants would be lower if compressor heat loss and friction in pipes were included. However, the losses would have higher impact for R290 and R717 because of high compressor outlet temperature and high viscosity compared to R744.

**Pressure drop calculations**

Pressure loss was calculated for the relevant evaporating temperatures for the selected refrigerants, and was included in the COP estimation. Results are tabulated below:

Table 4.6: Pressure loss in plate freezer for selected refrigerants and applicable evaporating temperatures

| | | $T_{e,avg}$ | | | | |
|---|---|---|---|---|---|---|
| | | -50 °C | -45 °C | -40 °C | -35 °C | -30 °C |
| R744 | $G$ [kg/sm$^2$] | 236 | 205 | 179 | 158 | 137 |
| | $dP$ [bar] | 0.55 | 0.39 | 0.29 | 0.22 | 0.16 |
| | $dT$ [K] | 1.96 | 1.2 | 0.77 | 0.52 | 0.34 |
| R290 | $G$ [kg/sm$^2$] | | | 130 | 113 | 97.8 |
| | $dP$ [bar] | | | 0.193 | 0.138 | 0.1 |
| | $dT$ [K] | | | 3.97 | 2.54 | 1.52 |
| R717 | $G$ [kg/sm$^2$] | | | | 33.9 | 28.9 |
| | $dP$ [bar] | | | | 0.129 | 0.076 |
| | $dT$ [K] | | | | 2.7 | 1.3 |

Applicable temperature was assumed to be corresponding temperature where pressure at the evaporator outlet is above 0.9 bar. This means for example limiting evaporating temperature, $T_e$, to -45 °C and -36 °C for R290 and R717 at the outlet, respectively.

Pressure loss depend on thermodynamical properties and mass flux squared. R717 has low mass flux, and therefore low pressure loss, in evaporator, due to high latent heat of evaporation. However, R717 (and R290) has high $\Delta T_{sat}/\Delta P_{sat}$, resulting in a larger drop in evaporating temperature for a given pressure loss. R744 on the other hand, has one of the lowest $\Delta T_{sat}/\Delta P_{sat}$ of all refrigerants [26].

Evaporating temperature was regarded as average temperature across evaporator. R290 has relative high temperature and pressure loss. Therefore, -45°C might not be an applicable evaporating temperature as the pressure at the outlet of evaporator and internal heat exchanger is below atmospheric pressure (0.7 bar). Also, -35°C for R717 is a questionable evaporating temperature, as the lowest pressure at the evaporator outlet is just below 0.9 bar.

### 4.3.2 Specific energy requirement and product capacity

Now that both freezing time and COP has been calculated, it was possible to estimate the specific energy requirement to freeze the fish, $q\left[\frac{kWh}{tonnefish}\right]$ and product capacity $\left[\frac{kgfish}{h}\right]$. Once

more, different plate temperatures and block thickness were evaluated.

Table 4.7: Key performance indicators for a plate freezer

| | | **Freezing time [min]** | | | **Energy use** [ $\frac{\text{kWh}}{\text{tonne}}$ ] | | | **Product capacity** [ $\frac{\text{kg}}{\text{h}}$ ] | | |
|---|---|---|---|---|---|---|---|---|---|---|
| Evaporating temperature [°C ] | | -50 | -40 | -30 | -50 | -40 | -30 | -50 | -40 | -30 |
| Block thickness [mm] | 50 | 56.00 | 68.80 | 93.10 | 64.62 | 46.78 | 35.18 | 438.6 | 375.4 | 294.7 |
| | 75 | 108.7 | 135.7 | 184.8 | 67.41 | 52.54 | 39.00 | 412.7 | 341.1 | 259.2 |
| | 100 | 173.5 | 219.2 | 301.3 | 74.30 | 57.40 | 43.24 | 387.6 | 313.6 | 233.4 |

Required energy use increases with reducing temperature, mainly because of lower COP, but also because of larger heat loss in freezer, for a longer time. At the same, product capacity can be increased by up to 66 %, by using low temperature systems.

Energy use was calculated using R744 COPs. For calculating product capacity, a reset time (defrost, unloading and loading of product) was set to 20 minutes. Also, a freezer with a 25 plates is assumed, corresponding to 1250 kg for 100 mm blocks. The amount of fish per batch is therefore smaller for thinner blocks. Nevertheless, the product capacity still increases with reduced thickness. This can be explained by the fact that freezing time is more or less dependent on thickness squared, while the amount of fish per batch is linearly dependent on thickness. However, too thin blocks might result in bad contact between fish and plates, and larger air voids in the frozen fish block. Following that logic, there might exist an optimum block thickness, regarding capacity. Further experiments and data on bulk densities are required to find this optimum block thickness.

Results from Table 4.7 can be used to calculate direct energy cost of the freezing process.

$$p = \text{Required energy} \cdot \frac{\text{Price per liter}}{\text{Energy density}} \cdot \frac{1}{\eta_g} \tag{4.2}$$

Depending on evaporating temperature and block thickness, price vary between 90 and 190 NOK/tonne (10-20 €/tonne), assuming industrial diesel price of 8.75 NOK/L and energy density of 35.8 MJ/L. Also, generator efficiency ($\eta_g$) is assumed to be 35%. Considering the sales price for cod is around 32000 NOK/tonne (3300€/tonne), it is clear that product capacity is more important than energy efficiency.

## 4.4 CTES

### 4.4.1 Storable energy

Method from chapter 3.5.1 was done to simulate compressor capacity and heat load from fish, illustrated in figure below:

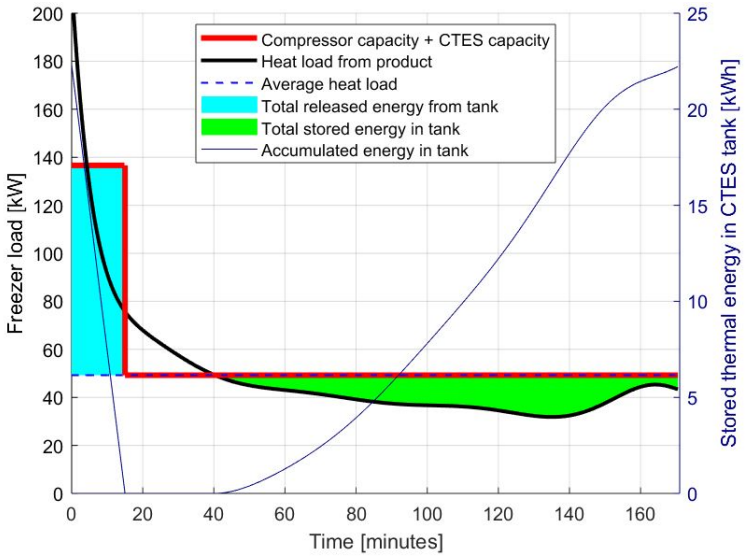


Figure 4.10: Heat load and total freezing capacity for 1250 kg fish in one plate freezer

Heat load from the fish is high in the beginning due to large temperature difference and high ice formation rate. After a while, 41 minutes, the heat load is smaller than the compressor capacity, meaning that it is possible to store the additional energy. Storing last throughout the freezing process and accumulates to around 22.2 at the end. This energy is released in the next freezing process, by condensing gas from the low pressure receiver, essentially helping the compressor to keep the low pressure. All the stored energy is now released in 15 minutes. This results in an added freezing capacity of around 89kW, 137kW in total. The added freezing capacity is enough the keep the pressure and temperature around the designed point, with very little variation.

### 4.4.2 Ice melting and dimensioning of CTES tank

One can imagine that the discharge, or melting, of the PCM tank would be the limiting factor, since it require larger heat transfer rates. Therefore, melting of PCM was modeled, described in chapter 3.5.2 and 2.4. Results from PCM melting thickness development is illustrated in figure 4.11.

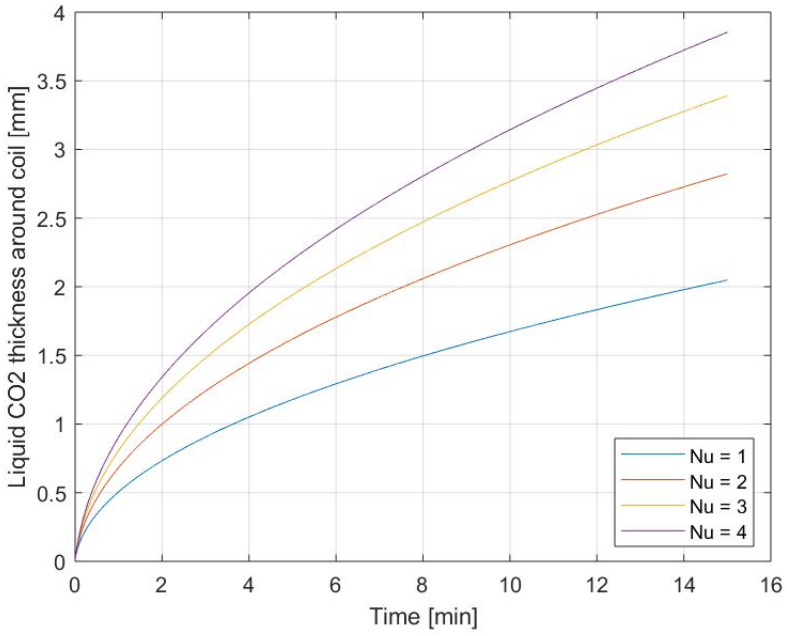


Figure 4.11: Liquid melted PCM layer development, for different Nusselt numbers

Results are dependent on the Nusselt number, as expected. Precise Nusselt number prediction is very complex. Small d/L, thickness of liquid layer divided by length of tube, generate large shear force between liquid moving up versus liquid going down. This will break up the typical circulation movement of one large circulation pattern along the whole pipe to smaller circulations. In light of this, it was chosen to implement the Nusselt number which relates convective heat transfer of moving fluid to a fluid at rest (essentially only conduction). Nu=3 means heat transfer three times as large compared to if the liquid would be at rest. Nusselt number tends to be around 2-4 for similar cases where natural convection is dominant.

Small Nusselt numbers results in a thin melted PCM liquid layer, meaning that more tubes, or larger heat transfer area (fins), are required. This is clear from the fact that 22.7 kWh of heat needs to be released and since the heat of fusion for $CO_2$ is fixed, the mass of solid PCM that needs to be melted is constant. Dimensioning tank properties are tabulated below.

Table 4.8: Dimensioning properties for the CTES tank

| | Nusselt number | | | |
|---|---|---|---|---|
| | 1 | 2 | 3 | 4 |
| Melted PCM thickness [mm] | 2.02 | 2.74 | 3.24 | 3.64 |
| No. of 1m tubes required | 1377 | 979 | 805 | 702 |
| Total volume of tank [L] | 614 | 501 | 451 | 422 |
| Mean heat transfer, $U[W/m^2K]$ | 264 | 372 | 452 | 518 |

The overall heat transfer coefficient, from the solid/liquid interface in PCM, to the inside of the tubes, is illustrated in figure below. The average value is tabulated in table 4.8

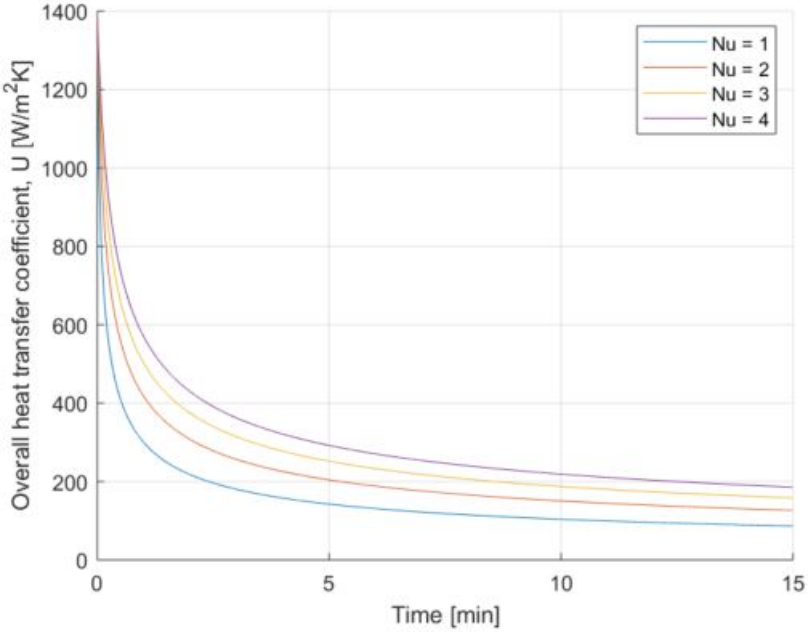


Figure 4.12: Overall heat transfer coefficient in CTES tank for different Nusselt numbers

In the beginning, the heat transfer is large due to low heat transfer resistance in the pipes. As the liquid layer starts to grow, the overall heat transfer is quickly dominated by the resistance of the liquid PCM. The high heat transfer might not be possible in real applications, thus, further research or experiments is required. Implementing fins to increase contact area is possible, and could be necessary to accomplish such high heat transfer rates. However, this will increase capital investment. Experiments or more precise numerical calculations is needed to validate the results.

### 4.4.3 Energy use and product capacity with CTES

One must not forget that the CTES system requires an additional compressor. A simple calculation was done to show that the CTES compressor is relatively small compared to the main heat pump compressors. Average mass flow was calculated by:

$$\Delta \dot{m}_{CTES} = \frac{\dot{Q}_{tot}}{\Delta S} = \frac{10.5kW}{219kJ/kg} = 0.048kg/s \tag{4.3}$$

Where $Q_{tot}$ is the averaged freezing capacity of the CTES tank in charge mode [kW/kg], and $\Delta S$ is the sublimation energy for the solid $CO_2$ [kJ/kg].

Compressor energy can be calculated by having data on $CO_2$ below, triple point. These are not easily gathered as most software focus on pressures above triple point. This thesis used data from Appendix B.

$$W_{c,CTES} = \dot{m}_{CTES}\Delta h = 0.048(701 - 649) = 2.5kW \tag{4.4}$$

Counting in that the CTES compressor's run time equals 75 % that of the main compressors, reveals that the CTES compressor power input is around 7% of the main compressors. This is a relatively small addition, but large enough to be considered in the main energy calculations.

Figure 4.10 reveals the mismatch in heat load and compressor capacity can be heavily downsized by use of CTES. In fact, pressure in the low pressure receiver is hardly influenced by the initially large heat load, with CTES system installed. Ideally, freezing times can be assumed to be close that of freezing times considering constant plate temperature. Table 4.9 evaluates the freezers KPIs, with and without a CTES system.

Table 4.9: Comparing dimensioning properties with and without CTES

| | With CTES | Without CTES | Difference [%] |
|---|---|---|---|
| Freezing time [min] | 168 | 174 | -3.17 |
| Energy use [kJ/kg] | 289 | 268 | 7.90 |
| Product capacity [kg/h] | 399 | 388 | 2.92 |

Table 4.9 reveals a decrease in freezing time by 3.17%, which results in increase of product capacity by 2.92%. The slight difference in product capacity increase and freezing time is because there was assumed a reset time (defrost and unloading/loading of product) of 20 minutes. Results conclude that both energy use and product capacity slightly increases with a CTES system installed. A relative small boat, like MS Arnøytind which have 3 freezers (1250 kg fish each), could potentially freeze 800kg more fish each day by implementing a CTES system. Further cost analysis must be done before concluding with potential profit. Thermal storage is in this thesis only evaluated for low temperature R744, but could in theory also be used for higher temperatures, displayed by R717 and R290.

# Chapter 5 Summary and Conclusions

In this thesis, a numerical freezing model was developed to predict the freezing time for fish in plate freezer. The freezing model was validated by conducting experiments on a phase changing test material in a $CO_2$ based, industrial plate freezer. Comparison from experiment and numerical model concluded a deviation of only 3 %. Furthermore, the pressure in the low receiver was modeled to cover the dynamic plate temperatures arising from insufficient compressor capacity. The pressure model was validated by comparison with data from similar facility.

Another model was made to estimate system efficiency, COP, for two different freezing systems using various natural refrigerants. Evaporating temperatures from -30 °C down to -50 °C was studied. $CO_2$ yields the lowest efficiencies, with COP ranging from 1.8 to 3.0 while COP for ammonia and propane was approximately 11 % higher for the same system. A $CO_2/NH_3$ cascade system was found to be on average 6 % more efficient than the pure $CO_2$ system.

For low temperature $CO_2$ systems, energy required to freeze fish was increased by 70 %, compared to -30°evaporating temperature for the same system. However, the freezing cost was calculated not to be significant to the total sales income. Freezing cost was estimated to be 90-190 NOK/tonne (10-20 €), while sales cost of frozen cod is around 32000 NOK/tonne (3263 €).

Focus was therefore redirected to freezing rate and product capacity increase, which is essential for fishermen. Before freezing, the fish is intermediately stored in RSW tanks, where temperature is around 0 °C. The time spent in this tank influences the fish quality. Furthermore, faster freezing enables the fishing vessel to catch more fish while there is fish present, by faster removal of fish in the RSW tanks. This ultimately reduces time at sea, and therefore cost and fuel usage for the vessel. Results revealed a product capacity increase of up to 66%, when freezing with -50 °C compared to -30°C. Even higher product capacity increase is possible when reducing fish block thickness. This is especially of interest when freezing pelagic fish, like mackerel and herring, which is smaller in size and can be closely packed, even in thin blocks.

A cold thermal storage system (CTES) was investigated, aiming to reduce the pressure elevation in the low receiver, which in turn causes prolonged freezing times. The CTES system utilized a shell and tube heat exchanger, containing PCM. Surplus "cold" energy from the freezing system was stored in the CTES tank by freezing the PCM. Likewise, when the compressor struggled to keep the low pressure, the stored energy was released, boosting the total refrigeration capacity. The CTES tank size was determined to be between 614 and 422 liters, and required 1377-702 tubes. When implementing the proposed CTES system, shorter freezing times was obtained. Results suggest a product capacity increase of 2.92% for a freezer with thermal storage solution.

# Chapter 6 Discussion

The numerical model fits experimental data very well, when comparing with test material with excellent contact with plates in the freezer. However, fish will have less contact with freezer plates due to the irregular shape of the product. Therefore, freezing times for fish is expected to be longer. This was modeled by implementing altered formulas for conductivity, assuming porous medias with a specified air void fraction. If possible, the numerical results presented in this thesis should be validated using industrial plate freezers and frozen fish. This was originally planned for the thesis, however, no plate freezer were available for testing.

When calculating COP for the different systems and refrigerants, simplified assumptions are made. COP will be reduced if all losses are included, but especially $CO_2$ can have less heat loss in compressors due to relative low compressor outlet temperature, and less friction loss in pipes due to low viscosity.

Results from the product capacity calculations demonstrates an increase, both when reducing evaporating temperature and fish block thickness. However, too thin fish blocks will result in poor contact between product and plate, in addition to higher air void fractions, which increases freezing time. Following this logic, there exists an optimum thickness, regarding product capacity. Better models, with correlation between fish size, block thickness and air void fraction, along with more experiments must be done to find this optimum thickness.

One might argue on the two-dimensional assumption when modeling the CTES tank. When charging and discharging the tank, heat transfer rates are likely to vary along the pipes. In discharge mode, gas starts to condense on the inside surface of the pipes, causing a buildup of a liquid boundary layer. The boundary layer acts as a thermal resistance, reducing the overall heat transfer coefficient and reducing the melting rate on the PCM side. The same problem arises when charging the tank. The dry ice particles generated in the bottom of the pipes must be sublimated before entering the compressor, or some kind of cyclone separator must be installed ahead of the compressor. If not, somewhere in the pipe, all dry ice is sublimated and very low heat transfer rates is achieved. Stratification of the liquid/solid PCM layer is the result of this, which is not a possible result for a two-dimensional analysis. Also, it is assumed noe sub cooling of the PCM, which often is the case for pure liquids. The effect of excluding the assumptions above might result in underestimation of size and number of tubes in the tank.

The chosen PCM for thesis thesis was $CO_2$, because of cost effectiveness, good temperature match and knowledge on the subject. $CO_2$ has very high energy storage density, roughly 400 $MJ/m^3$, but has generally low thermal conductivity due to its non polar structure. Maybe other

commercially available PCMs are better suited for the task, when considering volume of tank and achievable heat transfer rates.

More practical problems needs to be addressed, like control system, defrost, more than one freezer in parallel, plugging of ice in the CTES tank and perhaps the need for a "cold finger" when the freezing system is not running. A cold finger is a small heat pump unit maintaining the low temperature in liquid receiver and CTES tank, when the system is not running. Obviously, heat is leaking no matter how good insulated the components are.

## 6.1 Control system description

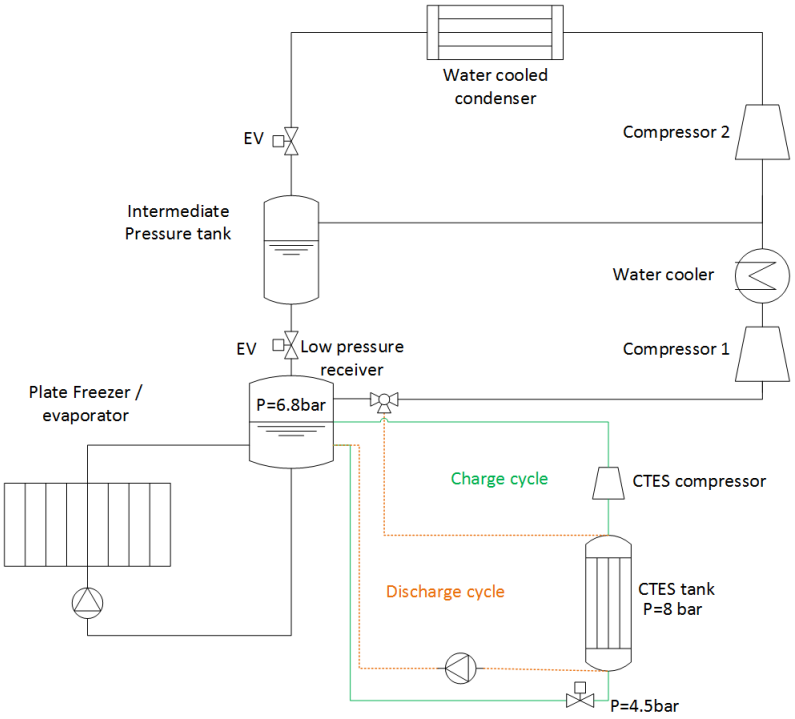


Figure 6.1: Suggested process diagram for a CTES add-on system

The most important control parameter in the freezing system, displayed in figure 6.1 is the pressure in low pressure receiver. As proven in this thesis, evaporating temperature is crucial for maximizing the product capacity of the system. The pressure in the receiver could be controlled by turning on/off the CTES system. This can replace frequency controlled compressors, which are expensive and more energy demanding.

Higher pressure than the designed 6.8 bar is a sign that the compressor cannot remove the gas generated by the freezer. This should signal a valve to open up for gas to be condensed in to the

CTES tank. Too low pressure is a sign that compressor capacity is higher than the heat load, and might generate solid $CO_2$ in the receiver and freezer, which is not desirable. This should signal the CTES compressor to start and the expansion valve in to the CTES tank to open, allowing liquid to be removed and sublimated refrigerant to re-enter the liquid receiver as gas. This will stabilize the pressure to the designed level. Frequency converter should, however, be installed on the small CTES compressor, since available energy to be stored is varying during the freezing process, see figure 4.10.

The liquid pump to the freezer should ensure enough liquid to be evaporated. Insufficient liquid delivery results in too excessive gas formation in the tubes, leading to low heat transfer. Too much liquid results in high pressure drop and oddly enough, also low heat transfer because of a different flow regime. Studies have shown that circulation ratios around 3-6 results yields optimum heat transfer. However, heat transfer quickly drop past 6, so a circulation rate of 3-4 is recommended. Circulation ratio cannot be measured directly, so to ensure sufficient liquid supply, the pump is controlled by the pressure drop through the freezer. Freezing system suppliers often have a designed pressure drop that has proven to be effective when it comes to heat transfer rates, so the pump can be frequency controlled to match that specific pressure drop.

The intermediate pressure is, by some suppliers, set to a constant value. For R744 systems with sea water cooling, a temperature of -10°C is sometimes set as design point. This may not be the most effective pressure level, but it ensures a more stable liquid level in both receivers, and stable low level compression.

Condensing temperature is mostly dependent on sea water temperature, which is relatively constant in the north sea ($9 \pm 5$°C). The sea water is supplied by a sea water pump, and condensing temperature will be somewhat dependent on the mass flow, delivered by this pump. A high mass flow results is higher power consumption, but also lower condensing pressure.

## 6.2 Multiple freezers in parallel

One important thing to notice is that this thesis assumes only one freezer supported by one simple compressor. In reality, it is common to have multiple freezers connected in parallel, supported by multiple compressors. Some fish trawlers are basically frozen fish factories at sea, capable of having over 10 ten plate freezers in addition to blast freezers and a large frozen storage. For these vessels, energy storage may not be needed, since the base heat load is huge and the fluctuations due to varying heat load is small in comparison.

However, it is of interest to look at fishing vessels, or land based facilities, having a few plate freezers in parallel. A smart strategy would be to start the freezers with an interval, of maybe

20 to 45 minutes. Then, peak heat load would be spread out instead of starting all the freezers at once, resulting in a huge peak heat load. If multiple compressors are used, some of the compressor capacity regulation may be done by turning on/off the compressors.

Below is a simulation of the total heat load in a system with 3 freezers.

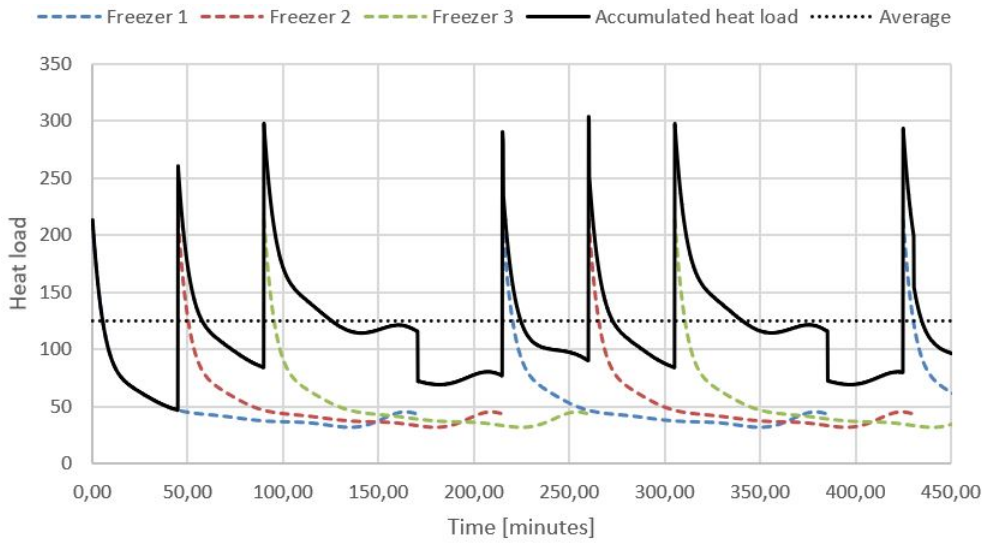


Figure 6.2: Three freezers in parallel, starting with intervals of 45 minutes

Figure 6.2 illustrates the respective and combined heat load of three plate freezers in parallel, with 45 minutes intervals. Maximum heat load is approximately 300 kW, and the dimensioning compressor capacity is approximately 115 kW, provided by two or three compressors. If thermal storage is used, the mismatch between compressor capacity and heat load can be reduced by the same principle shown in figure 4.10. Storage tank dimensions are likely to be equal as in table 4.8, since time between peaks are longer than time required to charge the tank. The tank was able to discharge almost at almost 100kW capacity for 15 minutes. Recharge time is shorter due to higher conductivity of dry ice, compared to liquid $CO_2$. As mentioned before, these results require more research and experimental validation.

MS Arnøytind used four 45 kW low stage compressors, adding up to a maximum capacity of 180 kW, whereas one of them is frequency controlled. As can be seen from figure 2.5, heat load rarely exceeds 180 kW, which is essentially an overdimensioned system, but is needed to keep the low pressure during peak loads. Also, a freezer storage with unknown load must be covered. If the system included a CTES system, a lower installed compressor capacity could be installed. The cost effectiveness of such a system is, for now, unknown. One would have to balance the reduction in price due to lower compressor capacity, and the added cost of a CTES system. Also, benefits of a possible increase in capacity must be included.

# Chapter 7 Proposal for Further Work

For further work on this project, the author recommends the following:

- **Validate numerical model** by doing experiments on fish in industrial freezer under real operating conditions. Also, gather data on air void fraction for different fish species and block thickness. Using these parameters, more precise results are available.
- Using the new model, block thickness can be optimized with regard to capacity.
- **Improving description of CTES system** using better models and/or experiments. As discussed in chapter 6, cost and effectiveness are two important criteria in determining if CTES should be installed on fishing vessels. Better models or experiments is needed before determining the rate of ice melting on the tubes. As suggested by the literature, heat transfer improvement methods, such as fins, could play an important role on size dimensioning of the tank. Other, more practical problems, such as control of the system, ice plugging in distribution system of the tank and what happens when the freezers are not running also needs clarification. Furthermore, other possible PCMs should be investigated. A project or master thesis on the cold thermal energy storage system alone is probably needed to get the information required.
- **Multiple freezers in parallel** has already been discussed in this thesis. Potential decrease in installed compressor capacity has not been sufficiently discussed. This should be investigated further.
- **Control system** should be described for the different components in freezing system.

# Appendix A Acronyms

**ASHRAE** American Society of Heating, Refrigerating and Air-Conditioning Engineers

**CFD** Computational Fluid Mechanics

**COP** Coefficient of Performance

**CTES** Cold Thermal Energy Storage

**EPT** Institute of Energy and Process engineering

**EV** Expansion Valve

**FTCS** Forward Time - Central Space

**GWP** Global Warming Potential

**KPI** Key Performance Indicators

**NOK** Norwegian Krone (Currency)

**NTNU** Norwegian University of Science and Technology

**ODP** Ozone Depletion Potential

**PCM** Phase Change Material

**R22** Chlorodifluoromethane (Refrigerant)

**R290** $C_3H_8$, Propane

**R744** $CO_2$ (Refrigerant)

**R717** $NH_3$, Ammonia

**RSW** Refrigerated Sea Water

**TC** Temperature Couple

**TES** Thermal Energy Storage

**TPS** Transient Plane Source

# Appendix B $CO_2$ data

## Dampftafel für $CO_2$ flüssig – dampfförmig

| $t$, °C | $T$, K | $p$, bar | Dichte, kg/m³ | | Enthalpie, KJ/kg | | Verd.-wärme kJ/kg | Entropie, kJ/(kg·K) | |
|---|---|---|---|---|---|---|---|---|---|
| | | | $\varrho_{liq}$ | $\varrho_{ga}$ | $h_{liq}$ | $h_{ga}$ | | $s_{liq}$ | $s_{ga}$ |
| +31 | 304,15 | 73,83 | 466,0 | 466,0 | 558,94 | 558,94 | 0 | 4,6365 | 4,6465 |
| +30 | 303,15 | 71,92 | 596,4 | 334,4 | 527,12 | 590,13 | 63,01 | 4,5444 | 4,7524 |
| +25 | 298,15 | 64,32 | 705,8 | 240,0 | 497,39 | 616,84 | 119,45 | 4,4497 | 4,8504 |
| +20 | 293,15 | 57,33 | 770,7 | 190,2 | 477,30 | 632,63 | 155,33 | 4,3827 | 4,9128 |
| +15 | 288,15 | 50,93 | 817,9 | 158,0 | 460,97 | 641,29 | 180,32 | 4,3292 | 4,9551 |
| +10 | 283,15 | 45,06 | 858,0 | 133,0 | 445,89 | 647,24 | 201,35 | 4,2781 | 4,9894 |
| + 5 | 278,15 | 39,72 | 893,1 | 113,0 | 431,66 | 650,84 | 219,18 | 4,2300 | 5,0179 |
| 0 | 273,15 | 34,85 | 924,8 | 96,3 | 418,68 | 653,69 | 235,01 | 4,1868 | 5,0472 |
| −5 | 268,15 | 30,45 | 953,8 | 82,4 | 405,74 | 654,86 | 249,12 | 3,9314 | 5,0698 |
| −10 | 263,15 | 26,47 | 980,8 | 70,5 | 393,94 | 655,65 | 261,71 | 4,0976 | 5,0924 |
| −15 | 258,15 | 22,89 | 1006,1 | 60,2 | 382,84 | 656,07 | 273,23 | 4,0570 | 5,1154 |
| −20 | 253,15 | 19,67 | 1029,9 | 51,4 | 372,33 | 656,36 | 284,03 | 4,0168 | 5,1380 |
| −25 | 248,15 | 16,81 | 1052,6 | 43,8 | 362,28 | 655,95 | 293,67 | 3,9779 | 5,1615 |
| −30 | 243,15 | 14,27 | 1074,2 | 37,0 | 352,49 | 655,49 | 303,00 | 3,9389 | 5,1854 |
| −35 | 238,15 | 12,02 | 1094,9 | 31,2 | 342,82 | 654,77 | 311,95 | 3,8996 | 5,2096 |
| −40 | 233,15 | 10,05 | 1115,0 | 26,2 | 333,23 | 653,62 | 320,62 | 3,8594 | 5,2348 |
| −45 | 228,15 | 8,33 | 1134,5 | 21,8 | 323,64 | 652,68 | 329,04 | 3,8184 | 5,2607 |
| −50 | 223,15 | 6,84 | 1153,5 | 18,1 | 314,05 | 651,34 | 337,29 | 3,7765 | 5,2883 |
| −55 | 218,15 | 5,55 | 1172,1 | 14,8 | 304,46 | 649,88 | 345,42 | 3,7334 | 5,3172 |
| −56,6 | 216,55 | 5,18 | 1177,9 | 13,8 | 301,32 | 649,33 | 348,01 | 3,7205 | |

bei 0 °C wird $h_{liq}$ = 418,68 kJ/kg (= 100 kcal/kg) und $s_{liq}$ = 4,1868 kJ/(kg · K) [(= 1 kcal/(kg · K)] gesetzt

## Dampftafel für $CO_2$ fest – dampfförmig

| $t$, °C | $T$, K | $p$, bar | Dichte, kg/m³ | | Enthalpie, kJ/kg | | Sublimationswärme kJ/kg | Entropie, kJ/(kg·K) | |
|---|---|---|---|---|---|---|---|---|---|
| | | | $\varrho_{sol}$ | $\varrho_{ga}$ | $h_{sol}$ | $h_{ga}$ | | $s_{sol}$ | $s_{ga}$ |
| −56,6 | 216,55 | 5,18 | 1512,4 | 13,84 | 105,55 | 649,33 | 543,78 | 2,8156 | 5,3273 |
| −60 | 213,15 | 4,10 | 1521,9 | 10,97 | 99,27 | 649,21 | 549,94 | 2,7863 | 5,3671 |
| −65 | 208,15 | 2,87 | 1534,6 | 7,74 | 89,97 | 648,41 | 558,44 | 2,7428 | 5,4261 |
| −70 | 203,15 | 1,98 | 1546,1 | 5,39 | 82,02 | 646,94 | 564,92 | 2,7043 | 5,4860 |
| −75 | 198,15 | 1,34 | 1556,5 | 3,71 | 75,07 | 645,02 | 569,95 | 2,6695 | 5,5467 |
| −78,9 | 194,25 | 0,98 | 1564,0 | 2,74 | 70,05 | 643,18 | 573,13 | 2,6435 | 5,5948 |
| −80 | 193,15 | 0,896 | 1566,1 | 2,51 | 68,71 | 642,63 | 573,92 | 2,6373 | 5,6095 |
| −85 | 188,15 | 0,584 | 1574,8 | 1,672 | 62,72 | 639,99 | 577,27 | 2,6059 | 5,6748 |
| −90 | 183,15 | 0,372 | 1582,2 | 1,087 | 56,90 | 637,06 | 580,16 | 2,5749 | 5,7435 |
| −95 | 178,15 | 0,231 | 1588,9 | 0,693 | 51,20 | 633,97 | 582,77 | 2,5431 | 5,8150 |
| −100 | 173,15 | 0,139 | 1595,2 | 0,428 | 45,55 | 630,74 | 585,19 | 2,5104 | 5,8908 |

Figure B.1: Relevant thermodynamic properties for R744

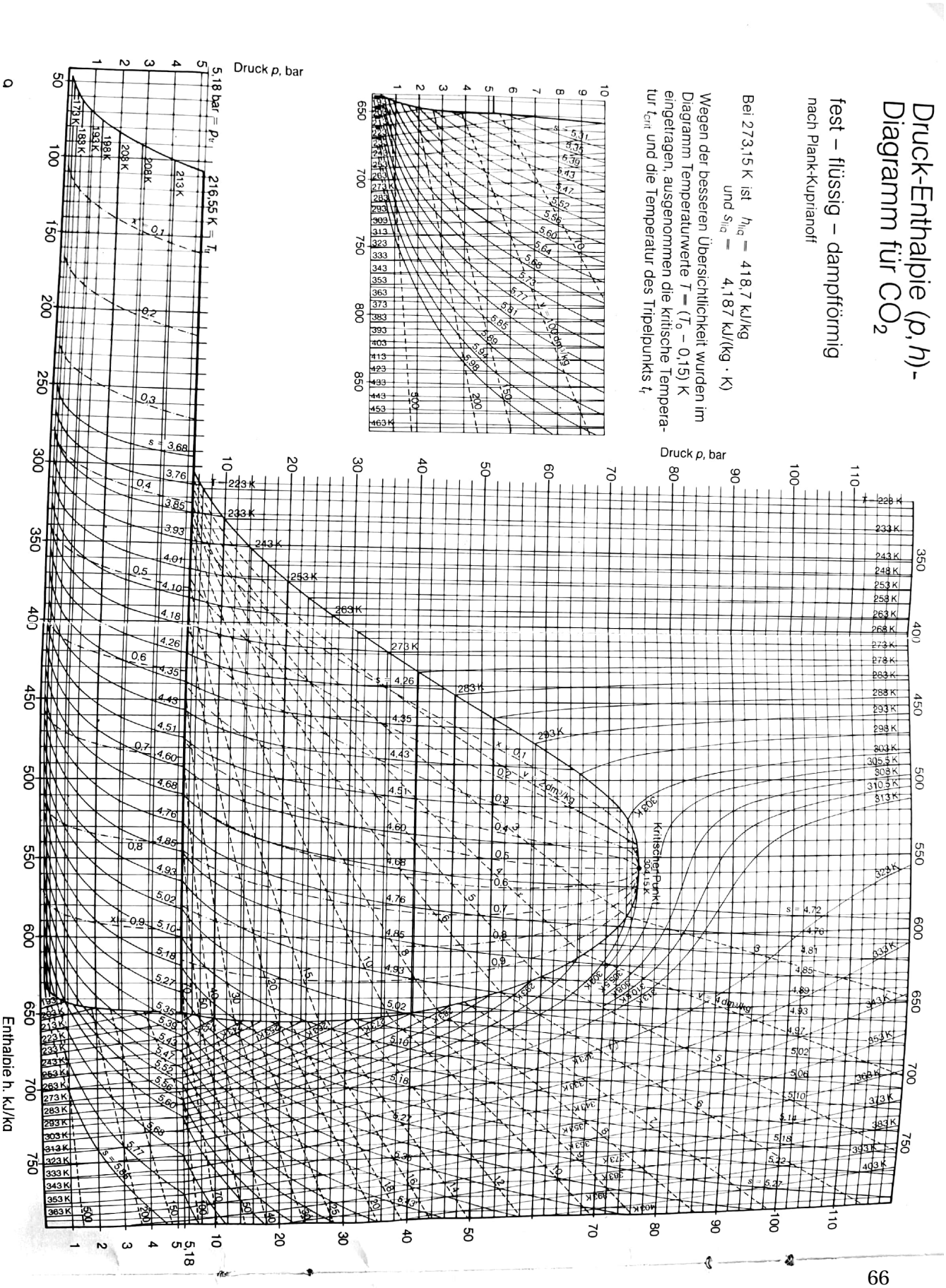


Figure B.2: PH diagram for R744

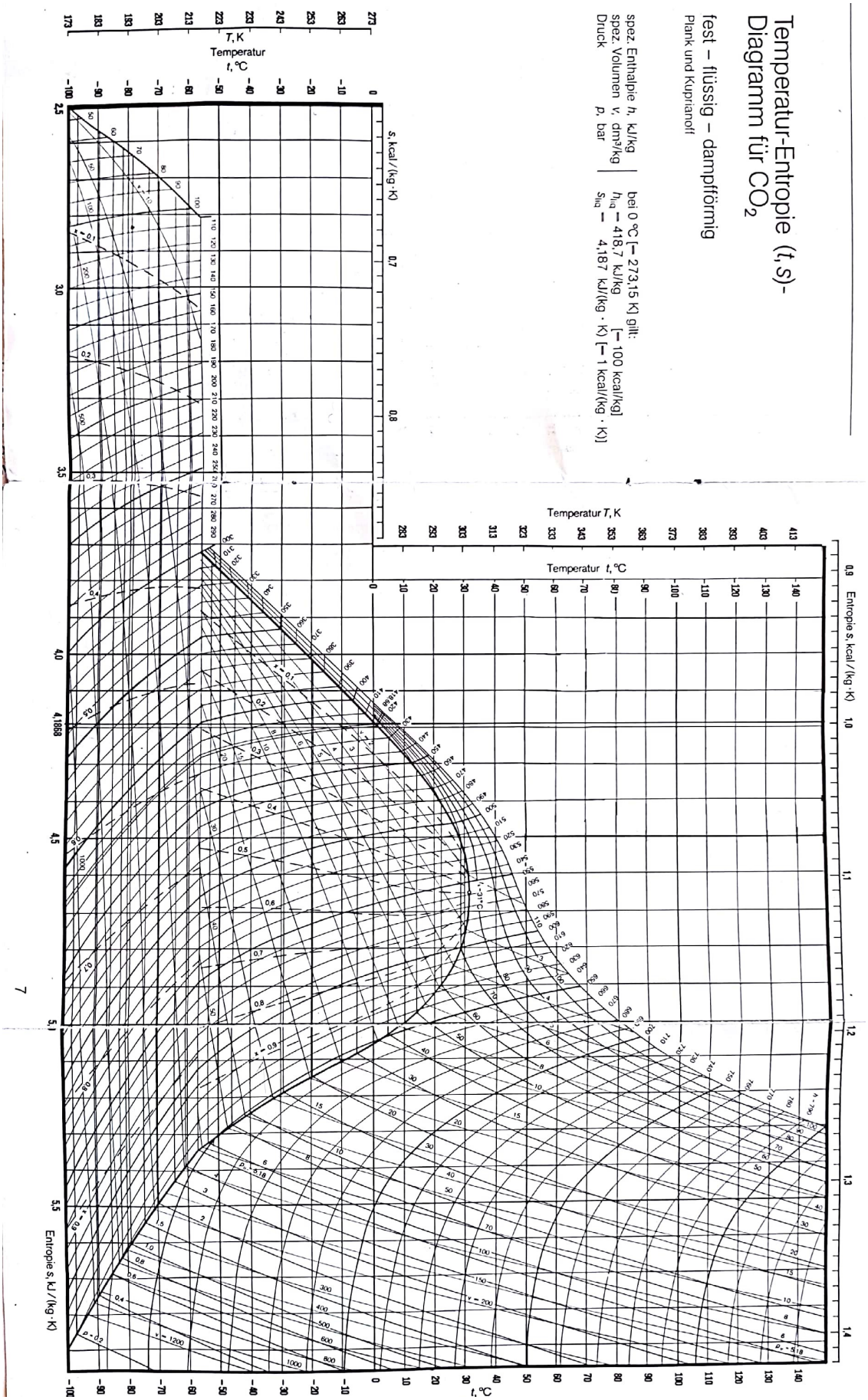


Figure B.3: TS diagram for R744

# Appendix C Draft Scientific Paper

The following paper is planned to be published in the 25$^{th}$ IIR International Congress of Refrigeration (ICR 2019) which is held in Montreal, Canada August 2019.

# Cold thermal energy storage with low-temperature plate freezing of fish on offshore vessels

**Espen H. VERPE[(a)(b)], Ignat TOLSTOREBROV[(b)], Alexis SEVAULT[(a)]**
(a) SINTEF Energy Research, P.O. Box 4761 Sluppen, NO-7465 Trondheim, Norway (b) Norwegian University of Science and Technology, Department of Energy and Process Engineering, Trondheim, 7491, Norway

## ABSTRACT

This paper investigates the contact freezing of fish with CO2 refrigeration system at a boat with respect to evaporating temperature and geometry of fish blocks. Cold thermal energy storage (CTES) was studied, aiming to decrease the elevation of receiver pressure, causing prolonged freezing times.

The numerical freezing model relied on the apparent heat capacity method and was validated with experiments, by freezing of test material in industrial plate freezer.

The fish production capacity could be increased by 66 % when using -50 ºC systems compared to -30 ºC for 100 mm fish blocks, while decreasing the block's thickness to 50 mm increased the production capacity by 13 %. Implementation of CTES system neglected increasing evaporating pressure and reduced the freezing time by 3.2 %.

Reduced evaporating temperature, thinner fish blocks and implementation of a CTES system proved to be beneficial, regarding product capacity, but got system efficiency.

Keywords: CTES, Plate Freezing, R744, Numerical Freezing Model, Energy Efficiency

## ACKNOWLEDGEMENTS

This publication has been partly funded by HighEFF - Centre for an Energy Efficient and Competitive Industry for the Future, an 8-year Research Centre under the FME-scheme (Centre for Environment-friendly Energy Research, 257632/E20). The authors gratefully acknowledge the financial support from the Research Council of Norway and partners of HighEFF. Also, thanks to Yves Ladam from Kuldeteknisk AS for supplying industrial plate freezer for experimental validation along with measurement data on land-based facilities.

## 1. INTRODUCTION

In the last decade, there has been an increase in natural refrigerants used in refrigeration systems. On offshore vessels, most systems use either R717 or R744. $CO_2$ has the ability to evaporate at temperatures as low as -50 ºC. Though operating at lower temperatures reduces freezing times, it also lowers system efficiency and requires higher installed compressor capacity.

This study focuses on plate freezing of fish onboard small fishing vessels, where compact equipment and high product capacity (kg frozen fish per day) is essential. Plate freezers are compact and uses plates, inside which the refrigerant evaporates, in direct contact with the fish to ensure fast freezing. Prediction of freezing times is an important parameter when designing freezing systems.

A new $CO_2$ system installed on a fishing vessel showed freezing time significantly longer than expected freezing time. This happened because the heat load from the product side varies during the freezing process, while the compressors are designed to have an optimum efficiency at a certain capacity. In addition, compressors are dimensioned for the average heat load, to avoid over dimensioning the system. This results in insufficient compressor capacity during peak heat load, leading to elevated pressure in the evaporator and prolonged freezing times.

This study investigates the possibility to optimize the freezing process and equipment on board boats, by installing a cold thermal energy storage (CTES) system. The CTES system stores energy, when the compressor capacity is larger than the heat load, and releases that energy when needed, typically in the beginning of the freezing process.

To obtain this aim the following measures were done:

1) Development of a numerical model for the freezing process
2) Development of a numerical model for the pressure in the receiver
3) Model validation using experiments and data from freezing facility
4) Suggestion of CTES system and effects on key performance indicators of freezing system

This paper is based on the main author's Master thesis [1], where more details and results can be found.

## 2. METHODS AND MATERIALS

### 2.1 Description of offshore $CO_2$ freezing system

This study is based on an offshore, two-stage, sea-water cooled, flooded evaporator, freezing system. A simplified model description is illustrated in Figure 1. The plate freezer has 24 stations and approximately 1250 kg capacity.

A model to estimate the system COP was established with refrigerant data from RnLib [2]. Reasonable assumptions included: isentropic efficiency of 0.7, sea water temperature of 8 °C, temperature difference of 5 K in condenser and pressure drop in evaporator and condenser estimated by methods found in [3], which encompasses acceleration loss, friction loss and height difference.

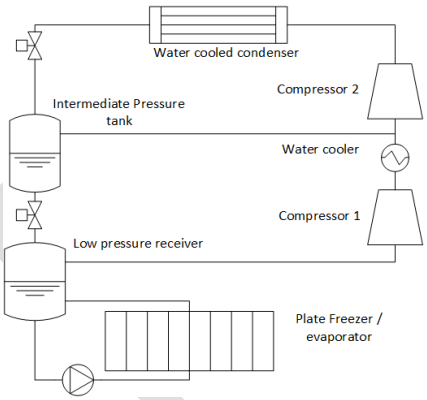


*Figure 1: Simplified model description of a two-stage freezing system*

### 2.2 Numerical description

#### 2.2.1 Freezing model

To be able to predict freezing times for various evaporating temperatures and fish block thicknesses, a numerical freezing model was made in MATLAB. The chosen method was to solve the two-dimensional heat diffusion equation, Equation 1, numerically by implicit finite difference method [4].

$$\frac{\partial}{\partial t}(\rho(T)c_a(T)\cdot T) = \vec{\nabla}\cdot\left(k(T)\cdot\vec{\nabla}T\right) \quad (1)$$

Equation 1 uses apparent heat capacity, $c_a$, which includes both latent and sensible energy, described by [5]. Other temperature dependent thermodynamic properties were calculated using methods described in ASHRAE [6]. Note that the conductivity for porous media was used, to compensate for larger air voids between the packed fish, resulting in more realistic thermal conductivity values than for a homogenous material.

Firstly, the boundaries were set to constant values, Dirichlet boundary condition, calculating required heat load, $Q$, to maintain boundary at constant temperature. It was recognized, however, such heat loads are not practically possible due to limited installed compressor capacity. Dynamic freezer inlet temperature was modelled as described in Section 2.2.2, which in turn became the more realistic, time dependent boundary conditions.

#### 2.2.2 Pressure receiver

Limited compressor capacity results in insufficient refrigerant gas removal from the low-pressure receiver, see Figure 1**.** Increased pressure elevates evaporating temperature in freezer, which in turn, increases freezing time. Therefore, a model was made, attempting to simulate the evaporating temperature during freezing of fish by assuming known installed compressor capacity and calculated heat load from fish product. A gas mass balance was set around the receiver, enabling the possibility to calculate specific volume, $\upsilon$ [$m^3$/kg], for the tank, see more details in [1]. The calculated liquid temperature was used as an input in the freezing model, described in Section 2.2.1, to simulate the dynamic plate temperature in the beginning of the freezing process.

### 2.2.3 Energy storage tank description

Increase in temperature and freezing time due to insufficient compressor capacity could, in theory, be eliminated by implementing a CTES system. In this study, a shell-and-tube heat exchanger containing PCM on the shell side was used to store energy, as suggested by [7]. Charging, or freezing, of PCM is done when surplus energy is available, in other words, when compressor capacity is larger than heat load from product. The same energy is released during the first 15 minutes of freezing, essentially helping the compressor to remove gas, by condensing it in the storage tank and melting the PCM, following the method described in [8], see Figure 2.

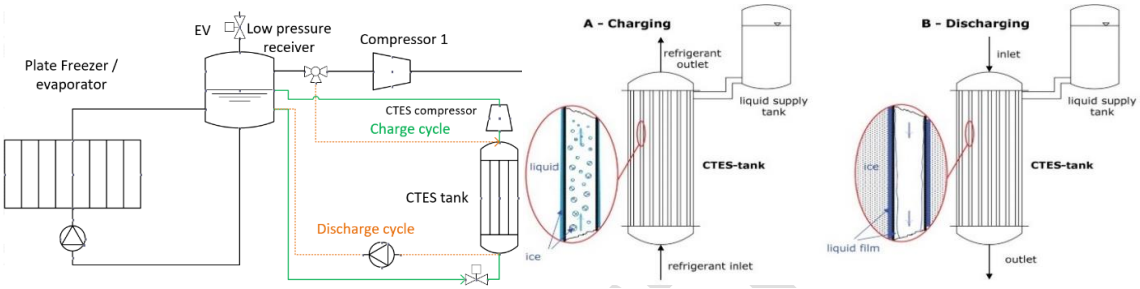


*Figure 2 Charge and discharge cycles for the CTES system with a close-up on the CTES tank*

The PCM was also chosen to be $CO_2$ due to matching phase changing temperatures and relative high thermal conductivity, which is a key factor to improve the heat transfer rates. To store energy around -50 ºC, the charging temperature of refrigerant must be below the triple point, indicating solid dry ice particles to be formed. In charge mode, the liquid from the receiver is expanded, generating solid ice to be sublimated in tubes, while PCM is freezing on the shell side. During discharge, gas is drawn from the receiver, helping the compressor to maintain low pressure, and is condensed when in contact with colder PCM. The PCM will be melted, releasing the stored energy. Dimensioning of equipment is fundamental, therefore PCM melting and freezing was modelled, based on the two-dimensional illustration in Figure 3.

Assuming heat is transferred from phase changing refrigerant, through metal pipes, liquid PCM and to the interface of phase changing PCM, an expression for the overall heat transfer coefficient is described by Equation 4 [10]

$$UA = \frac{2\pi L}{\frac{1}{r_i h_{conv}} + \frac{ln(r_o/r_i)}{k_{pipe}} + \frac{ln(r_{pcm}/r_o)}{k_{pcm}}} \quad (4)$$

Equation 4 is valid for liquid PCM at rest. However, buoyancy effects lead to heat transport by natural convection, resulting in higher heat transfer in liquid layer. Nusselt number, *Nu*, which relates heat transfer in convective fluids to pure conduction in fluids at rest, is defined in Equation 5 by:

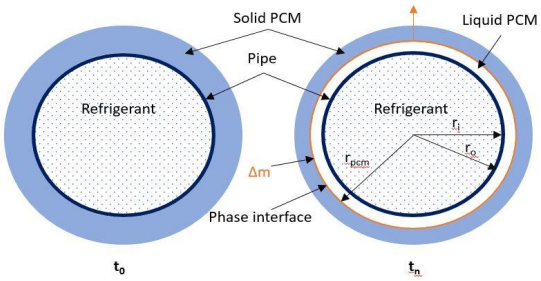


*Figure 3: Close-up on pipe in CTES tank during discharge*

| | Tube side | | Shell side |
|---|---|---|---|
| | Charge | Discharge | PCM |
| Temperature | -65 ºC | -49 ºC | -57 ºC |
| Pressure | 3 bar | 7 bar | 8 bar |

*Table 1: Suggested pressure and temperature levels in CTES tank [9]*

$$Nu = \frac{h}{k} d \quad (5)$$

Energy to freeze PCM can be expressed by:

$$Q = U \cdot A \cdot \Delta T = \frac{\Delta m \Delta H}{\Delta t} \quad (6)$$

Inserting equation 4 into equation 6, by use of equation (5) and expressing $\Delta m$ by known quantities, yields:

$$\Delta r = \frac{1}{\frac{1}{r_i h_{condens}} + \frac{ln(r_o/r_i)}{k_{pipe}} + \frac{ln(r_{pcm}/r_o)}{k_{pcm} Nu_d}} \cdot \frac{\Delta T \Delta t}{\Delta H \rho_{pcm} r_{pcm}^n} \quad (7)$$

Equation (7) describes melting radius $\Delta r$ for a time step $\Delta t$ and is being used to evaluate required amount of PCM and size of the tank. Pressures and temperatures assumed for the PCM tank are described in Table 1. Condensing heat transfer inside the tubes is complex to predict correctly. Therefore, values between 1700 and 4000 W/m$^{2}$·K, considered to be high and low boundaries in [11], were implemented for sensitivity analysis. Results concluded that they had a limited impact, since the heat transfer is dominated by PCM side. Aluminium pipe diameter was assumed to be 10 mm with 3-mm thick wall. The Nusselt number could not be determined precisely due to the complexity of the dynamics at play. Therefore, "most probable" Nusselt numbers between 1 and 4 were assumed.

## 2.3 Validation of models

To validate the numerical freezing model, a test material, consisting of agar-gel, was chosen due to good contact with plates, no internal circulation, high density of nucleation sites and convenience to monitor temperature. Thermal conductivity of the gel was measured using HotDisk TPS method. The test material was frozen in an industrial plate freezer, while measuring core temperature with a TC monitor [12]. Evaporating temperature was measured to be -49 ºC during the whole experiment, due to almost empty freezer, giving optimal conditions for constant plate temperature assumption.

Validation of pressure receiver model was done by comparing model results with data, gathered from land-based freezing facility.

# 3. RESULT AND DISCUSSION

## 3.1 Validating models

To validate the models, different strategies were chosen. The numerical freezing model was validated using experiments with the industrial plate freezer, conducted by the authors. The pressure receiver model was validated using data from similar land-based freezers.

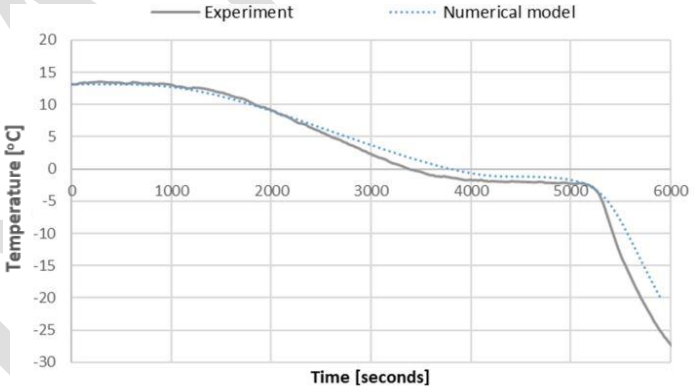


*Figure 4: Test material core temperature from experiments and numerical model during freezing in plate freezer*

### 3.1.1 Freezing time

In Figure 4, experimentally measured core temperature is compared to the numerical model. To achieve a core temperature of -20 ºC, there was only a difference of 2.9 % in freezing time.

Results from the numerical were in good agreement with the experimental data. One can therefore assume reasonable agreement also to frozen fish, provided correct model inputs.

### 3.1.2 Pressure in receiver

In Figure 5, the theoretical temperature is compared to measured temperatures in low-pressure receiver. The theoretical model overestimates the elevation of temperature, by 4 to 7 K. Possible reasons may be the unknown receiver tank size and the assumption of constant circulation rate in the freezer. In addition, the temperature peak seems sharper than in the experiments, which may be explained by different compressor control strategies.

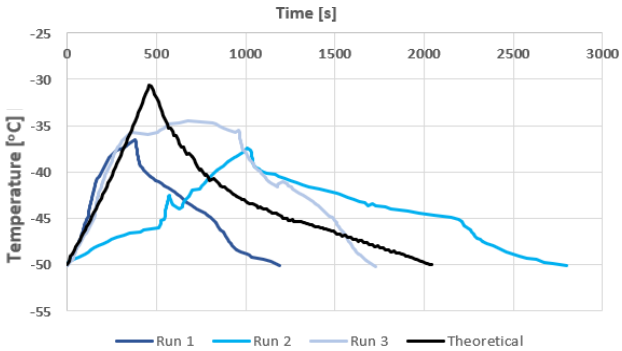


*Figure 5: Model prediction and measured data on temperature in lowpressure receiver during freezing*

Modelling pressure in a receiver is a complex task since it is influenced by a number of parameters, e.g., control of compressor, heat loss, liquid level, gas and liquid in non-equilibrium and other factors difficult to implement in numerical models. However, numerical results seems to be in agreement with experimental data.

## 3.2 Results from numerical models

### 3.2.1 COP of system

The efficiency of the freezing system in Figure 1 was estimated for different natural refrigerants and evaporating temperatures. Furthermore, a R744/R717 cascade system was included.

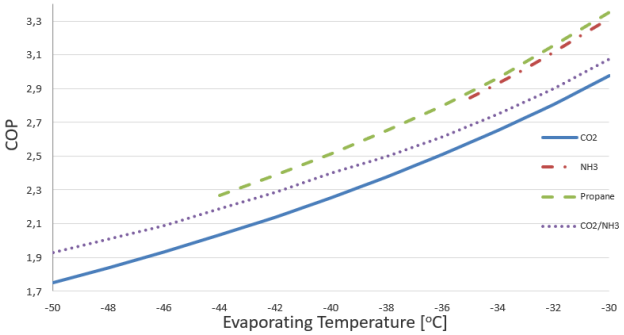


*Figure 6: COP for selected natural refrigerants, for different evaporating temperatures.*

$CO_2$ yields the lowest COP of the represented refrigerants, varying between 1.75 and 3.0. However, if more realistic assumptions are included for example pipe friction loss and compressor heat loss, the COP for $CO_2$ is expected to decrease less than the other refrigerants, due to specific thermodynamic properties.

### 3.2.2 Freezing time, energy use and product capacity

Various freezing curves are illustrated in Figure 7, representing different air void fractions which relates to packing factor of the fish. All runs are calculated for evaporating temperatures of -50 °C and plate thickness of 100 mm. A prolonged freezing time of up to 30 minutes highlights the importance of having high packing factor of the product. Factors that influence the packing factor are fish size and shape, block thickness and flexibility of fish (rigor mortis).

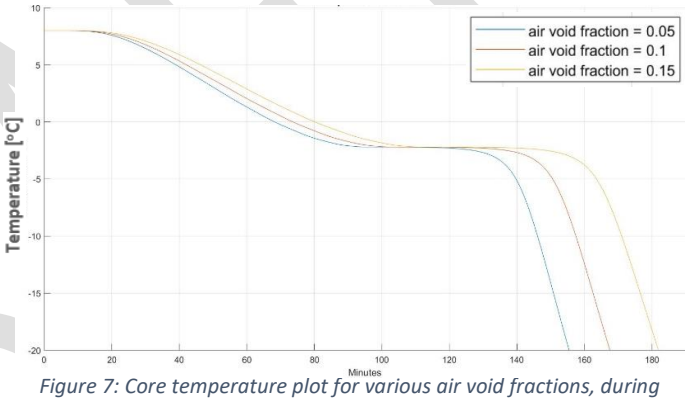


*Figure 7: Core temperature plot for various air void fractions, during freezing*

Based on the calculations of the freezing times and the system efficiency, the key performance indicators could be determined, as shown in Table 2. A freezer with 24 stations was assumed, corresponding to 1250 kg for 100 mm blocks.

| | | Freezing time[min] | | | Energy use [kWh/tonne] | | | Product capacity [%] | | |
|---|---|---|---|---|---|---|---|---|---|---|
| Evaporating temperature | | -50°C | -40 °C | -30 °C | -50 °C | -40 °C | -30 °C | -50 °C | -40 °C | -30 °C |
| Block thickness [mm] | 50 | 56.00 | 68.80 | 93.10 | 64.62 | 46.78 | 35.18 | 188 % | 161 % | 126 % |
| | 75 | 108.7 | 135.7 | 184.8 | 67.41 | 52.54 | 39.00 | 177 % | 146 % | 111 % |
| | 100 | 173.5 | 219.2 | 301.3 | 74.30 | 57.40 | 43.24 | 166 % | 134 % | 100 % |

Freezing times are calculated using dynamic plate temperatures, in accordance with Figure 5. Relative energy use is calculated using COPs for the $CO_2$ system, and a heat loss is included. Product capacity calculations are made assuming a reset time (defrost, unloading/loading of product) of 20 minutes.

The increase in energy use with the decrease in evaporation temperature can be explained by the decrease in COP and increase in heat loss, which have more impact than the decrease in freezing time. In addition, the energy use slightly decreases for thinner blocks since the freezing times seem to be dependent on thickness squared, while the mass is linearly dependent on thickness. The same argument is also valid when studying product capacity. Therefore, product capacity can be greatly increased, both

with reduction in evaporating temperature and plate thickness. However, too thin fish blocks might reduce surface contact and increase air void fraction.

### 3.2.3 Heat load in the system

Heat load was calculated by enthalpy difference in fish, using the freezing model. Figure 8 illustrates individual and total heat load of a system containing three plate freezers in parallel. The peaks represent the start of a new freezing process, which happens with 40 minutes intervals. Plate freezers using 24 100-mm block thickness and -50 ºC plate temperature are assumed. The dotted line indicates the average heat load, which generally yields the dimensioning of the installed compressor capacity.

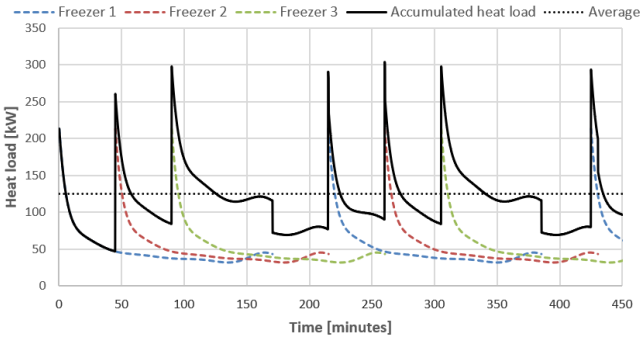


*Figure 8: Heat load for 3 plate freezers running in parallel, one after the other.*

It is clear from Figure 8 that peak heat loads are significantly higher than the installed compressor capacity, explaining the elevation in receiver temperature and possibly the longer freezing times demonstrated by comparing ideal freezing time to real freezing time.

## 3.3 Cold thermal energy storage

Figure 9 illustrates when, and how much, energy can be stored, for one 1250 kg freezer. In practice, the pressure in receiver determines whether the compressor capacity is higher than the heat load since this cannot be directly measured. Lower pressure than designed indicates surplus energy available and signals the expansion valve to open and starts the CTES compressor, see Figure 2. The amount of stored energy determines the discharge CTES capacity, at the designed discharge time. All results regarding CTES are calculated assuming -50 ºC R744 systems using 100 mm blocks.

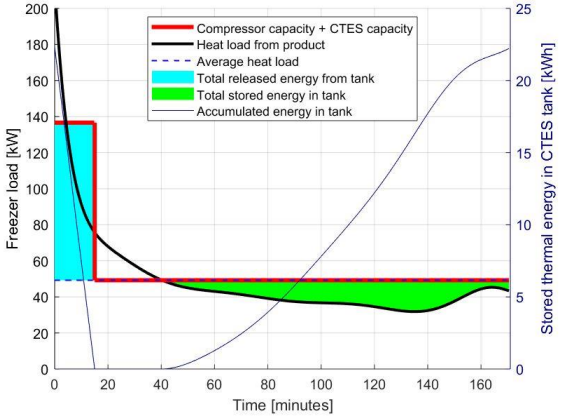


*Figure 9: Heat load, compressor capacity and discharged/accumulated thermal energy during freezing*

Compressor capacity matches the heat load far better when the CTES system is installed. This nearly eliminates the elevated receiver temperature, which would be the case if the compressor capacity was equal to the average heat load.

### 3.3.1 Ice melting and sizing of storage system

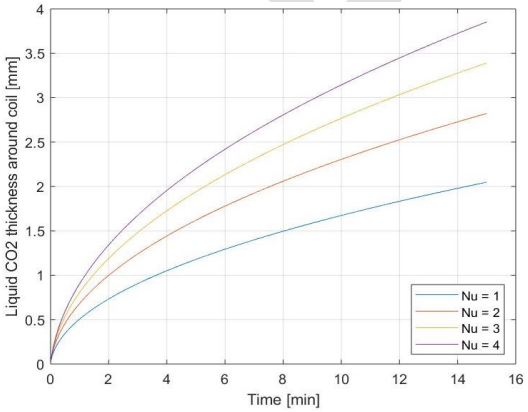


*Figure 10: Evolution of the liquid $CO_2$ thickness around the tube with time for various Nusselt numbers.*

To determine the number of tubes and the size of the storage tank, the melting of the PCM had to be modelled, since it is likely that discharging of the tank would be the dimensioning criteria due to the short time. The melting layer was modelled for different Nusselt numbers, determining the amount of PCM required for each 1 m long tube, as shown in Figure 11. The overall heat transfer coefficient is modelled accordingly. The total energy to be stored being already calculated, one can also determine the number of tubes and the total amount of PCM required, see Table 2.

The number of tubes and the total volume of the tank are especially interesting since they influence the capital investment cost and the space requirement, respectively. Around 0.5 $m^3$ takes up valuable space in a small machine room, but one might argue that a CTES system require less installed compressor capacity, since some of the heat load can be covered with the storage tank, which in turn reduce the number or the size of the compressors.

| | Nusselt Number | | | |
|---|---|---|---|---|
| | **1** | **2** | **3** | **4** |
| Melted PCM thickness [mm] | 2.02 | 2.74 | 3.34 | 3.64 |
| No. of 1m tubes required | 1377 | 979 | 805 | 702 |
| Total volume of tank [L] | 614 | 501 | 451 | 422 |
| Mean Heat transfer, U [$W/m^2K$] | 264 | 372 | 452 | 518 |

*Table 2: Dimensioning properties of CTES tank*

Methods of heat transfer enhancements, described in [7], may be needed to achieve the heat transfer rates, calculated in Table 3. The enhancement might also reduce the number of tubes and size, however, investment cost is likely to increase.

### 3.3.2 Effect on freezing system

Now, it is possible to calculate new freezing times, with nearly constant plate temperature, since higher effective compressor capacity, reduces the elevation in pressure and temperature in the receiver. From here, the potential benefits of installing a CTES system could be investigated.

| | With CTES | Without CTES | Difference [%] |
|---|---|---|---|
| Freezing time [min] | 168 | 174 | -3.17 |
| Specific energy use [kWH/tonne] | 80.2 | 74.3 | 7.94 |
| Product capacity [kg/h] | 399 | 388 | 2.92 |

*Table 3: Potential benefits of installing a CTES system*

Note the increase in energy use, as a relatively small CTES compressor is installed. Freezing time is decreased by over 3 %, due to lower plate temperature during the whole freezing process, which in turn results in 2.9 % capacity increase. Capacity and freezing time are not directly linked due to the assumed 20-min reset time, for defrost, unloading and loading of product.

## 4. CONCLUSION

After validation of the numerical freezing model for good contact, constant temperature, agar-gel, one might assume that the model is sufficient for fish freezing, provided correct input values. Prediction of pressure in receiver provided a good agreement with the experimental data, though, the pressure is erratic and varies from cycle to cycle. Furthermore, the model seems to yield higher peak temperature than the measured data, by 4 to 7 K.

Results from the freezing model imply that packing factor of the fish blocks has a major influence on freezing rate, with almost 30 minutes difference between 15 % and 5 % air fraction in the blocks. The factor with the largest influence on freezing time is the thickness of the blocks. However, excessively thin blocks might create large air voids for larger fish species, which, in turn, increases freezing time. Therefore, there might exist an optimum thickness defined by the fish size and achievable packing factor. More data on packing factors is needed to find the optimum block thickness. Decrease in block thickness and especially lower evaporating temperature, enabled by R744 systems, result in increased product capacity for the freezer, which is more relevant than energy reduction and freezing time. The freezing station is the bottleneck of the production line since it takes up to 4 hours for fish to be frozen. In some cases, the short-term storage on the boat (often refrigerated sea water (RSW) tanks) is filled up while there is still fish to be harvested. Vessels with installed R744 systems, having fast freezing rates, can therefore spend less time at sea for the same amount of fish, which in turn reduces operational costs and fuel consumption.

Implementing a CTES system within a low-temperature R744 system, using $CO_2$ as PCM and storing energy when compressor capacity is larger than heat load, was estimated to increase the product capacity by 2.9%. The storage tank practically eliminated the pressure increase in the receiver, by condensing the refrigerant gas that the compressor could not remove. The tank size was determined to be between

600 and 400 litres, depending on the achievable internal heat transfer rates. The tank required between 1400 and 700 tubes to be able to release the stored energy within 15 minutes.

## NOMENCLATURE

| | | | | | | | |
|---|---|---|---|---|---|---|---|
| $\rho$ | Density [kg/m$^3$] | $\dot{m}$ | Mass flow [kg/s] | $r$ | Radius [m] | $Q$ | Heat [W] |
| $c_a$ | Apparent heat capacity [J/(g·K)] | $\upsilon$ | Specific volume [m$^3$/kg] | $L$ | Length [m] | $U$ | Overall heat transfer coefficient [W/(m$^2$K)] |
| $T$ | Temperature [K] | $\dot{V}$ | Volume flow [m$^3$/s] | $h$ | Convective heat transfer [W/m$^2$·K] | $A$ | Area [m$^2$] |
| $k$ | Thermal conductivity [W/(m·K)] | $x$ | Vapour fraction [-] | $t$ | Time [s] | $H$ | Fusion energy [J/kg] |

## REFERENCES


[1] Verpe, Low Temperature Plate Freezing of Fish using R744 as Refrigerant and Cold Thermal Energy Storage, Norwegian University of Science and Technology, 2018.

[2] Returgass, "Stiftelsen Returgass," [Online]. Available: {http://www.returgass.no/om-oss/annen-informasjon/rn-lib/. [Accessed 2018].

[3] Sardeshpandea, Shastrib and Ranadea, "Two phase flow boiling pressure drop insmall channels," *International Journal of Heat and Fluid Flow,* 2014.

[4] Tannehill, Anderson and Pletcher, Computational Fluid Mechanics and Heat Transfer, 2nd ed., Tylor&Francis, 1997, pp. 137-138.

[5] Schwartzberg, "Effective heat capacities for the freezing and thawing of food," *Journal of Food Science,* 1976.

[6] American Society of Heating, Refrigeration and Air-Conditioning, ASHRAE handbook: Refrigeration, 2010.

[7] Agyenim, Hewitt, Eames and Smyth, "A review of materials, heat transfer and phase change problem formulation for latent heat thermal energy storage systems (LHTESS)," *Renewable and Sustainable Energy Reviews,* 2010.

[8] Hafner, Nordtvedt and Rumpf, "Energy saving potential in freezing applications by applying cold thermal energy storage with solid carbon dioxide," in *11th International Congress on Engineering and Food (ICEF11)* , 2011.

[9] "KNOWLEDGE SHARING REPORT – CO2 Liquid Logistics Shipping Concept (LLSC) Overall Supply Chain Optimization," Global CCS institute, 2011.

[10] Incropera, Dewitt, Bergman and Lavine, Principles of Heat and Mass Transfer, 7 ed., John Wiley & Sons, Inc., 2013, pp. 136-138.

[11] Zang, "Co2 condensation heat transfer coefficient and pressure drop in a mini-channel space condenser," *Experimental Thermal and Fluid Science,* 2012.

[12] Accsense, "Product leaflet," 2014. [Online]. Available: http://accsense.com/media/versalog/VersaLog-TC.pdf.

# Bibliography


[1] A. Watzinger, A. Lydersen, H. W. (1949). *Fiskefiletfrysing: Kontaktfrysing mellom kjøleplater*. Fiskedirektoratet.

[2] Abbasi, N. M. (2015). *Solving the advection PDE in explicit FTCS, Lax, Implicit FTCS and Crank-Nicolson methods for constant and varying speed. Accuracy, stability and software animation* . Master thesis at UCI.

[3] Accsense (2015). Product leaflet for tc monitor. http://accsense.com/media/versalog/VersaLog-TC.pdf.

[4] Agyenim et al. (2009). A review of materials, heat transfer and phase change problem formulation for latent heat thermal energy storage systems (lhtess). *Renewable and Sustainable Energy Reviews*.

[5] Agyenim et al. (2010). Heat transfer enhancement in a medium temperature thermal energy storage system using a multitube heat transfer array. *Renewable energy*.

[6] Armin et al. (2011). Energy saving potential in freezing applications by applying cold thermal energy storage with solid carbon dioxide. *11th International Congress on Engineering and Food (ICEF11)*.

[7] Armultra. Iqf freezers and plate freezers. http://www.armultra.co.uk/gallery/category.php?catID=11.

[8] Bonacina and Comini (1971). *On a numerical method for the solution of the unsteady state heat conduction equation with temperature dependent parameters*. XIIIth International Congress of Refrigeration.

[9] ChemicaLogic. Co2 tables. http://www.chemicalogic.com/Documents/co2_phase_diagram.pdf. PT-Diagram for CO2.

[10] Cleland (1977). *Heat transfer during freezing of foods and prediction of freezing times*. PhD thesis, Massey University, New Zealand.

[11] Cleland and Earle (1976). A comparison of freezing calculations including modification to take into account initial superheat. *Journal of Food science*.

[12] Cleland and Earle (1977). A comparison of analytical and numerical methods of predicting the freezing times of foods. *Journal of Food science*.

[13] Cleland and Earle (1979). Prediction of freezing times for foods in rectangular shapes. *Journal of Food science*.

[14] Crowley (1978). Numerical solution of stefan problems. *Journal of heat and mass transfer*.

[15] Danfoss Group (2016). Hfc phase down (regulation). http://refrigerants.danfoss.com/hfc/#/.

[16] Demirbas (2010). *Methane gas Hydrate*. Springer, 2nd edition.

[17] Dincer and Rosen (2001). Energetic, environmental and economic aspect of thermal energy storage systems for cooling capacity. *Applied Thermal Enginnering*.

[18] DSI-AS. Leaflet dsi v3 vertical plate freezer. http://www.dsi-as.com/products/dsi-vertical/v3/.

[19] DSI-AS. Natural refrigerants co2/nh3. http://www.dsi-as.com/fileadmin/Arkiv/Billeder/Product_Leaflets/Engelsk/dsi_CO2_english__NY.pdf. Product leaflet.

[20] Earle, R. and Earle, M. (2004). *Unit Operations in Food Processing*. The New Zealand Institute of Food Science & Technology (Inc.), web edition edition.

[21] Esen et al. (1997). Geometric design of solar aided latent heat storage dependent on various parameters and phase change materials. *Soluble Energy*.

[22] Fellows, P. (2009). *Food processing technology*. Woodhead Publishing, 3rd edition.

[23] Fernández, Dopazo, Uhía, and Diz (2012). Experimental analysis of the freezing process in a horizontal plate freezer with co2 as refrigerant in a cascade refrigeration system. *Taylor and Francis Online*.

[24] Finckh et al. (2011). Energy and efficiency comparison between standardized hfc and co2 transcritical systems for supermarket applications. *23rd IIR International congress of Refrigeration*.

[25] Granryd et al. (2005). *Refrigerating engineering*. Royal Institute of Technology, KTH: Department of Energy Technology.

[26] Hafner and Eikevik. "co2 as working fluid". Lectures notes at NTNU 2017.

[27] Heldmann et al. (2007). *Handbook of food engineering*. Taylor & Francis Group, 2nd edition.

[28] Hot Disk Instruments. Information kapton sensors. https://www.hotdiskinstruments.com/products-services/sensors/kapton-sensors/.

[29] Incropera et al. *Principles of Heat and Mass Transfer*. John Wiley Sons.

[30] International Institute of Refrigeration (2015). The role of refrigeration in the global economy. http://www.iifiir.org/userfiles/file/publications/notes/NoteTech_29_EN.pdf.

[31] International Organization for Standardization. Determination of thermal conductivity and thermal diffusivity — part 2: Transient plane heat source (hot disc) method. https://www.iso.org/obp/ui/#iso:std:iso:22007:-2:ed-2:v1:en.

[32] Lees (1966). A linear three level difference scheme for quasi linear parabolic equations. *Mathematics of computation*.

[33] Lenninger and Beverloo (1975). *Food process engineering*. Springer Netherlands, 2nd edition.

[34] Mallett (1993). *Frozen Food Technology*. Springer, 2nd edition.

[35] Maxim Integrated. ibutton temperature loggers with 8kb datalog memory ds1922l/ds1922t. https://datasheets.maximintegrated.com/en/ds/DS1922L-DS1922T.pdf. Product leaflet.

[36] Merymann (1963). *Food process*. 22, 81.

[37] Miles et al. (1983). Calculation of thermophysical properties of foods. *Physical properties of foods*.

[38] Nagaoka, Takaji, and Hohani (1955). *Experiments on the freezing of fish in air blast freezer*. IXth International Congress of Refrigeration.

[39] of Heating Refrigerating, A. S. and Engineers, A.-C. (2010). *ASHRAE Handbook: Refrigeration*. American Society of Heating, Refrigerating and Air-Conditioning Engineers, Inc., 2nd edition.

[40] Pham (2002). *CALCULATION OF PROCESSING TIME AND HEAT LOAD DURING FOOD REFRIGERATION*. AIRAH Conference.

[41] Planck (1941). Beitrage zur berechnung und bewertung der gefriergeschwindigkeit van lebensmitteln. *Beihefte Z ges Kalte-lnd*.

[42] Plank (1963). *El Empleo del Frio en Ia Induatria de la Alimentación*. Reverté, Barcelona.

[43] Rebellato, Giudice, and Comini (1978). Finite element analysis of freezing processes in foodstuffs. *Journal of Food science*.

[44] RJatal, Mannapperuma, and Singh (1989). A computer-aided method for the prediction of properties and freezing/thawing times of foods. *Journal of Food engineering*.

[45] Rose (1960). A method for calculating solutions of parabolic equations with a free boundary. *Mathematics of Computation*.

[46] Sardeshpandea, Shastrib, and Ranadea (2014). Two phase flow boiling pressure drop in small channels. *International Journal of Heat and Fluid Flow*.

[47] Schwartzberg (1976). Effective heat capacities for the freezing and thawing of food. *Journal of Food Science*.

[48] Sharma and Sagara (2005). Latent heat storage materials and systems: A review. *International Journal of Green Energy*.

[49] Stiftelsen Returgass. Rn-lib free download. http://www.returgass.no/om-oss/annen-informasjon/rn-lib/.

[50] SWEP. *Refrigerant Handbook*. https://www.swep.net/refrigerant-handbook/1.

[51] Valentas, Rotsteina, and Singh (1997). *Handbook of food engineering practice*. Taylor & Francis Group.

[52] Zang and Faghri (1996). Heat transfer enhancements in latent heat thermal energy storage systems by using the internally finned tube. *International journal of heat and mass transfer*.

[53] Zhang et al. (2012). Co2 condensation heat transfer coefficient and pressure drop in a mini-channel space condenser. *Experimental Thermal and Fluid Science*.